DEVELOPMENT OF ADVANCED
ADI-FDTD BASED TECHNIQUES FOR
ELECTROMAGNETICS AND MICROWAVE MODELING

by

Iftikhar Ahmed

Submitted

in partial fulfillment of the requirements

for the degree of

DOCTOR OF PHILOSOPHY

Major Subject: Electrical and Computer Engineering

at

DALHOUSIE UNIVERSITY

Halifax, Nova Scotia   July, 2006

Canada

DALHOUSIE UNIVERSITY

To comply with the Canadian Privacy Act the National Library of Canada has requested that the following pages be removed from this copy of the thesis:

Preliminary Pages
Examiners Signature Page
Dalhousie Library Copyright Agreement

Appendices
Copyright Releases (if applicable)

Table of Contents

List of Tables

List of Figures

x

List of Abbreviations

ABCs   Absorbing boundary conditions

ADI   Alternating direction implicit

BEM   Boundary element method

CE   Complex envelop

CFL   Courant-Friedrich-Levy

CN   Crank Nicolson

EM   Electromagnetic

FD   Frequency domain

FDM   Finite difference method

FDTD   Finite-difference time-domain

FDTLM   Frequency domain transmission line matrix

FEM   Finite element method

FFT   Fast Fourier transforms

FVTD   Finite volume time domain

MM   Mode matching method

MoL   Method of lines

MoM   Method of moments

MOMTD   Time domain method of moments

MRTD   Multiresolution time-domain

PDEs   Partial Differential Equations

PML   Perfectly matched layers

PSTD	Pseudospectral time-domain
RF	Radio frequency
SDA	Spectral domain approach
TD	Time domain
TDFEM	Time domain finite element method
TE	Transverse electric
TM	Transverse magnetic
TLM	Transmission line method

Dedication

This work is dedicated to my parents and sister.

Acknowledgements

First of all I am thankful of my supervisor Dr.Zhizhang (David) Chen for his valuable suggestions, assistance, encouragement and guidance throughout my research. The author also wishes to thanks other guiding committee members, for their advice and evaluation of this work.

Thanks to Dr. Sherwin Nugent for his advice on the theory of electromagnetics and wave propagations. I am also thankful to Dr. J. M. Chuang for his assistance in transmission line equations and some other complex mathematical equations.

I am grateful to all members of microwave and wireless research group from September 2001 to date for their company. My thank goes to Ms. Lorraine Devanthey for her help during my thesis writing.

ABSTRACT

With the development of more complicated structures in the field of electrical engineering, the importance of the computational electromagnetics increases. With computational electromagnetics, a designer can know what happens inside circuit structures, namely, which components or elements radiate and how signals travel and reflect. For microwave frequencies and wide band systems applications, time-domain methods are increasingly preferred of their capability in handling wide band signals. Among time domain methods, FDTD (Finite Difference Time Domain) method has attracted more attention due to its simplicity and direct applicability to Maxwell's equations. It has been used in a large number of applications, and FDTD based software has been developed commercially. Nevertheless, due to CFL (Courant-Friedrich-Levy) stability constraint and numerical dispersion error, it takes large memory and simulation time for electrically large and high Q structures. To circumvent the problems, many improved FDTD methods have been developed. For instance, to make FDTD method memory efficient, PSTD (Pseudospectral Time Domain) method was proposed, and to reduce its dispersive error MRTD (Multiresolution Time Domain) was developed. To remove the CFL constraint, unconditionally stable ADI-FDTD method was introduced recently, although it takes more memory and is more dispersive at larger time steps.

To further improve the computational efficiency, in this thesis, hybrid FDTD and ADI-FDTD method is introduced. By using this hybrid approach, advantages of both FDTD and ADI-FDTD methods can be taken. In it, FDTD is applied in coarse mesh and ADI-FDTD in fine mesh areas. The time step is the same as that of the FDTD region even with smaller cell size in ADI-FDTD region. In this way, optimum saving in memory and computation time can be achieved without sacrificing the accuracy.

Accuracy of the ADI-FDTD method deteriorates at larger time steps. To mitigate this problem, two different error-reduced ADI-FDTD methods are presented. These error-reduced methods are based on the more accurate Crank Nicolson (CN) method but the simulation procedure is like the ADI-FDTD method. In these methods, modified splitting error term, which is missing in ADI-FDTD formulation and causes inaccuracy, is introduced to reduce the errors. The first method is found to be more accurate than the second one, but both are better than the conventional ADI-FDTD method.

ADI-FDTD also has relatively large dispersion error in comparisons with the FDTD method. To reduce it, dispersion optimized ADI-FDTD methods with different cases are also developed in this thesis. In them, dispersion controlling parameters are introduced, which result in different degrees of dispersion controls.

In summery all the methods proposed in this thesis are aimed at improving the efficiency of FDTD method and the ADI-FDTD method. To improve computational efficiency an efficient hybrid method is introduced. To have better results with larger time steps, error-reduced ADI-FDTD methods are introduced, and to control the dispersion of ADI-FDTD method dispersion optimized ADI-FDTD methods are proposed. These proposed methods are then numerically tested for validity and effectiveness.

Chapter 1   Introduction

1.1   Introduction

Today, realistic simulation of large and complicated systems has become possible, due to increasing computation power of computers. For simulation purposes many analytical, semi analytical and numerical methods have been proposed and are in use. Such kinds of methods are being employed day by day for more accurate and efficient designs. Circuit and prototype design without proper prediction of results is proven to be expensive and time consuming. Accurate modeling and simulation of circuits can provide better prediction of circuit performance before circuit prototyping. In general, it is very difficult to get the analytical or semi analytical solutions of all kinds of circuit structures due to their complexity and variations. To handle the situation numerical methods are then used. On the other hand, due to increased computation power of computer, numerical methods, which were considered to be expensive in the past, start to play an important role today in solving the electromagnetic and RF/microwave structure problems. In addition, continuous improved accuracy and efficiency of these methods are also making them effective and popular. Many software packages based on these numerical methods have been developed commercially, although efforts to develop more refined numerical methods are still underway in both academia and industry.

There are two basic circuit designing CAD (Computer Aided Design) techniques, circuit-theory based and field-theory based. The circuit-theory based techniques are simpler and older than the field theory-based techniques. The circuit based techniques are used in terms of voltage and current. The field based circuit designing techniques are comparatively new and are applied in terms of electric and magnetic fields [1]. In them, Maxwell's equations are to be solved. The field based techniques are alternative to the circuit based techniques; they take a more microscopic view of a structure to be analyzed.

The main reason for using field based techniques is their generality to consider all electromagnetic effects including:

1) all loss mechanisms such as surface waves and radiation
2) parasitic coupling between elements
3) effect of compacting a circuit into small space
4) effect of package or housing on the circuit performance

With computer graphic technology, above effects can be visualized on screen, allowing deeper understanding of circuit operations.

However, in the field based methods, size of a structure is critical because of needed but limited computer resources. With the development of new efficient methods and high-speed computers, such a constraint is relaxing. Major applications of the field-based techniques are RF/microwave electronics, optical fiber communications, radar, satellite communications, aircrafts systems, electromagnetic compatibility, mobile communications, biomedical devices and antennas. These vast applications show the importance of computational electromagnetics.

The field-based techniques can be categorized into two types: frequency and time domain methods. The examples of the frequency domain methods are Method of Moment (MoM) and Finite Element Method (FEM) while the examples of the time domain methods are FDTD and ADI-FDTD. Frequency domain methods are efficient in narrow band solutions, while the time domain methods are efficient for wide band solutions. Although both have advantages in their own domains, the time domain methods are getting popular because of their ability of handling wideband signals and the availability of high power computers. A large number of time domain numerical methods have been developed [2-5]. Among them the FDTD method is the most popular due to its simplicity and generality. In the next section a brief review of both frequency and time dependent methods is presented.

1.2 Review of the State of-the-Art Numerical Methods

As described before, numerical methods fall into the following two broad categories:

A)   frequency domain

B)   time domain

These two categories are also known as time harmonic and transient methods, respectively. In terms of usage frequency domain methods are very old techniques as compared to time domain methods. Before 70's it was difficult to apply time domain methods because of the required large number of calculations and limited computer power. Therefore, frequency domain methods were more common. Frequency domain or harmonic methods are very efficient in narrow or moderate bandwidth applications, but not for wide bandwidth applications. Frequency domain methods can be obtained by replacing the time domain differential operator with $j\omega$ and time domain integral operator by $\frac{1}{j\omega}$ in Maxwell's equations [1]. Frequency domain methods are applicable and effective for linear problems. On the other hand, today the time domain or transient methods have become popular due to availability of the high power computers. These methods can cover a wide range of frequency spectrum in one simulation run. In addition, time domain methods can also be applied easily to non-linear structures.

A)   Frequency domain methods

With frequency domain methods the full wave frequency domain analysis of a problem can be done at any frequency of interest. These methods can be used to calculate frequency- dependent characteristics such as skin effect, losses, dispersion and reflection at discontinuities. They are good for steady-state conditions and become inefficient for transient analysis.

The following frequency domain methods, Finite Element Method (FEM), Method of Moment (MoM), Finite Difference Method (FDM), Frequency Domain Transmission Line Method (FDTLM), Method of Line (MoL), Spectral Domain Approach (SDA), Boundary Element Method (BEM), and Mode Matching (MM) are briefly explained here.

A1   FEM (Finite Element Method)

In 1968 FEM was applied for the first time in the field of electromagnetics by Silvester [1], although it had been applied in the field of civil and mechanical engineering. Today it is a well-known frequency domain method for electromagnetic and RF/microwave applications. It has been applied to both two-dimensional and three-dimensional problems. Commercial software based on this method have been developed for electromagnetics and RF/microwave applications, for example, HFSS by Ansoft [8], FEMLAB by COMSOL [9], QuickField by Tera Analysis [10], and FlexPDE by PDE Solutions [11].

FEM is effective for irregular boundaries and complex structures. It is also suitable for shielding applications with apertures. However, it is complex to understand and to prepare final equations for programming. In addition, it is not suitable for thin long wires and for applications where there is a large distance between a source and a measurement point. Although the FEM method is computationally expensive for complex structures such as thin film resonators, the availability of high-speed computers favors FEM over other frequency domain simulation techniques [12].

To solve a problem, FEM contains the following four steps [13]:
1) discretization of a structure into a finite number of elements or subregions that is known as finite element mesh.
2) derive the equations for elements or subregions defined in step 1.
3) assemble all subregions or elements obtained in the discretized structure.
4) solve the obtained resulting equations by the Iterative or Banded Matrix methods.

The FEM mesh usually contains non-overlapping polygonal regions or elements. Triangle and quadrilaterals are two well-known types of subregions or elements, but triangle is mostly used, due to the availability of wide range variety of triangular meshing techniques. The approximate solution of each element should follow the constraints: that requires continuity along the edges of the subregions and boundary conditions. Adaptive

meshing techniques [14-15] are also used to optimize the meshing in structures and to control the mesh density. A fine mesh can be used in the desired areas such as corners where field variation is rapid etc, and a coarse mesh in the rest of the areas. For open region structures FEM is not computationally economical. To handle open problems, hybrid techniques or absorbing boundary conditions have been developed with the FEM method [16].

A2   MoM (Method of Moments)

The MoM is one of the most well-known methods in frequency domain analysis of electromagnetics and RF/microwave circuits. It was used initially in civil and mechanical engineering and first introduced by R.F. Harrington to electromagnetics [17-18]. Basically, MoM uses two important concepts of electromagnetics: Green's function and superposition. In electromagnetics Green's function is like an impulse response of a circuit. For given boundaries (e.g. infinite free space or walls) and material bodies (e.g. dielectrics and ground planes) Green's function is used to find out the field at any position due to an extremely small uniform current element at a particular position. For an actual circuit that occupies a fixed area or volume current may have distributions along a surface and in a volume. By dividing the current on a surface into many small current elements, field components are measured by adding the contribution (or Green's function) from each current element (superposition) [19].

MoM is used normally to solve integral equations. It is a suitable method for long wire and objects with considerable distances among them [20]. Therefore, it is very effective for radiation and scattering problems. Based on MoM many commercial software packages have been developed such as momentum (ADS) by Agilent EEsof EDA [21], Ensemble by Ansoft [22], em by Sonnet software [23], IE3D by Zeland software [24], and EMSight by Applied wave research [25].

In general MOM is good for computing the homogeneous and layered dielectrics. It is difficult to apply MoM to nonlinear and non-homogeneous structures. To handle these

5

structures, hybrid methods [26] are used but they are still in the stage of infancy in development.

Normally MoM is categorized into two types [1]. The first category is closed-box MoM and the second is open-box moment method. In the closed-box moment method, box walls and circuits both are included in the formulation. Codes for these are made by using fixed resolution grid and an analytical Green's function is employed for fast computation. However, the closed-box moment method is not suitable for millimeter wave applications because the box wall may support some resonant modes that may cause interference with the original signals. Another issue is that grid resolution is fixed and cannot be varied.

In the open-box method, there is no need of fixed grid resolution; triangular and rectangular grids can be used for a structure. It is applied more often to open structures e.g. rectangular microstrip patch antennas. Nevertheless, in the open-box moment method, calculation of Green's function is slower than in the closed-box moment method. There is also need of image theory to implement symmetry and box walls. In addition, to find impedance in open case there is need of a separate 2-D solution [1]. Nonetheless, the moment method has worked very well for analyzing broad range of problems in the field of electromagnetic and RF/ microwave circuits.

A3   FDM (Finite Difference Method)

Finite difference method is used to solve partial differential equations, and it is one of the best-known methods that are applied to quasi-static problems. Quasi-static problems are those that are used when a structure is much smaller than wavelength. To get accurate results with FDM, a solution domain is first discretized into a collection of small cells. The discretized cell size should be small; otherwise there will be un-negligible dispersion errors due to discretization.

The FDM is one of the old numerical methods. It was widely studied from 1950 to 1970 and has been applied to many practical electromagnetics problems [27-28], including the

waveguide discontinuities problem [29-30]. FDM is attractive, straight forward and simple. To solve a problem with FDM normally three conditions have to be known before-hand [5][30-31]:

1) a partial differential equation to be solved, e.g., Laplace or Poisson's equation
2) a solution region where the equation is applied
3) boundary conditions within the solution region

With these conditions, FDM can be applied. For example, a two-dimensional Laplace equation problem can be solved with the finite difference method in the following steps:

Step1: divide the solution domain into a finite number of cells as shown in Fig 1.1.

Step2: Approximate the differential equation and boundary conditions by a set of linear algebraic equations as the result of replacing differentials with finite differences that is,

$$\nabla^2 V = \frac{\partial^2 V}{\partial x^2} + \frac{\partial^2 V}{\partial y^2} = 0 \tag{1.1}$$

is finite-differenced, which leads to

$$V_{i,j} = \frac{1}{4}(V_{i,j-1} + V_{i,j+1} + V_{i-1,j} + V_{i+1,j}) \tag{1.2}$$

Equation (1.2) is the discretized solution of equation (1.1) with $\Delta x = \Delta y$. It shows that the field value at a point is the averages of those at the four neighboring points (see Fig 1.1).

Step3: Solve the resultant set of algebraic equations obtained in Step2 by either an Iteration Method or Banded Matrix Method.
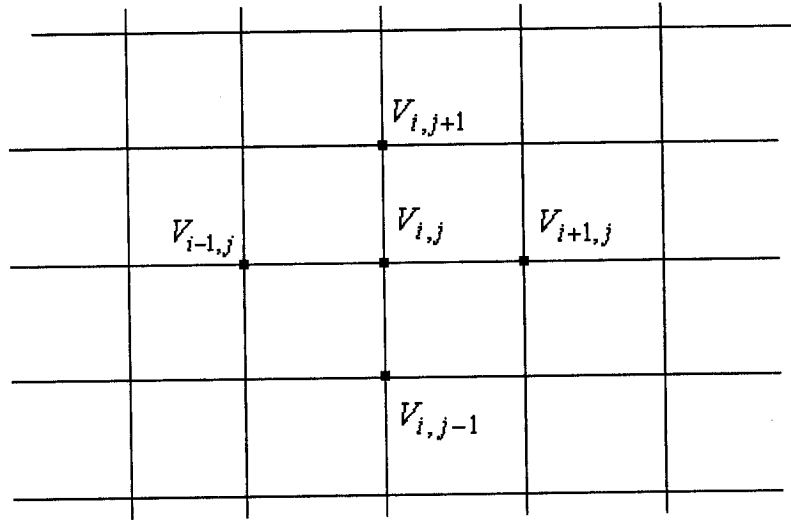
Fig. 1.1 Finite difference for Laplace's equation

A4   FDTLM (Frequency Domain Transmission Line Matrix)

The FDTLM method [32] is an extended form of the TLM method [33], and was introduced by Jin and Vahldieck in 1992. In general, FDTLM has approximately the same advantages and disadvantages compared to the TD-TLM as frequency domain methods have in comparison with time domain methods.

In FDTLM, a structure under study is discretized into meshes of transmission lines connected with symmetrical condensed nodes. The FDTLM method is assumed to be in steady state conditions, while the field interactions are represented or solved with connecting and scattering matrices. In addition to many other applications, the FDTLM method is efficient for thin layer structures as compared to the TD-TLM method [34-35]. By using absorbing boundary conditions, this method can also be applied to open structures efficiently [36].

A5   MoL (Methods of Lines)

The method of lines (MoL) is a method that is used to solve PDEs (partial differential

equations) in which time derivative is solved by using the ordinary differential equations and the spatial derivatives by finite differences. MoL is a semi-analytical method, and is used as one of the standard tools for many practical, complex electromagnetic problems [37]. It was originally developed by a mathematician to solve the boundary value problems [38-39]. R. Pregla, from Fern Universitat, Hagen, Germany, applied it first to electromagnetics [40], and many other researchers [41-43] followed latter. This method has results better than the finite difference method, and has been applied to many applications successfully.

The basic concept of MoL is that a differential equation is usually discretized in one or two dimensions but remains analytical in the remaining directions. Due to the discretization in some directions and analytical solution in the remaining directions, it has qualities of both finite difference and analytical methods. In MoL, the following five steps are needed [43]:

1) divide the given structure into layers
2) discretize the given structure in one or two directions
3) make transformation to obtain decoupled ordinary differential equations
4) take the inverse transformation and apply the boundary conditions
5) obtain the solutions after solving the equations.

MoL does not have any problem with relative convergence and it also does not support spurious modes. It has certain advantages like efficient computation and less programming effort, due to its property of having the merits of both analytical and finite difference method. Perfectly absorbing boundaries have been introduced in MoL; with them, it can also solve open structures very efficiently and is not limited to closed solution domains.

A6   SDA (Spectral Domain Analysis)

This method is known both as SDM (Spectral Domain Method) and SDA (Spectral

Domain Approach). SDA is the Fourier- transformed version of the integral equation method, and has been applied to microstrip and other printed lines structures [44]. Many commercial packages using this method such as VUSTLSn Model- LINMIC+/N (AC Microwave), MMICTL- LINMIC+/N (AC Microwave), MCPL model - Ansoft Designer (Ansoft) and SFPMIC- LINMIC+/N (AC Microwave) [1] are available. SDA was proposed by Itoh and Mittra in 1973. They applied it to the calculation of dispersion characteristics of microstrip line. This technique is basically a modification of Galerkin's approach adopted for applications in the Fourier transform or spectral domain [45]. In general, the spectral domain analysis is a combination of analytical and numerical techniques. It is very suitable for the solution of boundary value problems in microwave and millimeter wave integrated circuits [46], or the applications where there is interface between air and dielectric [47]; this is why the method is mostly applied to microstrip-like structures. This method is highly effective due to its analytical preprocessing. However this method has certain limitations. It is applicable to very thin layer conductor strips and is not suitable for finite thickness strips. Discontinuity in the substrate of the sideward direction is not permitted. In spite of these limitations, SDA is still one of the most widely used numerical techniques [44].

A7   BEM (Boundary Element Method)

Boundary Element Method is an extension of the Finite Element Method (FEM) and is obtained by applying the finite element method to Boundary Integral Equations (BIE) [48]. In other words, it is a combination of the two methods, FEM and BIE, with the advantages of both methods. It makes possible modeling of arbitrarily curved boundaries with FEM and small mesh volume with BIE [49]. BEM method can deal with inhomogeneous materials in a simple and efficient way [50]. BEM only requires discretization at the boundaries. Therefore, the size of the solution matrix is small compared to the FEM method and can be solved efficiently. Another important advantage of this method is that there is no need to use absorbing boundary conditions because fields at infinite distance are accounted for by using Green's function [50]. The commercial software ELECTRO by Integrated Engineering Software is based on this

method [1]. BEM was also hybridized with other methods such as FEM and BEM [51], and MoM and BEM [52], etc. The main disadvantage of BEM is that the matrix it involved is usually a full matrix.

A8   MM (Mode Matching Method)

This method is used usually when the solution domain structure is divided into two or more regions. Each region has a set of well defined analytical solutions of Maxwell's equations that satisfy all the boundary conditions excluding at the intersections. When the solutions in each region are orthonormal, they are known as normal modes. The main concept of this method can be divided into two steps: Step 1 is the expansion of the unknown fields in the individual region in terms of their respective normal modes and Step 2 is the interface of the regions with continuity conditions [53]. It is appropriate for two and three dimensional structures including scattering and eigenvalue problems. MM is efficient for a structure where modes are known analytically. This method has been used to many structures, comparatively to regular [53] than complex structures. Many new modifications in mode matching method have been made and are underway to increase the efficiency of this method [54-57]. However, there is still need of further research in this method to increase its efficiency.

B)   Time domain methods

Time domain methods are relatively easy to apply to non-linear structures, and provide solutions for a wide spectrum of frequencies. The output of time domain methods is in time domain, and Fourier transform is used to convert it into frequency domain. Time domain methods were not very popular before the 1970's due to heavy calculation requirements, but after the development of high-speed computer technology these methods are becoming more and more popular. A large number of commercial software packages have been developed based on these time domain methods, and are efficient. However, for structures with resonances, the time domain methods take long CPU time.

11

Some of the well known time domain methods are Finite Difference Time Domain (FDTD), Transmission Line Matrix (TLM), Alternating Direction Implicit FDTD (ADI-FDTD), Multiresolution Time Domain (MRTD), Pseudospectral Time Domain (PSTD), Method of Moments Time domain (MoMTD), Finite Element Time Domain method (FEMTD), Complex Envelop (CE-FDTD), and Finite Volume Time Domain (FVTD). They are reviewed in the following sections.

B1   FDTD (Finite Difference Time Domain)

FDTD (Finite Difference Time Domain) method was proposed by Yee in 1966 [2]. Since then Maxwell's equations based FDTD has become one of the most popular time domain methods, and has been applied to almost all kinds of structures [3]. The reason for its popularity is that it deals directly with Maxwell's equations without pre-processing. However, due to the explicit nature of the method, it has the Courant Friedrich Levy (CFL) condition:

$$\Delta t \leq \frac{1}{c\sqrt{\dfrac{1}{\Delta x^2} + \dfrac{1}{\Delta y^2} + \dfrac{1}{\Delta z^2}}}$$

This constraint is a disadvantage because the time step has to be small and within this limit. As a result, CPU time will be large.

There are many commercial software packages available based on this method, such as X-FDTD by Remcom, Concerto by Vector Fields, Microwave Studio 4.0 by Computer Simulation Technology (CST) [1], SEMCAD X by Schmid & Partner Engineering AG [58] and FIDELITY by Zeland Software [59].

There are six main reasons that make the FDTD method popular in industry and academia [4]:

1) FDTD is a well defined method; sources of error have been well studied and can be estimated.

2) FDTD can deal with impulsive behaviors naturally. In other words, FDTD can compute the impulse response of an electromagnetic system with a single simulation run.

3) Due to the explicit nature of FDTD, it does not encounter the difficulties of linear algebra that limits the size of electromagnetics models.

4) FDTD can handle new structures by re-orientation of the mesh instead of the new formulation.

5) FDTD method is becoming more and more CPU-time efficient, thanks to rapidly increasing computer power.

6) FDTD allows visualization of solutions in time domain, a natural way in which physical events occur.

Numerous papers have been written about FDTD. It has been applied to all kinds of problems where electromagnetic fields are present. They include high-speed digital and microwave circuits, electromagnetic effects on the human body, biomedical devices (pacemakers, MRI), radars, heating effects on integrated circuits and food items, microwave filters and amplifiers, optical structures and bio-photonics, cellular telephones, LTTC, MEMS, NEMS and metamaterials.

B2   TLM (Transmission Line Matrix)

TLM method was first proposed by Johns and Beurle in 1971[60]. This method is basically derived from Maxwell's equations using the finite difference approximation [61] and method of moment [62]. It has resemblance to the transmission line network, as can be seen from its name.

In TLM method, the solution domain is divided into grids and nodes of grids are connected with each other through transmission lines. Voltage and current terms are used, instead of electric and magnetic fields, as in the case of FDTD. However, they are analogous. Voltage corresponds to the electric field and current corresponds to the magnetic field. When a current or a voltage impulse is used as a source and incident onto

13

a node, as shown in Fig 1.2, it will be reflected, scattered and transmitted to the neighboring nodes as shown in Fig. 1.3. The transmitted impulses will become the incident impulses to the neighboring nodes.
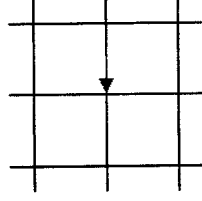
Fig. 1.2 Incident impulse at a node for   Fig. 1.3 Reflected and transmitted impulse
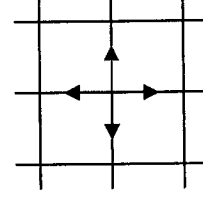
              TLM method   at a node

The impulse scattering and propagation in the TLM mesh can be mathematically represented as:

$$\left[V_k^r\right] = [S]\left[V_k^i\right] \qquad (1.3) \qquad\qquad \left[V_{k+1}^i\right] = [C]\left[V_k^r\right] \qquad (1.4)$$

where $[S]$ and $[C]$ are scattering and connection matrix respectively, V_k^r and V_k^i are the vectors of reflected and incident impulses at the k_{th} time step. It is possible to combine equations (1.3) and (1.4) but it is easy if both are handled separately [1].

In three-dimensional cases, the symmetrical condensed node (SCN) was presented by Johns in 1986 [60] (see Fig. 1.4) and is the most extensively used. The SCN consists of six branches with two transmission lines in each branch. The main advantage of these symmetrical condensed nodes is that all the coupled field components are available at the center of a node as well as at the cell boundaries. In almost all the modern TLM simulators, this node technique is used with some variations.

TLM method is like FDTD and approximately has the same limitations as FDTD. It is not suitable for applications where there are long distances between sources and points of

interest. As well, it takes long simulation times when there is need of fine grids. Both FDTD and TLM can be used for a wide range of applications. Simulation engineers normally chose either FDTD or TLM based on their familiarity with it.

Both methods are effective for nonlinear applications and can run on parallel processing systems. In general case the simulation time for the same size of matrix for both FDTD and TLM is less than those of MoM and FEM [1]. No computer can store unlimited data. To limit the extent of an open structure, absorbing boundary conditions (to act as an infinite region or free space) are also needed for TLM [63]. The MEFiSTO-3D Pro by Faustus Scientific [64] is a well-known TLM-based software available commercially.
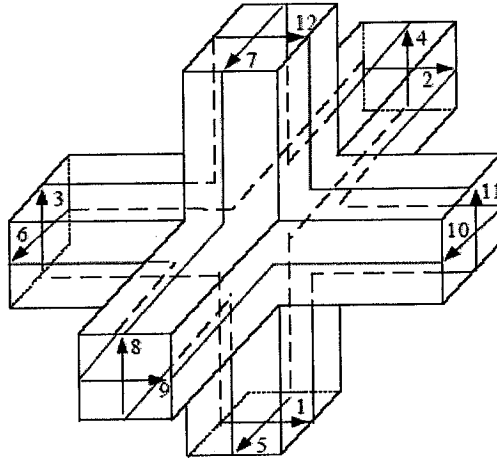
Fig. 1.4 Three - dimensional SCN for TLM method

B3   ADI-FDTD (Alternating Direction Implicit – FDTD)

ADI-FDTD [65-66] is an extended unconditionally stable version of FDTD. Its unconditional stability proof was presented in 2000 by Zheng, Chen and Zhang [66]. This is why that this method is also known as ZCZ algorithm [4]. The CFL-condition is removed with the uses of the ADI scheme. Due to the CFL-free nature of this method,

15

larger time steps can be taken, which reduce the number of iterations and therefore the simulation time. The total number of time steps N_{sim} needed to complete the simulation can be calculated with the following formula [4]:

$$N_{sim} = \frac{T_{sim}}{\Delta t_{max}}$$

where T_{sim} is the simulated time and is related to period T of λ_{min}, Δt_{max} is the time step selected with respect to the CFL limit. This method has been used in many applications including RF/microwave circuits, optical structures, effects of electromagnetic fields on the human body and dispersive material structures. The first EM simulator based on this method is SEMCAD X [67]. One disadvantage of this method is that it takes more simulation memory as compared to FDTD, but overall advantages of this method overcome the disadvantage of memory. The reason is explained in more detail in Chapter 2.

B4   MRTD (Multiresolution Time Domain)

MRTD was introduced by Krumpholz and Katehi [68-69]. This method has the potential to solve the memory problems associated with FDTD by reducing the grid density close to the Nyquist sampling rate. Due to the reduced grid density, MRTD is very efficient for certain types of applications. For example, in the case of 3-D microstrip transmission line analysis, an MRTD method runs seven times faster than FDTD and gets the same results. The foundation of MRTD is dependent on the scaling and wavelet functions and the application of the multiresolution analysis in coincidence with the MoM-based discretization of Maxwell equations. In MRTD, rectangular pulse functions are used for time variation while scaling and wavelet functions are used for spatial variation [70-71]. This method can save considerable computation cost in terms of CPU time and memory. However, this method has the some constraints like the FDTD method:

1)   time steps should follow the CFL limit for stability.

2)   Source and measuring point positions must be selected carefully.

3)   Long simulation time is required for electrically long or high Q-factor structures.

16

4)   Additional Discrete Fourier Transform or FFT is required to get results in frequency domain to convert time domain results.

5)   Boundary conditions are difficult to implement because high- order nature of the scheme.

To circumvent the problem, Chen and Zhang, presented eigen-based spatial-MRTD and ADI-MRTD [72-73]. To retain advantages of both MRTD and ADI-FDTD, Sarris and Katehi presented hybrid technique for both methods [74].

MRTD method has been applied to printed transmission lines, patch antennas, planar structures, multilayer package, waveguide discontinuities, RF MEMS structures, nonlinear circuits, high-frequency active devices and other complex microwave structures.

B5   PSTD (Pseudo Spectral Time Domain)

PSTD was proposed by Liu in 1997 [75]. PSTD like FDTD is also used to solve Maxwell's equation but the difference is that it uses FFT instead of finite difference to represent spatial derivatives. In PSTD [77-79], only two cells per wavelength are needed as compared to 10 cells per wavelength as a rule of thumb for the conventional FDTD. This is due to the higher order nature of Fourier transform. The main drawback in the PSTD is the wraparound effect (late time corruption effect on solution by waves propagating from other periods as the result of FFT periodicity) and boundary condition implementations. The wraparound effect however can be removed by using Perfectly Matched Layer (PML) [76].

PSTD method can also be formulated with non-Fourier form. For instance, Chebyshev PSTD method was proposed in [80]. It has advantages and disadvantages similar to the Fourier PSTD but with π cells per wavelength for homogeneous and smooth varying structures. In the case of inhomogeneous or multidomain structures, multidomain Chebyshev PSTD was developed [81] and has been applied to complex scattering

structures. It requires a bit more computer resources as compared to Fourier based PSTD, due to π cells per wavelength.

PSTD also has the CFL constraint. To remove CFL, CFL-free ADI-PSTD was introduced [82]. ADI-PSTD is more efficient than the PSTD methods, especially with Chebyshev PSTD. Overall, as compared to FDTD, PSTD method is less dispersive and is efficient. The disadvantage is the preprocessing that it requires as well as the boundary condition implementations.

B6   MoMTD (Method of Moment in Time Domain)

MoMTD is another time-domain method for solving electromagnetic problems. In it, Time Domain Integral Equations (TDIEs) are first formulated and then MoM is applied to those equations [83]. This method is an extended form of the MoM that is applied to Frequency Domain Integral Equations (FDIEs). In MoMTD, marching-on-in-time procedure is used to handle the time domain dependencies. This time domain method contains the same kind of advantages and disadvantages over MoM as does time-domain over the frequency domain methods [84]. MoMTD is very good for simulation of thin wire structures because MoMTD is applied to electric field integral equations that are very suitable for thin wire structures like thin wire antenna. MoMTD can also be easily hybridized with other time domain methods; for example it was hybridized with FDTD to improve simulation efficiency [85]. Another hybrid ADI-FDTD/MoMTD technique was also developed and applied for ground penetration radar [86].

B7   FETD (Finite Element Time Domain)

FETD method is also known as Time Domain Finite Element Method (TDFEM). This method introduces the advantages of time domain method into finite element method, which is traditionally a frequency domain method. Initially a time domain algorithm was developed by combining the Finite Element analysis with SPICE capabilities [87]. However, after the development of a new stand alone FETD method, it has become more

18

popular. FETD method is reported to be better than the FDTD based methods as long as the time step convergence to final solution is faster than the conditionally stable FDTD method [88]. In1995, unconditional stable FETD method was presented by Gedney and Navsariwala [89].

For complex structures with curved boundaries, the FETD method is more advantageous than the FDTD method. To get the advantages of both methods in complex structures, hybrid FETD and FDTD method was introduced [90]. This hybrid method was applied to via-hole grounded microstrip; FETD was applied to via-hole for curved boundaries and FDTD to the rest of the plane area.

The FETD method was extended to solve nonlinear microwave circuits [91] in addition to other applications, including PML terminations [92]. A hybrid method that combines FDTD, FETD and MoMTD methods was proposed and applied in [93]. It has the advantages of all three methods; FDTD deals with arbitrary material properties, MoMTD deals with thin wire structure, while FETD accurately models the curved geometries.

B8   FVTD (Finite Volume Time Domain)

The FVTD method deals with the Integral Maxwell's equations instead of the differential ones [94-95]. FVTD equations in integral form are given as:

$$\int_v \frac{\partial \vec{B}}{\partial t} dv = -\oint_s n \times \vec{E} da - \int_v \vec{J}_m dv$$

$$\int_v \frac{\partial \vec{D}}{\partial t} dv = -\oint_s n \times \vec{H} da - \int_v \vec{J}_e dv$$

where v is an arbitrary volume, s is surface enclosing volume v and n is a unit surface normal.

FVTD is effective for non-rectangular structures as compared to stair case solutions with the FDTD method. FVTD, cell size can be selected with respect to the shape of the structure [96].

A major disadvantage with the FVTD method is that it needs larger amounts of information and computational time as compared to the FDTD method. To overcome this problem, a hybrid approach known as FVHG (Finite Volume Hybrid Grid) method was introduced [97-98]. In FVGH, a structure is divided into two types of grids i.e. unstructured grids and rectangular grids. FVTD is used for unstructured grids and FDTD is used for rectangular grids. In this way, the advantages of both methods FDTD and FVTD can be obtained with better results and efficiency than their parent methods.

B9   CE-FDTD (Complex Envelop FDTD)

CE-FDTD is a new technique [99-100]. In the conventional FDTD method, time step is selected with respect to the maximum frequency of the source after the CFL condition is satisfied. In bandpass-limited applications, time step is selected with respect to the bandwidth of the source rather than its maximum frequency as in the conventional FDTD. This allows time step selection considerably larger than the conventional FDTD. The CE-FDTD was developed on such a basis.

The stability and dispersion of the CE-FDTD is presented in [101-102]. It is found that to make the CE-FDTD stable, carrier frequency must be between $\varpi_{th1} < \varpi < \varpi_{th2}$ where ϖ_{th1} and ϖ_{th2} are the lower and upper limits of threshold frequencies. More specifically,

$$\varpi > \varpi_{th1} = 2\sqrt{\left(\frac{c}{\Delta x}\right)^2 + \left(\frac{c}{\Delta y}\right)^2 + \left(\frac{c}{\Delta z}\right)^2 - \left(\frac{1}{\Delta t}\right)^2}$$

$$\varpi > \varpi_{th2} = 2\sqrt{\left(\frac{c}{\Delta x}\right)^2 + \left(\frac{c}{\Delta y}\right)^2 + \left(\frac{c}{\Delta z}\right)^2}$$

It was also stable even above $\varpi > \varpi_{th2}$. It was concluded that when ϖ was in between the set range or above the set range, the algorithm is stable. It was observed that when the

carrier frequency is higher than ϖ_{th1} and even higher than ϖ_{th2}, the system was more efficient and Δt can go up to 104 times of the CFL [102].

In short, CE-FDTD is less accurate than the conventional FDTD but works with larger time steps [102]. Therefore, to obtain some benefits, an implicit technique known as CE-ADI-FDTD was introduced [103]. It was found that this technique was better than the conventional ADI-FDTD method for narrow bandwidth or bandpass electromagnetic applications. With the same time step, CE-ADI-FDTD was less dispersive than ADI-FDTD and more dispersive than the conventional FDTD.

1.3   Motivation of Thesis

The motivation of this thesis is to develop new efficient numerical methods and improvements in the existing ADI-FDTD method. In this efforts hybrid ADI-FDTD/FDTD, Error Reduced ADI-FDTD and dispersion optimized ADI-FDTD methods are presented. A brief explanation is given below on the rationale that these methods are presented.

Since the introduction of FDTD by K.S. Yee in 1966, it has been applied to many applications successfully. However, CFL is the one of the major constraints for its efficiency in computing high Q-factor and electrically large size structures. This constraint increases computation resources for certain applications. To remove this constraint, Zheng, Chen and Zhang proposed a 3D unconditionally stable ADI-FDTD method. They proved the unconditional stability and showed dispersion analysis for this method. This method requires two-step simulation as compared to FDTD, and therefore it takes more memory. On the other hand, it can use a time step larger than the conventional FDTD and saves CPU time. To take advantages of both FDTD and ADI-FDTD methods, a hybrid ADI-FDTD/FDTD method is proposed in this thesis. This proposed method is efficient and effective.

The Crank Nicolson FDTD (CN-FDTD) method is more accurate than the ADI-FDTD method but it takes more computer resources comparatively. The higher accuracy of CN-

21

FDTD method is due to a splitting term that is not present in ADI-FDTD. Consequently, to reduce the splitting error of the conventional ADI-FDTD method and obtain results close to CN-FDTD, new methods known as Error Reduced ADI-FDTD(ER-ADI-FDTD) methods are proposed in this thesis. These methods incorporate the modified splitting error term in order to reduce the splitting errors. They have a formulation pattern like the CN-FDTD method but a simulation pattern like ADI-FDTD method. They improve the accuracy of the ADI-FDTD method to a level comparable to the CN-FDTD method.

The conventional ADI-FDTD method has higher dispersion at larger time steps that reduces its effectiveness of unconditional stability. To reduce this dispersion, DO-ADI-FDTD (Dispersion Optimized ADI-FDTD) methods are presented in this thesis. These DO-ADI-FDTD methods are applied to 1-D, 2-D and 3-D cases and the results show the reductions in errors.

In short, the aim of this thesis is to develop new efficient numerical schemes that can improve the accuracy of the ADI-FDTD method. The details of these techniques are explained in the remaining chapters.

1.4   Scope and Organization of Thesis

This thesis concerns the development of advanced ADI-FDTD based techniques for electromagnetic and microwave modeling. It consists of the following chapters.

Chapter 2 briefly reviews the FDTD method, its stability and dispersion. In addition to this, constraints of the method are explained. This method forms the base for the ADI-FDTD. A brief review of the ADI-FDTD method is then presented. These methods lay the foundation for Hybrid ADI-FDTD/FDTD, error reduced ADI-FDTD and dispersion optimized ADI-FDTD methods proposed in this thesis.

Chapter 3 describes the 2-D hybrid ADI-FDTD/FDTD method. It is applied to different structures for validation and is compared with the conventional FDTD method.

Chapter 4 illustrates the 3-D hybrid ADI-FDTD/FDTD method. It is then compared with the conventional 3-D FDTD method by considering different applications.

Chapter 5 describes error-reduced ADI-FDTD methods as the new extensions of the conventional ADI-FDTD method. These new methods are based on CN- FDTD (Crank Nicolson-FDTD), but their simulation procedure is similar to the conventional ADI-FDTD. After obtaining the formulations for these methods numerical experiments are conducted. Results are obtained and compared with the results obtained from other methods for validations.

In Chapter 6 new techniques to control the dispersion error of the conventional ADI-FDTD method are proposed. A 1-D DO-ADI-FDTD (Dispersion Optimized ADI-FDTD) case is considered and explained first, and then is extended to 2-D and 3-D cases. In all these cases, results are compared with the conventional ADI-FDTD method and explained.

Chapter 7 presents summary of the thesis and directions for future work.

Chapter 2   FDTD and ADI-FDTD Methods

2.1   Introduction

In this chapter a brief review of the Finite Difference Time Domain (FDTD) method and the associated problems are presented. This method forms the basis for the ADI-FDTD and its extended methods. Kane S. Yee presented the FDTD method in 1966 [2]. Since then, many new algorithms have been presented based on it [4]. The FDTD method has been applied to different areas like military defense, medical, high speed communications and computing, agricultural and the food industry [4][104-110].

The FDTD method is derived directly from the Maxwell's differential equations:

$$\nabla \times \vec{H} = \frac{\partial \vec{D}}{\partial t} + \vec{J} \tag{2.1}$$

$$\nabla \times \vec{E} = -\frac{\partial \vec{B}}{\partial t} \tag{2.2}$$

where $\vec{E}$ and $\vec{H}$ are electric and magnetic field intensity, and $\vec{D}$ and $\vec{B}$ are electric and magnetic flux densities respectively. In homogeneous and source free regions, $\vec{J} = 0$. In addition,

$$\vec{D} = \varepsilon \vec{E} \tag{2.3}$$

$$\vec{B} = \mu \vec{H} \tag{2.4}$$

with ε and μ being the constant permittivity and permeability of the medium respectively. Equations (2.3) and (2.4) hold for isotropic, dispersion-free, linear media only. The equations (2.1) and (2.2) are also known as Ampere's circuit law and Faraday's law respectively.

The vector curl equations (2.1) and (2.2), coupled with equations (2.3) and (2.4), can be expanded into a scalar form:

$$\frac{\partial E_x}{\partial t} = \frac{1}{\varepsilon}\left(\frac{\partial H_z}{\partial y} - \frac{\partial H_y}{\partial z}\right) \qquad (2.5)$$

$$\frac{\partial E_y}{\partial t} = \frac{1}{\varepsilon}\left(\frac{\partial H_x}{\partial z} - \frac{\partial H_z}{\partial x}\right) \qquad (2.6)$$

$$\frac{\partial E_z}{\partial t} = \frac{1}{\varepsilon}\left(\frac{\partial H_y}{\partial x} - \frac{\partial H_x}{\partial y}\right) \qquad (2.7)$$

$$\frac{\partial H_x}{\partial t} = \frac{1}{\mu}\left(\frac{\partial E_y}{\partial z} - \frac{\partial E_z}{\partial y}\right) \qquad (2.8)$$

$$\frac{\partial H_y}{\partial t} = \frac{1}{\mu}\left(\frac{\partial E_z}{\partial x} - \frac{\partial E_x}{\partial z}\right) \qquad (2.9)$$

$$\frac{\partial H_z}{\partial t} = \frac{1}{\mu}\left(\frac{\partial E_x}{\partial y} - \frac{\partial E_y}{\partial x}\right) \qquad (2.10)$$

Now for any function F of space and time, denote

$$F\big|_{i,j,k}^{n} = F(x = i\Delta x, y = j\Delta y, z = k\Delta z, t = n\Delta t)$$

where $\Delta x, \Delta y, \Delta z$ are space increments, Δt is the time increment, i, j, k and n are real number or integers.

After applying the second-order accurate central finite difference approximation to the equations (2.5) to (2.10), the resulting equations can be used for programming. For instance equations (2.5) and (2.8) are discretized and have the form:

$$E_x\Big|_{i+\frac{1}{2},j,k}^{n+1} = E_x\Big|_{i+\frac{1}{2},j,k}^{n} + \frac{\Delta t}{\varepsilon}\left[\frac{H_z\Big|_{i+\frac{1}{2},j+\frac{1}{2},k}^{n+\frac{1}{2}} - H_z\Big|_{i+\frac{1}{2},j-\frac{1}{2},k}^{n+\frac{1}{2}}}{\Delta y}\right]$$

$$-\frac{\Delta t}{\varepsilon}\left[\frac{H_y\Big|_{i+\frac{1}{2},j,k+\frac{1}{2}}^{n+\frac{1}{2}} - H_y\Big|_{i+\frac{1}{2},j,k-\frac{1}{2}}^{n+\frac{1}{2}}}{\Delta z}\right] \qquad (2.11)$$

$$H_x\Big|_{i,j+\frac{1}{2},k+\frac{1}{2}}^{n+\frac{1}{2}} = H_x\Big|_{i,j+\frac{1}{2},k+\frac{1}{2}}^{n-\frac{1}{2}} + \frac{\Delta t}{\mu}\left[\frac{E_y\Big|_{i,j+\frac{1}{2},k+1}^{n} - E_y\Big|_{i,j+\frac{1}{2},k}^{n}}{\Delta z}\right]$$

$$-\frac{\Delta t}{\mu}\left[\frac{E_z\Big|_{i,j+1,k+\frac{1}{2}}^{n} - E_z\Big|_{i,j,k+\frac{1}{2}}^{n}}{\Delta y}\right] \qquad (2.12)$$

From equations (2.11) and (2.12) it is apparent that the electric field is obtained with the magnetic field of previous time at four different neighboring locations. The magnetic field can be obtained with the electric field of previous time at four neighboring locations. The grid arrangement for the field components are shown in Fig. 2.1.

2.2   Numerical Stability

FDTD is an explicit method with six electric and magnetic field components at each cell. As an explicit method, it is conditionally stable. The condition for the stability is known as CFL (Courant-Friedrichs-Levy) limit [104]:

$$\Delta t \leq \frac{1}{c\sqrt{\dfrac{1}{\Delta x^2} + \dfrac{1}{\Delta y^2} + \dfrac{1}{\Delta z^2}}}$$

where c is the velocity of light. As can be seen, Δt should always be less than or equal to the above said limit to maintain the stability; otherwise the FDTD algorithm will become

unstable. To keep the above condition fulfilled, space increments should be selected properly, The *CFL* condition is derived under the assumption that μ and ε are constant. Therefore if μ and ε are variables, a precise stability criterion is difficult to obtain [2].
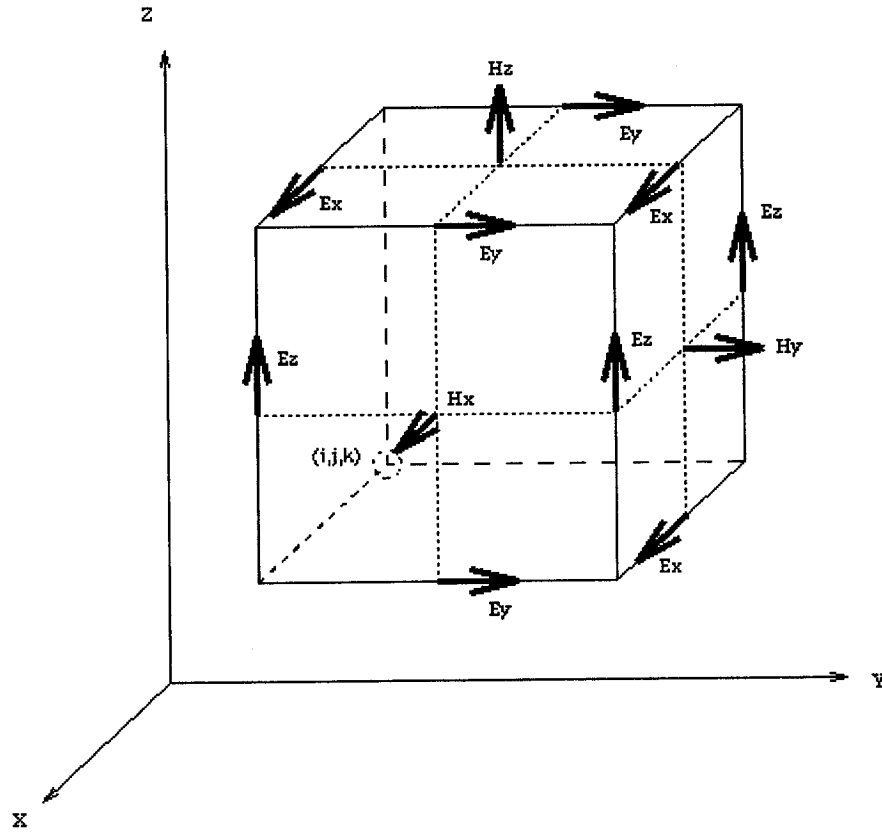
Fig. 2.1 Graphical representation of the FDTD or Yee cell

2.3   Numerical Dispersion

In communication technology, "dispersion" is used to describe any process by which an electromagnetic signal propagating in a physical medium is degraded and dispersed. It is because the various wave components (i.e., frequencies) of the signal have different propagation velocities within the physical medium.

The FDTD algorithm deals with electromagnetic waves propagating in a discretized or discrete space, which exhibit different propagation velocities with different frequencies and with different directions. They cause phase errors and delays. As a result they lead to

non-physical property such as broadening and ringing of a pulsed waveform, imprecise cancellation of multiple scattered waves, anisotropy, and pseudorefraction. The numerical dispersion is a significant feature in the FDTD modeling that must be understood for its accuracy limits, particularly for electrically large geometries [4] [111-113].

For explanatory purposes, in the three-dimensional FDTD case, consider a normalized, lossless region with $\mu=1$, $\varepsilon=1$ and $c=1$. Let $j=\sqrt{-1}$, and the Maxwell's equations in spectral domain [4][104] are:

$$j\nabla \times \vec{V} = \frac{\partial \vec{V}}{\partial t} \tag{2.13}$$

where

$$\vec{V} = \vec{H} + j\vec{E} \text{ and}$$

$$\left. \vec{V} \right|_{i,j,k}^{n} = V_0 e^{j\left(\omega n\Delta t - \tilde{k}_x\, i\Delta x - \tilde{k}_y\, j\Delta y - \tilde{k}_z\, k\Delta z\right)} \tag{2.14}$$

$\tilde{k}_x$, $\tilde{k}_y$, $\tilde{k}_z$ are wavenumber in the x, y and z directions and ω is the angular frequency of the sinusoidal traveling wave. By putting the wave expression (2.14) into equation (2.13) and simplifying the resulting equations, the FDTD dispersion equation is found as:

$$\left(\frac{1}{c\Delta t}\right)^2 \sin^2(\frac{1}{2}\omega\Delta t) = \frac{1}{\Delta x^2}\sin^2(\frac{1}{2}\tilde{k}_x\, \Delta x) + \frac{1}{\Delta y^2}\sin^2(\frac{1}{2}\tilde{k}_y\, \Delta y) + \frac{1}{\Delta z^2}\sin^2(\frac{1}{2}\tilde{k}_z\, \Delta z) \tag{2.15}$$

where $\vec{k}_x = \tilde{k}\cos\phi\sin\theta$, $\vec{k}_y = \tilde{k}\sin\phi\sin\theta$, $\vec{k}_z = \tilde{k}\cos\theta$, θ and ϕ define the propagation directions.

The phase velocity can then be determined by using the formula: $V_p = \dfrac{2\pi f}{\tilde{k}}$

The determined phase velocity V_p can be different from the velocity of light c for varying wavelength, grid discretization and the direction of propagation (i.e. θ and ϕ). In contrast to the numerical dispersion, dispersion relation of a plane wave in a continuous medium is given as:

$$\omega^2 \mu\varepsilon = k_x^2 + k_y^2 + k_z^2 \text{ or } \left(\frac{\omega}{c}\right)^2 = \left(k_x\right)^2 + \left(k_y\right)^2 + \left(k_z\right)^2 \tag{2.16}$$

Equation (2.15) is different from equation (2.16) but it approaches equation (2.16) when Δt, Δx, Δy and Δz tend to zero. To ensure accurate solutions, small cell sizes and time steps need to be taken. The result is large memory and long simulation time.

2.4   Absorbing Boundary Conditions

Like with all other numerical methods, open structures to be simulated need to have open boundaries or absorbing boundary conditions (ABC). Modeling and simulating these open regions properly is very important. This is because improperly selected boundary conditions lead to not only false results but also unstable solutions during simulation. The absorbing boundaries absorb the wave impinging on them and therefore simulate the infinite space. A large number of absorbing boundary conditions have been developed so for, e.g. Mur's ABC [119], Liao's ABC [120], PML (Perfectly matched layer) [121], UPML (Uniaxial PML) [122], CPML (Convolutional PML) [123] and GPML (Generalized PML) [124]. Among them, PML initially proposed by Berenger in 1994 has attracted more attention due to its absorbing efficiency. It features in the matching of the plane waves of arbitrary incidence, polarization and frequency at the boundaries while damping the energy inside the PML region. To obtain the perfectly matched planar interface, loss parameters, that are consistent with a dispersionless medium, are selected. Also a vector field component is divided into two orthogonal components, and therefore

twelve components instead of six in Maxwell's original equations are computed. Each of these twelve components satisfies the coupled set of first order partial differential equations. This concept was also introduced into the second order FDTD scheme [4] by Berenger.

Based on Beregner's PML compact PML were also developed e.g. Uniaxial PML (UPML) and Convolutional PML (CPML). They are advanced versions of PML with a higher computational efficiency than the original PML. In this thesis, CPML is used as an absorbing boundary condition, due to its efficiency as compared to conventional PML. The significance of CPML is that its formulation is independent of the material medium or the host medium. It means that the formulations will remain unchanged for generalized media such as inhomogeneous, dispersive, lossy, anisotropic, or non-linear media. It can also absorb the evanescent waves and also provide memory-savings as compared to the conventional PML.

2.5   ADI-FDTD

To tackle the CFL constraint in the FDTD method, an unconditionally stable FDTD method known as ADI-FDTD was proposed in [6-7]. This method is based on Peaceman –Rachford algorithm [125]. The absorbing boundary conditions used for the FDTD method also can be used for this method.

In the ADI-FDTD method, computations of Maxwell's equations are partitioned into two steps. For example, for E_x component,

$$\frac{\partial E_x}{\partial t} = \frac{1}{\varepsilon}\left(\frac{\partial H_z}{\partial y} - \frac{\partial H_y}{\partial z}\right)$$

(2.17)

The ADI-FDTD computation procedure is as follows:

Step # 1

$$
\frac{E_x\Big|_{i+\frac{1}{2},j,k}^{n+\frac{1}{2}} - E_x\Big|_{i+\frac{1}{2},j,k}^{n}}{\Delta t/2} = \frac{1}{\varepsilon}\left[\frac{H_z\Big|_{i+\frac{1}{2},j+\frac{1}{2},k}^{n+\frac{1}{2}} - H_z\Big|_{i+\frac{1}{2},j-\frac{1}{2},k}^{n+\frac{1}{2}}}{\Delta y} - \frac{H_y\Big|_{i+\frac{1}{2},j,k+\frac{1}{2}}^{n} - H_y\Big|_{i+\frac{1}{2},j,k-\frac{1}{2}}^{n}}{\Delta z}\right] \quad (2.18)
$$

Step # 2

$$
\frac{E_x\Big|_{i+\frac{1}{2},j,k}^{n+1} - E_x\Big|_{i+\frac{1}{2},j,k}^{n+\frac{1}{2}}}{\Delta t/2} = \frac{1}{\varepsilon}\left[\frac{H_z\Big|_{i+\frac{1}{2},j+\frac{1}{2},k}^{n+\frac{1}{2}} - H_z\Big|_{i+\frac{1}{2},j-\frac{1}{2},k}^{n+\frac{1}{2}}}{\Delta y} - \frac{H_y\Big|_{i+\frac{1}{2},j,k+\frac{1}{2}}^{n+1} - H_y\Big|_{i+\frac{1}{2},j,k-\frac{1}{2}}^{n+1}}{\Delta z}\right] \quad (2.19)
$$

This way of formulations gives unconditionally stable results. Its stability and dispersion calculations are like that of the FDTD method, but are unconditionally stable [126]. Although this method is unconditionally stable, it takes more memory and has larger dispersions at larger time steps. In the next chapters, to handle the disadvantage of both FDTD and ADI-FDTD methods and to obtain their advantages, hybrid FDTD/ADI-FDTD, error reduced ADI-FDTD and dispersion-optimized ADI-FDTD methods are proposed and described in detail.

2.6   Conclusion

This chapter presents a brief review of FDTD and ADI-FDTD. It is necessary to understand the methods proposed in the succeeding chapters. Methods presented in the following chapters solve the constraints associated with these methods.

Chapter 3   Two Dimensional Hybrid ADI-FDTD and FDTD Method

3.1   Introduction

Since the FDTD algorithm developed by Yee [2], it has been applied successfully to a broad range of problems [3]. Nevertheless, its computational efficiency is limited by its two inherent physical constraints: the numerical dispersion and the Courant-Friedrich-Levy (CFL) stability condition. The first condition demands small spatial discretization steps and the second condition small time steps. These conditions lead to large computation memory and CPU time requirements for electrically large structures. The first condition has been improved with the development of high-order schemes, such as the Multi-Resolution Time-Domain (MRTD) method [70] and the Pseudo-Spectral Time-Domain (PSTD) techniques [127]. The second condition has been removed with the recent development of the unconditionally stable alternating direction implicit finite-difference time-domain (ADI-FDTD) method [6][7].

The problem of large memory and long CPU time arises particularly in FDTD applications when a structure that contains electrically small geometric features, including sharp conducting edges, is modeled. To have the highest possible computational efficiency, efficient techniques have been proposed that incorporate *a priori* knowledge of the field behaviors near these fine structures into the FDTD algorithms with little increase of computational expenditures [128-129]. However, they require the field behaviors to be known and analytical processing to be done beforehand. Alternatively, the so-called subgridding schemes [130] can be used (see Fig. 3.1). In these subgridding schemes, fine numerical grids or meshes are applied to solution regions surrounding the fine geometric features where strong field variations occur. In the rest of the solution domain, coarse grids or meshes are still used in order to minimize the memory usage. A scheme is required to interface the fine grid and the coarse grid, both in space and in time, since the fine grids possess different spatial and temporal properties and conditions.

32

Fine mesh ← ··· → Coarse mesh
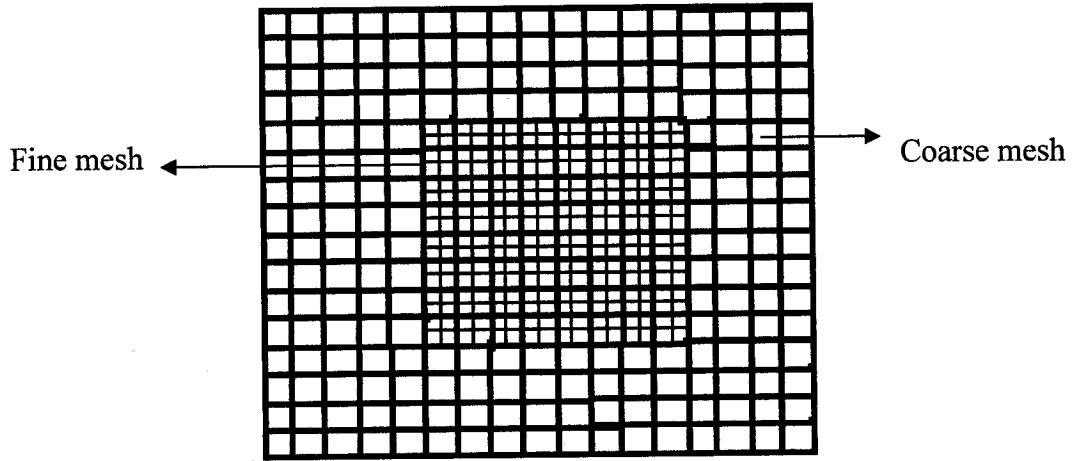
Fig. 3.1 An example of a subgridded scheme

In the subgridding scheme based purely on the conventional FDTD [130-131], one of the critical issues is to interface the two grids in time. In a fine grid, the time step has to be small, as stipulated by the CFL condition due to the fine grid cell sizes. However, in the coarse grid, the time step can be much larger. The result is that the two grids are simulated with two different time steps, or they simply are not synchronized. Consequently, a very carefully designed scheme is needed to interface the two grids, not only in space, but also in time where they are joined. Past experience has proven that unless the small time step for the fine grid is also applied to the coarse grid, an interfacing scheme often leads to instability or an overly complicated technique, which may still have a late-time stability problem [132].

In this chapter, a hybrid technique that combines FDTD and ADI-FDTD methods for subgridding is proposed to circumvent the problem. The solution domain is divided into coarse grid regions and fine subgridded regions whenever necessary. The conventional FDTD grid is then applied to the coarse grid regions, while the ADI-FDTD is used in the finely subgridded regions. Because of the unconditional stability of the ADI-FDTD, a large time step can then be taken for the fine grids. In other words, the same uniform time step can now be used in both the coarse and the fine grid regions across the whole solution domain. One of the immediate benefits is that an interfacing scheme needs only to be developed in space, but not in time. The other advantage is that such a scheme

minimizes the memory requirements since the relatively memory-expensive ADI-FDTD is applied only in the fine-grid regions that need it. In comparison with subgridding schemes using solely the conventional FDTD, the hybrid method allows for the use of a much larger time step and therefore reduces the CPU time. In comparison between the subgridding scheme using purely ADI-FDTD schemes, the hybrid method minimizes the use of the memory because the conventional FDTD algorithm is applied to the coarse mesh region.

In the following sections, the hybrid subgridding scheme is introduced for 2D case. Numerical validations of the proposed hybrid method and conclusions are also presented at the end of this chapter.

3.2   The 2-D Hybrid Method

To illustrate the proposed scheme clearly, consider the two-dimensional case. Without loss of generality, Fig 3.2 shows a typical interface at $x=0$ between a coarse grid region ($x<0$) and a dense grid region ($x>0$).
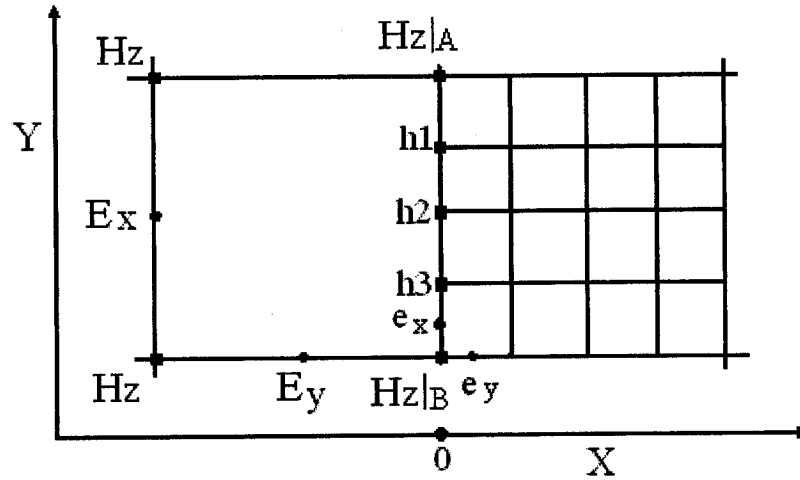
Fig. 3.2 Interface between coarse and fine mesh

For simplicity, a TE-to-z mode is considered. The related Maxwell's equations are:

34

$$\frac{\partial E_x}{\partial t} = \frac{1}{\varepsilon}\left(\frac{\partial H_z}{\partial y}\right)$$

(3.1)

$$\frac{\partial E_y}{\partial t} = -\frac{1}{\varepsilon}\left(\frac{\partial H_z}{\partial x}\right)$$

(3.2)

$$\frac{\partial H_z}{\partial t} = \frac{1}{\mu}\left(\frac{\partial E_x}{\partial y} - \frac{\partial E_y}{\partial x}\right)$$

(3.3)

The conventional FDTD method is now applied to the coarse grid for $x<0$ while the ADI-FDTD method is used in the dense grid region for $x>0$.

The corresponding FDTD equations applied to the $x<0$ region are:

$$E_x\Big|_{i+\frac{1}{2},j}^{n+1} = E_x\Big|_{i+\frac{1}{2},j}^{n} + \frac{\Delta t}{\varepsilon}\left[\frac{H_z\Big|_{i+\frac{1}{2},j+\frac{1}{2}}^{n+\frac{1}{2}} - H_z\Big|_{i+\frac{1}{2},j-\frac{1}{2}}^{n+\frac{1}{2}}}{\Delta y}\right]$$

(3.4)

$$E_y\Big|_{i,j+\frac{1}{2}}^{n+1} = E_y\Big|_{i,j+\frac{1}{2}}^{n} - \frac{\Delta t}{\varepsilon}\left[\frac{H_z\Big|_{i+\frac{1}{2},j+\frac{1}{2}}^{n+\frac{1}{2}} - H_z\Big|_{i-\frac{1}{2},j+\frac{1}{2}}^{n+\frac{1}{2}}}{\Delta x}\right]$$

(3.5)

$$H_z\Big|_{i+\frac{1}{2},j+\frac{1}{2}}^{n+\frac{1}{2}} = H_z\Big|_{i+\frac{1}{2},j+\frac{1}{2}}^{n-\frac{1}{2}} + \frac{\Delta t}{\mu}\left[\frac{E_x\Big|_{i+\frac{1}{2},j+1}^{n} - E_x\Big|_{i+\frac{1}{2},j}^{n}}{\Delta y}\right] - \frac{\Delta t}{\mu}\left[\frac{E_y\Big|_{i+1,j+\frac{1}{2}}^{n} - E_y\Big|_{i,j+\frac{1}{2}}^{n}}{\Delta x}\right]$$

(3.6)

where n indicates the nth time step, and i and j correspond to the position ($x=i\Delta x, y=j\Delta y$). Δx and Δy are the space increments in the x and y directions in the coarse grid region ($x<0$).

The corresponding ADI-FDTD equations applied to the $x>0$ region are:

$$E_x\Big|_{i+\frac{1}{2},j}^{n+1} = E_x\Big|_{i+\frac{1}{2},j}^{n} + \frac{\Delta t}{\varepsilon}\left[\frac{H_z\Big|_{i+\frac{1}{2},j+\frac{1}{2}}^{n+1} - H_z\Big|_{i+\frac{1}{2},j-\frac{1}{2}}^{n+1}}{\Delta y'}\right]$$

(3.7)

$$E_y\Big|_{i,j+\frac{1}{2}}^{n+1} = E_y\Big|_{i,j+\frac{1}{2}}^{n} - \frac{\Delta t}{\varepsilon}\left[\frac{H_z\Big|_{i+\frac{1}{2},j+\frac{1}{2}}^{n} - H_z\Big|_{i-\frac{1}{2},j+\frac{1}{2}}^{n}}{\Delta x'}\right] \tag{3.8}$$

$$H_z\Big|_{i+\frac{1}{2},j+\frac{1}{2}}^{n+1} = H_z\Big|_{i+\frac{1}{2},j+\frac{1}{2}}^{n} + \frac{\Delta t}{\mu}\left[\frac{E_x\Big|_{i+\frac{1}{2},j+1}^{n+1} - E_x\Big|_{i+\frac{1}{2},j}^{n+1}}{\Delta y'} - \frac{E_y\Big|_{i+1,j+\frac{1}{2}}^{n} - E_y\Big|_{i,j+\frac{1}{2}}^{n}}{\Delta x'}\right] \tag{3.9}$$

for the first sub-step, and

$$E_x\Big|_{i+\frac{1}{2},j}^{n+2} = E_x\Big|_{i+\frac{1}{2},j}^{n+1} + \frac{\Delta t}{\varepsilon}\left[\frac{H_z\Big|_{i+\frac{1}{2},j+\frac{1}{2}}^{n+1} - H_z\Big|_{i+\frac{1}{2},j-\frac{1}{2}}^{n+1}}{\Delta y'}\right] \tag{3.10}$$

$$E_y\Big|_{i,j+\frac{1}{2}}^{n+2} = E_y\Big|_{i,j+\frac{1}{2}}^{n+1} - \frac{\Delta t}{\varepsilon}\left[\frac{H_z\Big|_{i+\frac{1}{2},j+\frac{1}{2}}^{n+2} - H_z\Big|_{i-\frac{1}{2},j+\frac{1}{2}}^{n+2}}{\Delta x'}\right] \tag{3.11}$$

$$H_z\Big|_{i+\frac{1}{2},j+\frac{1}{2}}^{n+2} = H_z\Big|_{i+\frac{1}{2},j+\frac{1}{2}}^{n+1} + \frac{\Delta t}{\mu}\left[\frac{E_x\Big|_{i+\frac{1}{2},j+1}^{n+1} - E_x\Big|_{i+\frac{1}{2},j}^{n+1}}{\Delta y'} - \frac{E_y\Big|_{i+1,j+\frac{1}{2}}^{n+2} - E_y\Big|_{i,j+\frac{1}{2}}^{n+2}}{\Delta x'}\right] \tag{3.12}$$

for the second sub-step.

Note that in the ADI-FDTD equations (3.7)-(3.12), $\Delta x'$ and $\Delta y'$ are the space increments in the x and y directions in the dense grid region ($x>0$). They are different from the space increments, Δx and Δy of equations (3.4)-(3.6), in the coarse grid region ($x<0$).

In order to synchronize the simulations between the FDTD and the ADI-FDTD, the time step Δt taken for the ADI-FDTD is the same as for the conventional FDTD. Thus, one single full ADI-FDTD iteration amounts to two FDTD iterations. However the time step is same for both methods, which is Δt. In doing so, the interpolation of the fields at the interface ($x=0$) between the FDTD and ADI-FDTD grids needs to be carried out only in space. An example is shown in Fig 3.2, where the field quantity to be interpolated

36

between the dense and coarse grids is H_z. A simple linear interpolation scheme is employed. More specifically, the in-between values of H_z, denoted as h_1, h_2 and h_3, can be obtained as follows:

$$h_1 = \frac{3}{4} H_z|_A + \frac{1}{4} H_z|_B$$ (3.13)

$$h_2 = \frac{1}{2} H_z|_A + \frac{1}{2} H_z|_B$$ (3.14)

$$h_3 = \frac{1}{4} H_z|_A + \frac{3}{4} H_z|_B$$ (3.15)

Note that in Fig 3.2, it is assumed that the dense grid is four times denser than the coarse grid, or mesh ratio is four. For a general ratio of m, the above equation can be easily written as:

$$h_l = \frac{m-l}{m} H_z|_A + \frac{l}{m} H_z|_B$$ (3.16)

where $h_l, l = 1,2,...,m-1$, are the field values to be interpolated in between points A and B.

It should be pointed out here that the relatively large time-step applied in the dense grid will not cause unacceptable numerical dispersion errors as long as the time step does not cause unacceptable errors in the coarse grid. This occurs because the ADI-FDTD and FDTD present similar dispersion errors if their time and spatial step sizes are comparable [126]. In our case, the ADI-FDTD actually has a smaller grid size than the FDTD. Therefore, the numerical dispersion error in the dense grid should not be larger than the coarse grid.

3.3   Numerical Validations

The hybrid scheme described above is first applied to a two-dimensional finned waveguide and to an insulated fin line. Since these structures were also solved in [133-

134] with the other techniques, comparisons and validations of the proposed scheme can be made. The finned waveguide computed in our study has dimensions a = 2b = 64mm. The cross section is shown in Fig. 3.3. Because of the symmetry of the structure, only one-quarter of the waveguide needs to be modeled (as shown in Fig 3.4), where M and E represent magnetic and electric walls respectively. The fin length considered is equal to b/4. Because of the expected rapid changes of the fields around the fin, a dense mesh is applied in the vicinity of the fin. The ratio of the coarse grid cell size to the fine grid cell size was set to four.
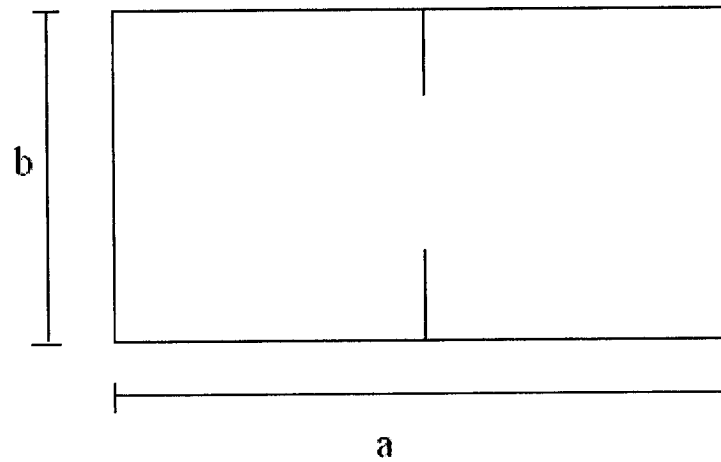
Fig. 3.3 Cross section of the finned waveguide
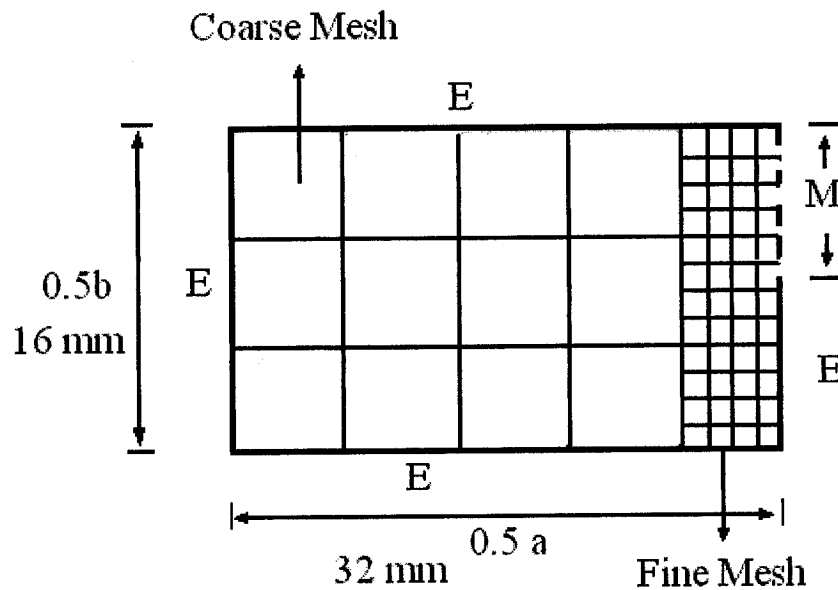
Fig. 3.4 One quarter of Fig 3.3

As described earlier the ADI-FDTD is applied in the fine grid region and the conventional FDTD is applied in the coarse grid region. The following relationships between the dense and coarse grid sizes were chosen:

$$\Delta x^{\prime} = \frac{\Delta x}{4}$$

and

$$\Delta y^{\prime} = \frac{\Delta y}{4}$$

Three different cell sizes $\Delta x^{\prime} = \Delta y^{\prime} = \Delta l = 0.5mm, 0.25mm,$ and $0.125mm$ were computed with $\Delta t = \frac{2\Delta l}{c}$, where $c = 3 \times 10^{8} m/s$ is the speed of light in the vacuum. For reference purposes, a separate pure FDTD simulation was also run with a uniform grid whose cell size was equal to the dense grid cell size of the hybrid method. The reason for taking a uniformly fine FDTD grid is that the FDTD can achieve a level of accuracy similar to that of the proposed method as shown below. The comparison made under such a condition can then be deemed fair.

Table 3.1 shows the computer resources used by the proposed hybrid method. For comparison, Table 3.2 shows the computer resources used by the pure FDTD method. In both cases, the computer used is a Dell XPS T600 with 600 MHz CPU and 256MB of RAM.

Table 3.1 Computer resources used by the hybrid method
for the finned waveguide

Size of fine mesh cell (mm)	Normalized cut-off frequency obtained	Time for simulation (Seconds)	Memory used by program
.5	0.2241	2	632K
.25	0.2263	13	708K
.125	0.2271	99	992K

Table 3.2 Computer resources used by the conventional FDTD

for the finned waveguide

Size of fine mesh cell (mm)	Normalized cut-off frequency obtained	Time for simulation (Seconds)	Memory used by program
.5	0.2249	3	688K
.25	0.2267	20	936K
.125	0.2273	313	1912K

Figures 3.5, 3.6 and 3.7 are the graphical representations of Tables 3.1 and 3.2. Fig. 3.5 shows that the proposed hybrid method is slightly less accurate than the conventional FDTD due to the dispersion problem. For both methods, however, the smaller the cell size, the more accurate the results. Both methods converge to the same solution, as the cell size tends to zero. When the cell size will be very small, i.e. approaches zero, both methods will converge to the same point and give the analytical solution value; this value then can be used as a reference to measure the error for both methods. Figs. 3.6 and 3.7 indicate that the proposed hybrid method takes less CPU time and memory than the FDTD.
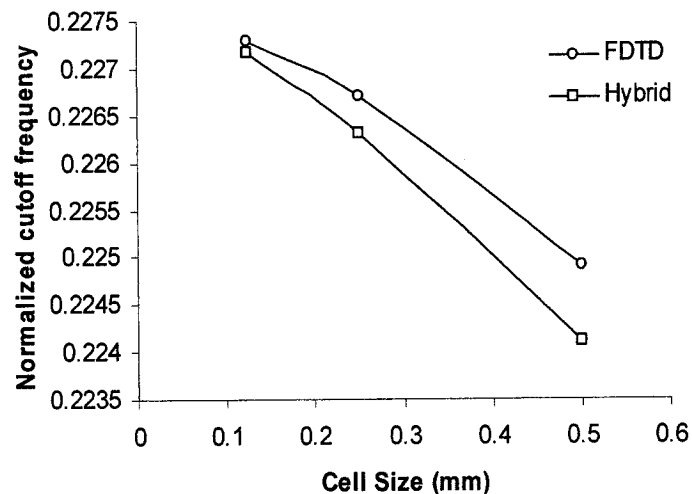
Fig. 3.5 Normalized cut-off frequencies obtained vs. cell size
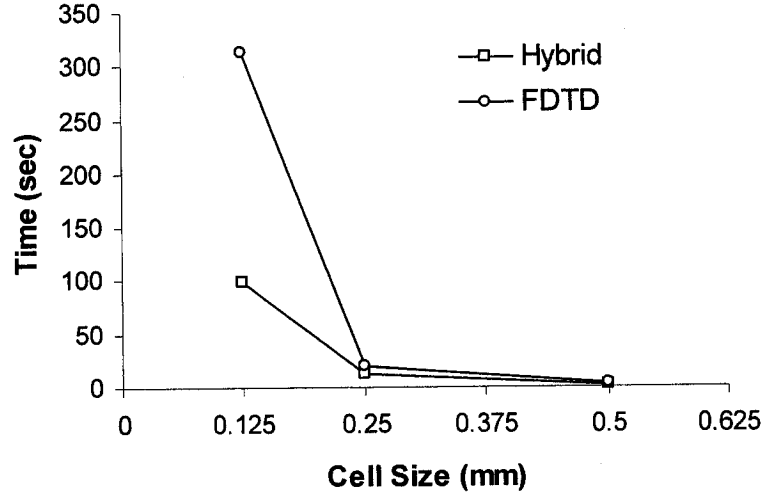
Fig. 3.6 Computation time vs. cell size
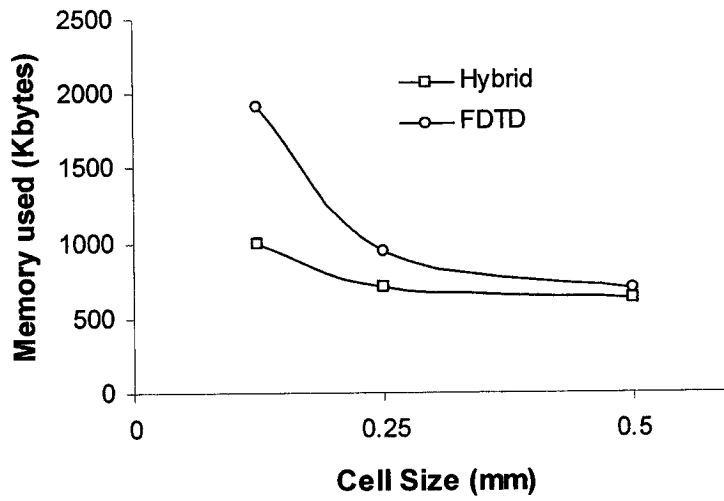
Fig. 3.7 Computer memory used vs. cell size

More specifically, when a fine cell size of $0.125mm$ is used, the proposed method uses about half the memory required by the FDTD, whereas the CPU time is about one third of that used by the FDTD. As a result, we conclude that the proposed hybrid method is superior to the pure FDTD method when a fine grid is required.

Another two-dimensional structure that was simulated with the hybrid method was an insulated fin line structure. Its geometry was the same as that of the finned waveguide except for the addition of insulation having permittivity of 2.2 around the fin (Fig. 3.8). Again, for reference, a separate FDTD was computed with a uniform grid whose cell size is equal to the dense grid cell size of the hybrid method. In the simulations with the hybrid method, the coarse grid cell size, $\Delta x = \Delta y$, was fixed at 1mm, while the fine grid cell size, $\Delta x' = \Delta y'$, was varied from 1 mm to $0.25mm$. The simulation results are shown in Fig. 3.9. These results indicate the differences in cutoff frequencies computed with both the hybrid method and the FDTD method for increasing insulation width. As can be seen, differences between the two methods are small and decrease as the width increases. In the above simulation, the ADI-FDTD fine grid regions occupy only a small portion of the whole solution domain. Consequently, the saving in memory is obvious. In the subsequent experiments, we intentionally increased the areas of the dense grid regions and examined the associated computer resources used.
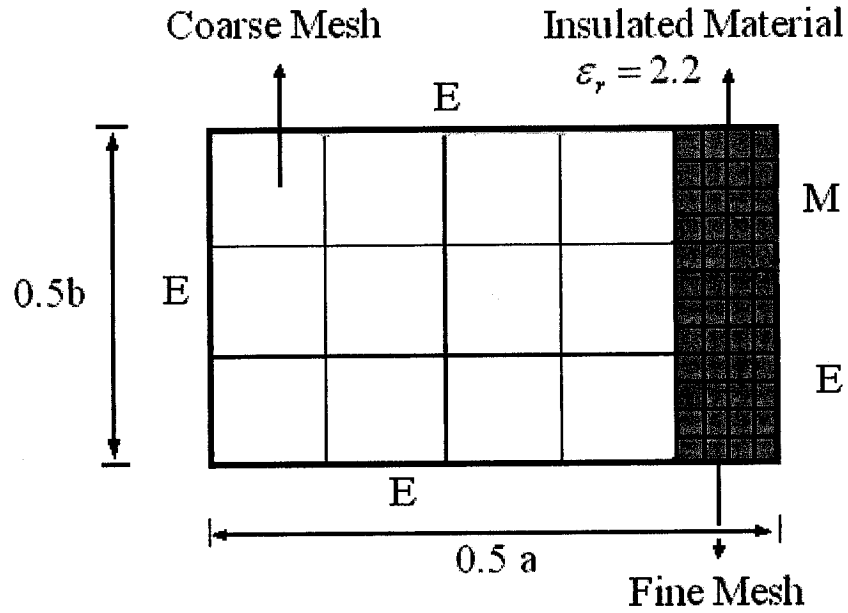
Fig. 3.8 One quarter of Fig 3.3 with insulation in fine mesh area
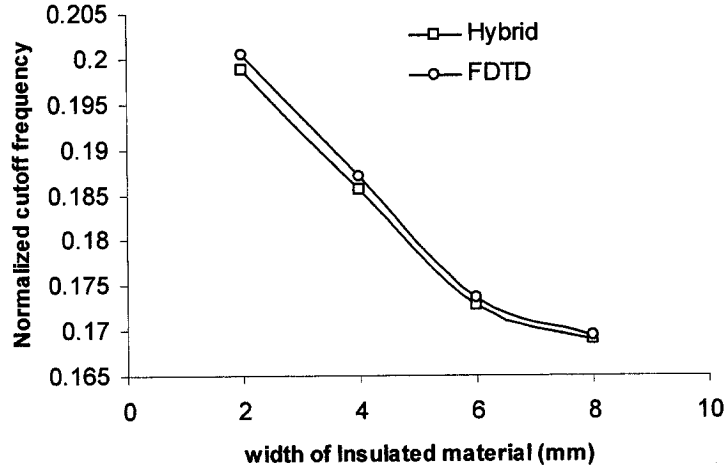
Fig. 3.9 Normalized cut-off frequencies obtained vs. width of insulator material

Figure 3.10 shows a cavity that is 50% filled with a FDTD grid and the rest 50% filled with an ADI-FDTD grid. The cavity size was $16mm$ x $8mm$. The coarse grid cell size was fixed at $1mm$ while the dense grid cell size was varied with different ratios of coarse to dense grid cell sizes.

Fig. 3.11 shows the relative errors when different cell size ratios are used. To measure the relative error analytical frequency was used as a reference. Fig. 3.12 presents memory used by the hybrid method and the FDTD method versus grid size ratios. Fig. 3.13 presents the CPU time used by the two methods with different grid size ratios.

As seen, it is observed that as the cell size ratio increases the errors decrease, memory used by the hybrid method is slightly higher than that required by the FDTD also. When the dense ADI-FDTD grid occupies 50% of the solution domain, the memory used by the hybrid method starts to be larger than that used by the FDTD alone. This is due to the fact that the ADI-FDTD method computes more components than the FDTD method. Although the hybrid method starts to use more memory, the CPU time required by the proposed hybrid method is still less than that of the FDTD, especially in the case of large grid size ratios.

Coarse mesh
(FDTD)

Fine mesh
(ADI-FDTD)

Grid size ratio 1:2

Coarse mesh
(FDTD)

Fine mesh
(ADI-FDTD)

Grid size ratio 1:3

44
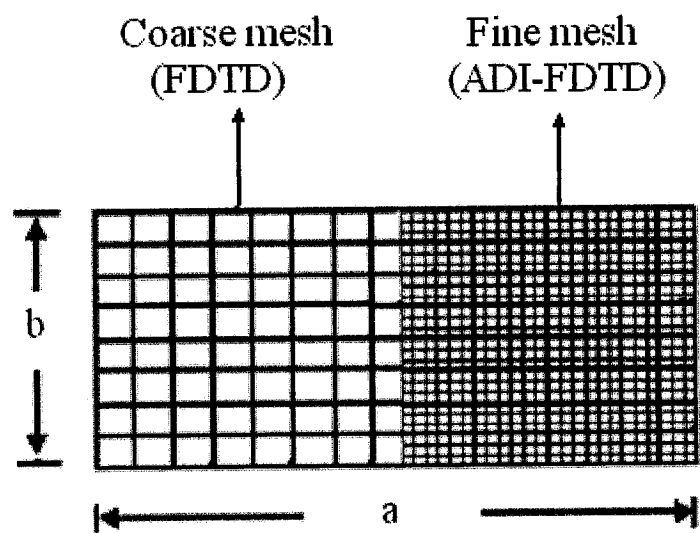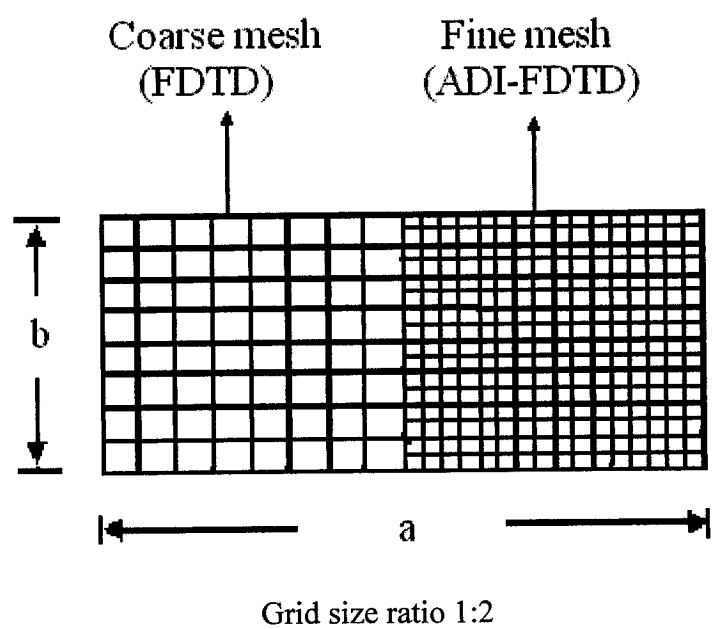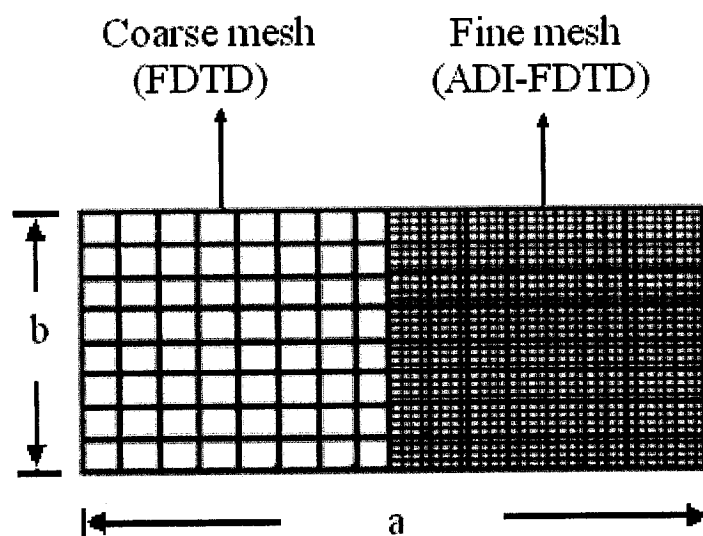
Grid size ratio 1:4

Fig. 3.10 Layout of the grids for cavity with different cell ratio
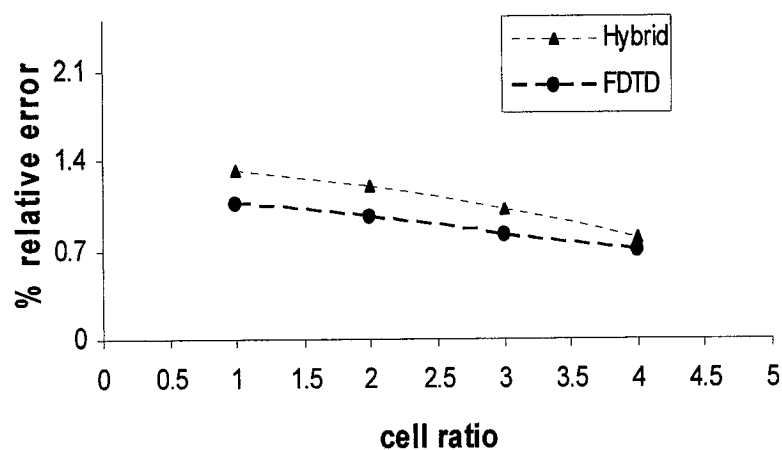
Fig. 3.11 Error vs. grid size ratio for cavity with different cell ratio
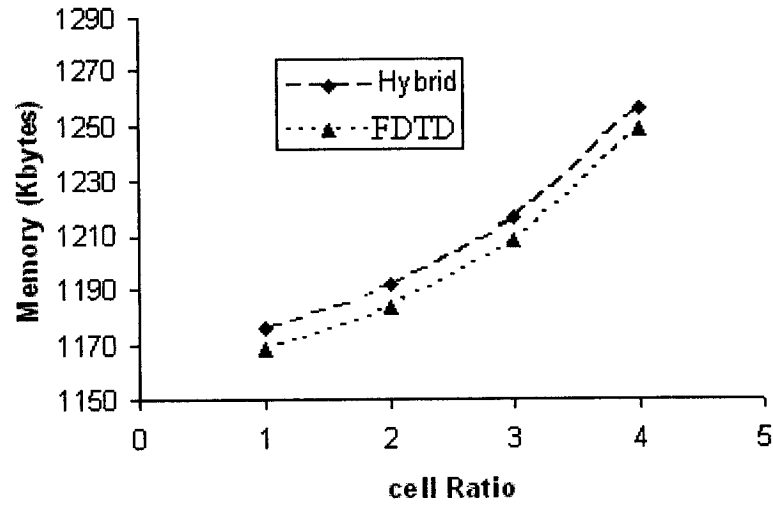
Fig. 3.12 Memory used vs. grid size ratio for cavity with different cell ratio
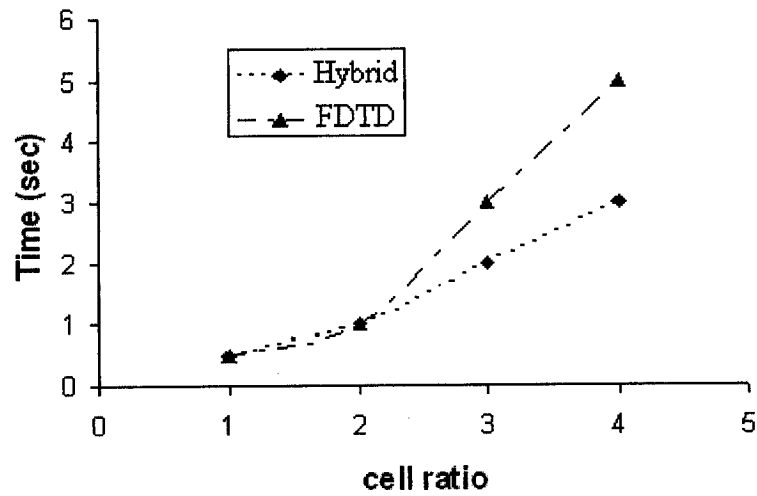
Fig. 3.13 Computation time vs. grid size ratio for cavity with different cell ratio

In all, it is concluded that the proposed hybrid method is effective and efficient for numerical subgridding, provided subgridding regions do not occupy a large portion of the solution domain. In the 2D case, they should not exceed 50% of the domain.

3.4   Conclusions

In this chapter, a hybrid scheme is presented that allows the interfacing of conventional FDTD grids and ADI-FDTD grids. Consequently, a solution domain that is divided into locally coarse and locally dense mesh regions can now be computed more efficiently; FDTD is applied in the coarse grid regions and ADI-FDTD is employed in the dense grid regions. In this way, the time step can be made uniform across the whole solution domain while the CPU and memory requirements are kept to a minimum. It is observed from the numerical experiments that the hybrid method is particularly effective when a fine mesh is required for regions surrounding fine geometrical features such as sharp conducting edges. Approximately the same solution accuracy can be obtained with less time and memory resources than with the conventional FDTD using a uniformly fine mesh. It is also observed that the hybrid method is valid for 2D applications. Finally, it is noted that special care needs to be taken in order to achieve better efficiency with the proposed hybrid method: the dense ADI-FDTD region should not occupy a large portion of the whole solution domain.

Chapter 4   Three Dimensional Hybrid FDTD and ADI-FDTD Method

4.1   Introduction

The finite-difference time-domain (FDTD) method has been used in many fields since it was firstly reported [1-4]. To make it more efficient, hybrid schemes have been proposed in the past. Those were aimed at taking advantage of the methods that are efficient with different conditions. For instance, the FDTD method has been interfaced with many other methods such as TLM that has less numerical dispersion and MoM that is effective for modeling open regions [135-136]. In this chapter, to save memory and computation time, a three dimensional hybrid FDTD and ADI-FDTD technique is proposed. In it, the ADI-FDTD is applied to fine mesh and the FDTD to coarse mesh. A subgridding interface is then developed and the associated interpolation is applied in space domain only. This technique is efficient for the applications in which there is need of fine subgrids. It leads to savings in memory and computation time.

Usually for applications where fine meshes are applied, the FDTD method requires long simulation time due to the small time step stipulated by the FDTD inherent CFL stability condition. To tackle this problem, the unconditionally stable ADI-FDTD method can be applied since it does not have the CFL stability condition. However, the ADI-FDTD normally requires more memory than the FDTD method. Therefore, it will be efficient not to apply the ADI-FDTD but the FDTD to wherever fine meshes are not needed. This leads to a subgridding scheme where an interfacing algorithm is needed to connect the FDTD-applied coarse mesh and the ADI-FDTD-applied fine mesh. In such a way, advantages of both FDTD and ADI-FDTD methods are utilized and the uses of the computation resources are optimized.

In this chapter, the FDTD method is hybridized with the recently developed ADI-FDTD method [6-7]. The ADI-FDTD is an implicit technique while the FDTD is an explicit one. Therefore, the proposed method hybridizes an explicit method with an implicit method. The 2-D hybrid method was described in the previous chapter. In this chapter, it is

extended to the 3-D. This chapter is divided into the following sections: development of 3-D hybrid technique, numerical experiments with RF/microwave, optical, and planar structures, and conclusions are presented at the end.

4.2   The 3-D Hybrid Technique

A typical interface between the ADI-FDTD fine mesh and the FDTD coarse mesh is illustrated in Fig 4.1. The mesh ratio of 1:2 is taken simply for clear illustration purpose. Equations for the 3-D FDTD and ADI-FDTD used for interfacing are given as:

FDTD equations

$$
E_x\Big|_{i+\frac{1}{2},j,k}^{n+1} = E_x\Big|_{i+\frac{1}{2},j,k}^{n} + \frac{\Delta t}{\varepsilon}\left[\frac{H_z\Big|_{i+\frac{1}{2},j+\frac{1}{2},k}^{n+\frac{1}{2}} - H_z\Big|_{i+\frac{1}{2},j-\frac{1}{2},k}^{n+\frac{1}{2}}}{\Delta y}\right]
$$

$$
- \frac{\Delta t}{\varepsilon}\left[\frac{H_y\Big|_{i+\frac{1}{2},j,k+\frac{1}{2}}^{n+\frac{1}{2}} - H_y\Big|_{i+\frac{1}{2},j,k-\frac{1}{2}}^{n+\frac{1}{2}}}{\Delta z}\right] \tag{4.1a}
$$

$$
E_y\Big|_{i,j+\frac{1}{2},k}^{n+1} = E_y\Big|_{i,j+\frac{1}{2},k}^{n} + \frac{\Delta t}{\varepsilon}\left[\frac{H_x\Big|_{i,j+\frac{1}{2},k+\frac{1}{2}}^{n+\frac{1}{2}} - H_x\Big|_{i,j+\frac{1}{2},k-\frac{1}{2}}^{n+\frac{1}{2}}}{\Delta z}\right]
$$

$$
- \frac{\Delta t}{\varepsilon}\left[\frac{H_z\Big|_{i+\frac{1}{2},j+\frac{1}{2},k}^{n+\frac{1}{2}} - H_z\Big|_{i-\frac{1}{2},j+\frac{1}{2},k}^{n+\frac{1}{2}}}{\Delta x}\right] \tag{4.1b}
$$

$$
E_z\Big|_{i,j,k+\frac{1}{2}}^{n+1} = E_z\Big|_{i,j,k+\frac{1}{2}}^{n} + \frac{\Delta t}{\varepsilon}\left[\frac{H_y\Big|_{i+\frac{1}{2},j,k+\frac{1}{2}}^{n+\frac{1}{2}} - H_y\Big|_{i-\frac{1}{2},j,k+\frac{1}{2}}^{n+\frac{1}{2}}}{\Delta x}\right]
$$

$$
- \frac{\Delta t}{\varepsilon}\left[\frac{H_x\Big|_{i,j+1/2,k+\frac{1}{2}}^{n+\frac{1}{2}} - H_x\Big|_{i,j-\frac{1}{2},k+\frac{1}{2}}^{n+\frac{1}{2}}}{\Delta y}\right] \tag{4.1c}
$$

$$H_x\Big|_{i,j+\frac{1}{2},k+\frac{1}{2}}^{n+\frac{1}{2}} = H_x\Big|_{i,j+\frac{1}{2},k+\frac{1}{2}}^{n-\frac{1}{2}} + \frac{\Delta t}{\mu}\left[\frac{E_y\Big|_{i,j+\frac{1}{2},k+1}^{n} - E_y\Big|_{i,j+\frac{1}{2},k}^{n}}{\Delta z}\right]$$

$$-\frac{\Delta t}{\mu}\left[\frac{E_z\Big|_{i,j+1,k+\frac{1}{2}}^{n} - E_z\Big|_{i+\frac{1}{2},j,k+\frac{1}{2}}^{n}}{\Delta y}\right] \tag{4.1d}$$

$$H_y\Big|_{i+\frac{1}{2},j,k+\frac{1}{2}}^{n+\frac{1}{2}} = H_y\Big|_{i+\frac{1}{2},j,k+\frac{1}{2}}^{n-\frac{1}{2}} + \frac{\Delta t}{\mu}\left[\frac{E_z\Big|_{i+1,j,k+\frac{1}{2}}^{n} - E_z\Big|_{i,j,k+\frac{1}{2}}^{n}}{\Delta x}\right]$$

$$-\frac{\Delta t}{\mu}\left[\frac{E_x\Big|_{i+\frac{1}{2},j,k+1}^{n} - E_x\Big|_{i+\frac{1}{2},j,k}^{n}}{\Delta z}\right] \tag{4.1e}$$

$$H_z\Big|_{i+\frac{1}{2},j+\frac{1}{2},k}^{n+\frac{1}{2}} = H_z\Big|_{i+\frac{1}{2},j+\frac{1}{2},k}^{n-\frac{1}{2}} + \frac{\Delta t}{\mu}\left[\frac{E_x\Big|_{i+\frac{1}{2},j+1,k}^{n} - E_x\Big|_{i+\frac{1}{2},j,k}^{n}}{\Delta y}\right]$$

$$-\frac{\Delta t}{\mu}\left[\frac{E_y\Big|_{i+1,j+\frac{1}{2},k}^{n} - E_y\Big|_{i,j+\frac{1}{2},k}^{n}}{\Delta x}\right] \tag{4.1f}$$

ADI FDTD

Here are the equations for 3D ADI-FDTD method [7]:

Step 1

$$\frac{E_x\Big|_{i+\frac{1}{2},j,k}^{n+\frac{1}{2}} - E_x\Big|_{i+\frac{1}{2},j,k}^{n}}{\Delta t/2}$$

$$= \frac{1}{\varepsilon}\left[\frac{H_z\Big|_{i+\frac{1}{2},j+\frac{1}{2},k}^{n+\frac{1}{2}} - H_z\Big|_{i+\frac{1}{2},j-\frac{1}{2},k}^{n+\frac{1}{2}}}{\Delta y} - \frac{H_y\Big|_{i+\frac{1}{2},j,k+\frac{1}{2}}^{n} - H_y\Big|_{i+\frac{1}{2},j,k-\frac{1}{2}}^{n}}{\Delta z}\right] \tag{4.2a}$$

50

$$\frac{E_y\big|_{i,j+\frac{1}{2},k}^{n+\frac{1}{2}} - E_y\big|_{i,j+\frac{1}{2},k}^{n}}{\Delta t / 2}$$

$$= \frac{1}{\varepsilon}\left[\frac{H_x\big|_{i,j+\frac{1}{2},k+\frac{1}{2}}^{n+\frac{1}{2}} - H_x\big|_{i,j+\frac{1}{2},k-\frac{1}{2}}^{n+\frac{1}{2}}}{\Delta z} - \frac{H_z\big|_{i+\frac{1}{2},j+\frac{1}{2},k}^{n} - H_z\big|_{i-\frac{1}{2},j+\frac{1}{2},k}^{n}}{\Delta x}\right]$$

(4.2b)

$$\frac{E_z\big|_{i,j,k+\frac{1}{2}}^{n+\frac{1}{2}} - E_z\big|_{i,j,k+\frac{1}{2}}^{n}}{\Delta t / 2}$$

$$= \frac{1}{\varepsilon}\left[\frac{H_y\big|_{i+\frac{1}{2},j,k+\frac{1}{2}}^{n+\frac{1}{2}} - H_y\big|_{i-\frac{1}{2},j,k+\frac{1}{2}}^{n+\frac{1}{2}}}{\Delta x} - \frac{H_x\big|_{i,j+\frac{1}{2},k+\frac{1}{2}}^{n} - H_x\big|_{i,j-\frac{1}{2},k+\frac{1}{2}}^{n}}{\Delta y}\right]$$

(4.2c)

$$\frac{H_x\big|_{i,j+\frac{1}{2},k+\frac{1}{2}}^{n+\frac{1}{2}} - H_x\big|_{i,j+\frac{1}{2},k+\frac{1}{2}}^{n}}{\Delta t / 2}$$

$$= \frac{1}{\mu}\left[\frac{E_y\big|_{i,j+\frac{1}{2},k+1}^{n+\frac{1}{2}} - E_y\big|_{i,j+\frac{1}{2},k}^{n+\frac{1}{2}}}{\Delta z} - \frac{E_z\big|_{i,j+1,k+\frac{1}{2}}^{n} - E_z\big|_{i,j,k+\frac{1}{2}}^{n}}{\Delta y}\right]$$

(4.2d)

$$\frac{H_y\big|_{i+\frac{1}{2},j,k+\frac{1}{2}}^{n+\frac{1}{2}} - H_y\big|_{i+\frac{1}{2},j,k+\frac{1}{2}}^{n}}{\Delta t / 2}$$

$$= \frac{1}{\mu}\left[\frac{E_z\big|_{i+1,j,k+\frac{1}{2}}^{n+\frac{1}{2}} - E_z\big|_{i,j,k+\frac{1}{2}}^{n+\frac{1}{2}}}{\Delta x} - \frac{E_x\big|_{i+\frac{1}{2},j,k+1}^{n} - E_x\big|_{i+\frac{1}{2},j,k}^{n}}{\Delta z}\right]$$

(4.2e)

$$\frac{H_z\big|_{i+\frac{1}{2},j+\frac{1}{2},k}^{n+\frac{1}{2}} - H_z\big|_{i+\frac{1}{2},j+\frac{1}{2},k}^{n}}{\Delta t / 2}$$

$$= \frac{1}{\mu}\left[\frac{E_x\big|_{i+\frac{1}{2},j+1,k}^{n+\frac{1}{2}} - E_x\big|_{i+\frac{1}{2},j,k}^{n+\frac{1}{2}}}{\Delta y} - \frac{E_y\big|_{i+1,j+\frac{1}{2},k}^{n} - E_y\big|_{i,j+\frac{1}{2},k}^{n}}{\Delta x}\right]$$

(4.2f)

<u>Step 2</u>

$$\frac{E_x\big|_{i+\frac{1}{2},j,k}^{n+1} - E_x\big|_{i+\frac{1}{2},j,k}^{n+\frac{1}{2}}}{\Delta t / 2}$$

$$= \frac{1}{\varepsilon}\left[\frac{H_z\big|_{i+\frac{1}{2},j+\frac{1}{2},k}^{n+\frac{1}{2}} - H_z\big|_{i+\frac{1}{2},j-\frac{1}{2},k}^{n+\frac{1}{2}}}{\Delta y} - \frac{H_y\big|_{i+\frac{1}{2},j,k+\frac{1}{2}}^{n+1} - H_y\big|_{i+\frac{1}{2},j,k-\frac{1}{2}}^{n+1}}{\Delta z}\right]$$

(4.3a)

$$\frac{E_y\big|_{i,j+\frac{1}{2},k}^{n+1} - E_y\big|_{i,j+\frac{1}{2},k}^{n+\frac{1}{2}}}{\Delta t / 2}$$

$$= \frac{1}{\varepsilon}\left[\frac{H_x\big|_{i,j+\frac{1}{2},k+\frac{1}{2}}^{n+\frac{1}{2}} - H_x\big|_{i,j+\frac{1}{2},k-\frac{1}{2}}^{n+\frac{1}{2}}}{\Delta z} - \frac{H_z\big|_{i+\frac{1}{2},j+\frac{1}{2},k}^{n+1} - H_z\big|_{i-\frac{1}{2},j+\frac{1}{2},k}^{n+1}}{\Delta x}\right]$$

(4.3b)

$$\frac{E_z\big|_{i,j,k+\frac{1}{2}}^{n+1} - E_z\big|_{i,j,k+\frac{1}{2}}^{n+\frac{1}{2}}}{\Delta t / 2}$$

$$= \frac{1}{\varepsilon}\left[\frac{H_y\big|_{i+\frac{1}{2},j,k+\frac{1}{2}}^{n+\frac{1}{2}} - H_y\big|_{i-\frac{1}{2},j,k+\frac{1}{2}}^{n+\frac{1}{2}}}{\Delta x} - \frac{H_x\big|_{i,j+\frac{1}{2},k+\frac{1}{2}}^{n+1} - H_x\big|_{i,j-\frac{1}{2},k+\frac{1}{2}}^{n+1}}{\Delta y}\right]$$

(4.3c)

$$\frac{H_x\big|_{i,j+\frac{1}{2},k+\frac{1}{2}}^{n+1} - H_x\big|_{i,j+\frac{1}{2},k+\frac{1}{2}}^{n+\frac{1}{2}}}{\Delta t / 2}$$

$$= \frac{1}{\mu}\left[\frac{E_y\big|_{i,j+\frac{1}{2},k+1}^{n+\frac{1}{2}} - E_y\big|_{i,j+\frac{1}{2},k}^{n+\frac{1}{2}}}{\Delta z} - \frac{E_z\big|_{i,j+1,k+\frac{1}{2}}^{n+1} - E_z\big|_{i,j,k+\frac{1}{2}}^{n+1}}{\Delta y}\right]$$

(4.3d)

$$\frac{H_y \Big|_{i+\frac{1}{2},j,k+\frac{1}{2}}^{n+1} - H_y \Big|_{i+\frac{1}{2},j,k+\frac{1}{2}}^{n+\frac{1}{2}}}{\Delta t / 2}$$

$$= \frac{1}{\mu}\left[\frac{E_z \Big|_{i+1,j,k+\frac{1}{2}}^{n+\frac{1}{2}} - E_z \Big|_{i,j,k+\frac{1}{2}}^{n+\frac{1}{2}}}{\Delta x} - \frac{E_x \Big|_{i+\frac{1}{2},j,k+1}^{n+1} - E_x \Big|_{i+\frac{1}{2},j,k}^{n+1}}{\Delta z} \right]$$

(4.3e)

$$\frac{H_z \Big|_{i+\frac{1}{2},j+\frac{1}{2},k}^{n+1} - H_z \Big|_{i+\frac{1}{2},j+\frac{1}{2},k}^{n+\frac{1}{2}}}{\Delta t / 2}$$

$$= \frac{1}{\mu}\left[\frac{E_x \Big|_{i+\frac{1}{2},j+1,k}^{n+\frac{1}{2}} - E_x \Big|_{i+\frac{1}{2},j,k}^{n+\frac{1}{2}}}{\Delta y} - \frac{E_y \Big|_{i+1,j+\frac{1}{2},k}^{n+1} - E_y \Big|_{i,j+\frac{1}{2},k}^{n+1}}{\Delta x} \right]$$

(4.3f)

It is difficult to handle equations (4.2) and (4.3) directly because both sides of the equations contain the unknown E and H components. To handle this problem, these equations are re-arranged and decoupled. After decoupling and simplifications, one of the equations (here equation 4.2a) is given below:

$$-\left(\frac{\Delta t^2}{4\mu\varepsilon\Delta y^2}\right)E_x \Big|_{i+\frac{1}{2},j+1,k}^{n+\frac{1}{2}} + \left(1 + \frac{\Delta t^2}{2\mu\varepsilon\Delta y^2}\right)E_x \Big|_{i+\frac{1}{2},j,k}^{n+\frac{1}{2}} - \left(\frac{\Delta t^2}{4\mu\varepsilon\Delta y^2}\right)E_x \Big|_{i+\frac{1}{2},j-1,k}^{n+\frac{1}{2}}$$

$$= E_x \Big|_{i+\frac{1}{2},j,k}^{n} - \frac{\Delta t^2}{4\mu\varepsilon\Delta y\Delta x}\left(E_y \Big|_{i+1,j+\frac{1}{2},k}^{n} - E_y \Big|_{i,j+\frac{1}{2},k}^{n} - E_y \Big|_{i+1,j-\frac{1}{2},k}^{n} + E_y \Big|_{i,j-\frac{1}{2},k}^{n} \right)$$

$$+ \frac{\Delta t}{2\varepsilon\Delta y}\left(H_z \Big|_{i+\frac{1}{2},j+\frac{1}{2},k}^{n} - H_z \Big|_{i+\frac{1}{2},j-\frac{1}{2},k}^{n} \right) - \frac{\Delta t}{2\varepsilon\Delta z}\left(H_y \Big|_{i+\frac{1}{2},j,k+\frac{1}{2}}^{n} - H_y \Big|_{i+\frac{1}{2},j,k-\frac{1}{2}}^{n} \right)$$

This equation contains the tridiagonal matrix on the left hand side, and can be solved easily.

A similar procedure can be applied to all other electric field components. There is no need to decouple magnetic field components because after calculating values of electric fields these can be put into a magnetic field component equation to find the magnetic field. In other words a tridiagonal matrix is applied to electric fields only.

53

To interface these methods for three dimensional cases, interpolation is used at the interface of FDTD and ADI-FDTD methods or at the interface of the coarse and fine meshes (as illustrated in Fig 4.1). Because the time step taken with the ADI-FDTD can be made the same as that with the FDTD meshes, simple linear interpolation can be applied. This interpolation procedure is an extension of the interface of the 2-D hybrid method. In other words, if the mesh ratio is an integer, the interpolation equation shown below can be used:

$$h_l = \frac{m-l}{m} H_z \mid_A + \frac{l}{m} H_z \mid_B$$

where $h_l, l = 1,2,...,m-1$, are the field values to be interpolated at the mid points in between two points A and B. For example in the case of Fig. 4.1, only h_1 is the value to be found at the middle point of A and B for H filed, as the mesh ratio is 1:2, or $m = 2$. Similarly the boundary values for E fields at interface used by the ADI-FDTD can be obtained from FDTD by interpolation.
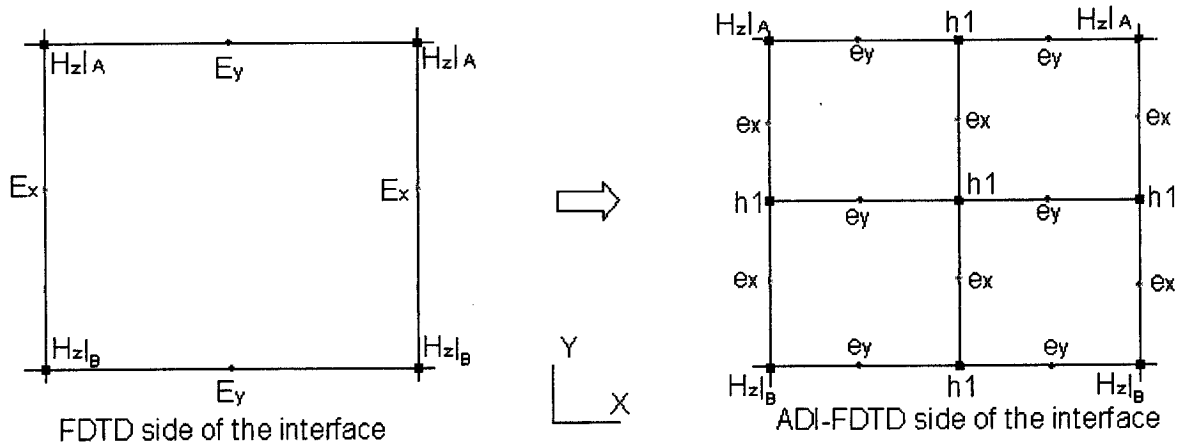
Fig. 4.1(a) Interface between the FDTD and ADI-FDTD mesh for one surface
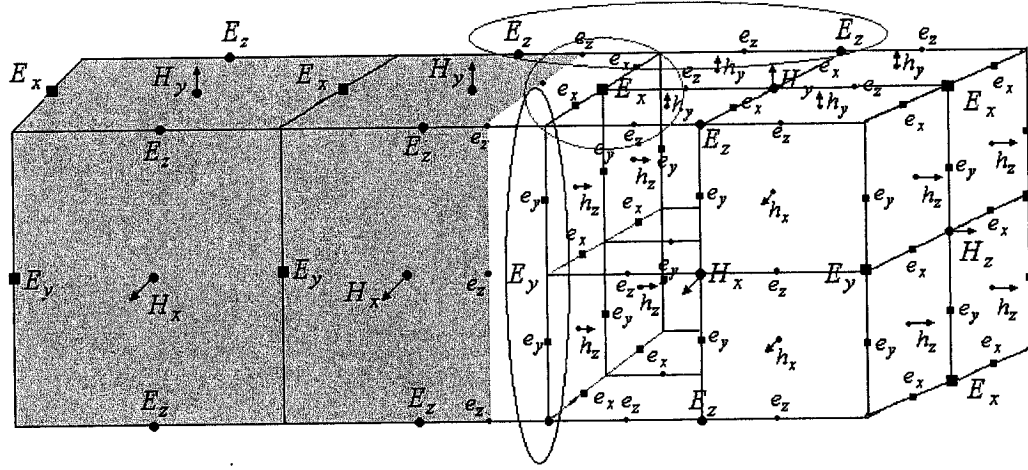
Fig. 4.1(b) Interface between the FDTD and ADI-FDTD mesh for three sides

Fig. 4.1 Interface between the FDTD and ADI-FDTD mesh

4.3   Numerical Experiments

In this sections 3-D hybrid approach is applied to RF/microwave, optical and planar structures.

4.3.1   RF/microwave Structures

For validation purpose, the 3-D hybrid technique was applied to four applications in RF/microwave range: a homogenous cavity, an inhomogeneous cavity, a waveguide with capacitive iris of zero thickness [138-139], and a waveguide with inductive iris of zero thickness [139-140]. In the first application, a homogeneous cavity with dimensions of 8*mm* x 8*mm* x 8*mm* was computed since an analytical solution was readily available. One-half of the cavity was filled with the coarse FDTD grid, while the other half was filled with the dense ADI-FDTD grid. The results are shown in Table 4.1 (for a grid size ratio of 1:2 and a coarse grid cell size (FDTD) of 0.333*mm*). It can be observed that the error of the hybrid method is below 0.88%. This indicates that the proposed hybrid method is also effective in the three dimensional case.

Table 4.1 Computed and analytical results for the homogeneous cavity

Modes	Analytical frequency (GHz)	Computed frequency Hybrid method (GHz)	% Relative Error
TM110	26.51	26.58	0.26
TM210	41.93	42.30	0.88
TM220	53.30	53.10	-0.37
TM320	67.60	67.50	-0.15
TM330	79.55	79.20	-0.44

In the second application an inhomogeneous cavity consisted of two halves, the first half filled with air and the second filled with dielectric material of permittivity 64. The dimensions used were $1m$ x $2m$ x $1.5m$. The FDTD was applied in the air filled region and ADI-FDTD in the dielectric region; the cell size used for the FDTD was 0.1m and for the ADI–FDTD 0.05m. Results obtained for cavity are shown in Table 4.2. From this, it can be observed that the hybrid technique presents solutions very close to those of the analytical and the FDTD results. The differences are less than 1% (FDTD results were obtained with a uniform mesh whose cell size was equal to the fine mesh cell size of the hybrid method).

Table 4.2 Results and relative error for inhomogeneous cavity

Analytical frequency(MHz)	Computed frequency with FDTD	Computed frequency with Hybrid method	%Relative error with FDTD	%Relative error with Hybrid method
18.63	18.61	18.60	0.11	0.16
27.17	27.12	27.30	0.19	-0.48
32.88	32.67	32.70	0.64	0.54

In the third application, a waveguide with capacitive iris was considered as shown in Fig

4.2. The waveguide has a cross section of 7*mm* x 3.5*mm* and the gap *d* between the two irises is 2.75*mm*. CPML absorbing boundary conditions were applied to both ends of the waveguide with 10 CPML layers. As shown in Fig. 4.3, the denser ADI-FDTD mesh is applied to the area around the iris, while the coarser FDTD mesh is applied to the rest of the region. The cell size used for FDTD was 0.5*mm* and the cell size for ADI-FDTD was
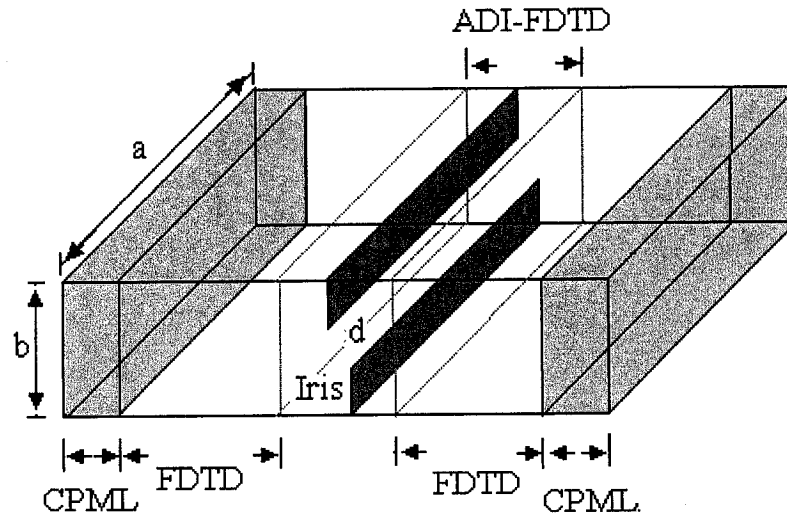
Fig. 4.2 Waveguide with the capacitive iris
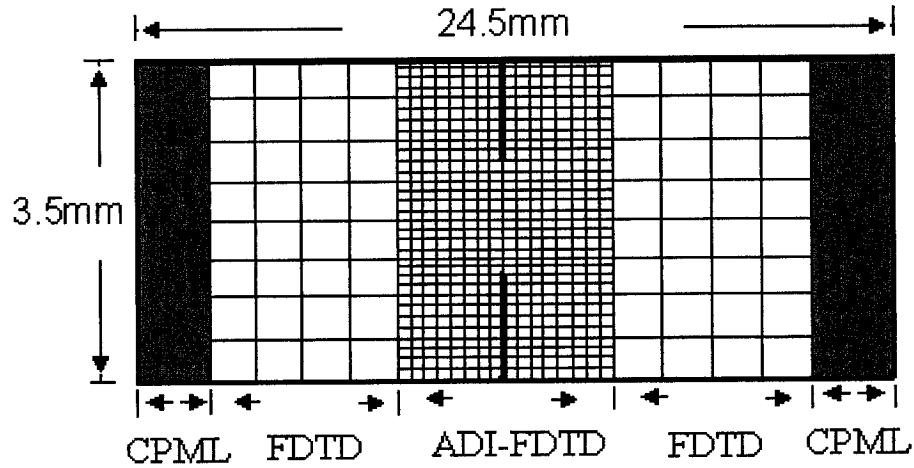
Fig. 4.3 Side view of capacitive iris waveguide with subgridding ratio 1:4

varied and taken as 0.25mm, 0.166mm and 0.125mm, respectively. They amount to the mesh ratios of 1:2, 1:3 and 1:4, respectively.

The CPML formulations used are given as follows:

$$\frac{\partial E_x}{\partial t} = \frac{1}{\varepsilon_0}\left(\frac{\partial H_z}{\partial y} - \frac{\partial H_y}{\partial z}\right)$$

$$E_x\Big|_{i+\frac{1}{2},j,k}^{n+1} = E_x\Big|_{i+\frac{1}{2},j,k}^{n} + \frac{\Delta t}{\varepsilon_0}\left[\frac{H_z\Big|_{i+\frac{1}{2},j+\frac{1}{2},k}^{n+\frac{1}{2}} - H_z\Big|_{i+\frac{1}{2},j-\frac{1}{2},k}^{n+\frac{1}{2}}}{K_y\Delta y} - \frac{H_y\Big|_{i+\frac{1}{2},j,k+\frac{1}{2}}^{n+\frac{1}{2}} - H_y\Big|_{i+\frac{1}{2},j,k-\frac{1}{2}}^{n+\frac{1}{2}}}{K_z\Delta z}\right]$$
$$+ \Psi_{exy}\Big|_{i+\frac{1}{2},j,k}^{n+\frac{1}{2}} - \Psi_{exz}\Big|_{i+\frac{1}{2},j,k}^{n+\frac{1}{2}} \tag{4.4a}$$

$$\Psi_{exy}\Big|_{i+\frac{1}{2},j,k}^{n+\frac{1}{2}} = b_y \Psi_{exy}\Big|_{i+\frac{1}{2},j,k}^{n-\frac{1}{2}} + a_y\left(\frac{H_z\Big|_{i+\frac{1}{2},j+\frac{1}{2},k}^{n+\frac{1}{2}} - H_z\Big|_{i+\frac{1}{2},j-\frac{1}{2},k}^{n+\frac{1}{2}}}{K_y\Delta y}\right) \tag{4.4b}$$

$$\Psi_{exz}\Big|_{i+\frac{1}{2},j,k}^{n+\frac{1}{2}} = b_z \Psi_{exz}\Big|_{i+\frac{1}{2},j,k}^{n-\frac{1}{2}} + a_z\left(\frac{H_y\Big|_{i+\frac{1}{2},j,k+\frac{1}{2}}^{n+\frac{1}{2}} - H_y\Big|_{i+\frac{1}{2},j,k-\frac{1}{2}}^{n+\frac{1}{2}}}{K_z\Delta z}\right) \tag{4.4c}$$

where

$$b_i = e^{-\left(\frac{\sigma_i}{k_i}+\alpha_i\right)\frac{\Delta t}{\varepsilon_o}} \tag{4.4d}$$

$$a_i = \frac{\sigma_i}{\left(\sigma_i k_i + k_i^2 \alpha_i\right)}\left(e^{-\left(\frac{\sigma_i}{k_i}+\alpha_i\right)\frac{\Delta t}{\varepsilon_o}} - 1\right) \tag{4.4e}$$

In above equations $i = x$ or y or z , $\alpha_i = 0.08$, $k_i = 15$, and $\sigma_i = \sigma_{opt} = \dfrac{m+1}{150\pi\sqrt{\varepsilon_r}\Delta l}\Big|_{m=4}$

$\Delta l (= \Delta x = \Delta y = \Delta z)$ is the cell size of the FDTD mesh. Note that only one equation is given above for FDTD CPML; other equations have the similar forms and can be found in [142-143]. The beauty of the CPML is that it is independent of the host medium, i.e. the same formulations can be used for all media either lossy or lossless. It is also more efficient than the conventional PML. This is the reason that it has been adopted for our proposed method.

In the fourth application, the waveguide with an inductive iris (shown in Fig.4.4) was considered. The dimensions were also the same as those used in the second application except the gap was now 4.95*mm*. The subgridding parameters used were also the same as those used in the second application. Table 4.3 shows the memory and computation time used for the waveguide with capacitive iris. The computation time and the memory used by the inductive iris case (the fourth application) are the same as for the capacitive iris case (the third application) because the dimensions are the same as in the capacitive iris case. For comparison purpose, the FDTD of a uniform mesh was also used to compute the structures. The cell size of the FDTD mesh was equal to the fine ADI-FDTD cell size of the hybrid method. For notation purposes, we denote the FDTD results with the mesh ratio number of the corresponding hybrid method. For instance, FDTD 1:4 means that the FDTD cell size is taken the same as that of the dense cell size used in the hybrid method with mesh ratio of 1:4. As seen from Table 4.3, the CPU time used by the hybrid method is less than half of that used by the FDTD, while the memory used is also less than that used by the FDTD method. Figs. 4.5 and 4.6 show the computed reflection coefficients S11 obtained for the capacitive and inductive iris cases. As can be seen, the hybrid method presents results that are of similar accuracy to that of the FDTD but with less memory and CPU time.

ADI-FDTD

a

b

d

FDTD

CPML   Iris   FDTD   CPML
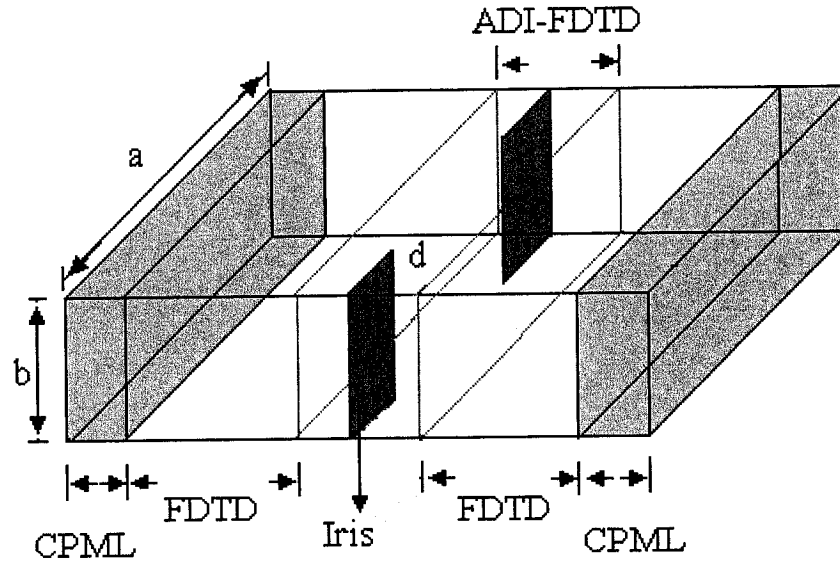
Fig. 4.4 Waveguide with the inductive iris

Table 4.3 Computer resources used for FDTD and Hybrid method for different mesh ratio

Ratio	FDTD Memory (Kbytes)	FDTD Time (Sec)	Hybrid Memory (Kbytes)	Hybrid Time (Sec)
1:2	8640	55	6136	19
1:3	25428	369	10868	151
1:4	57524	1639	20176	732

60
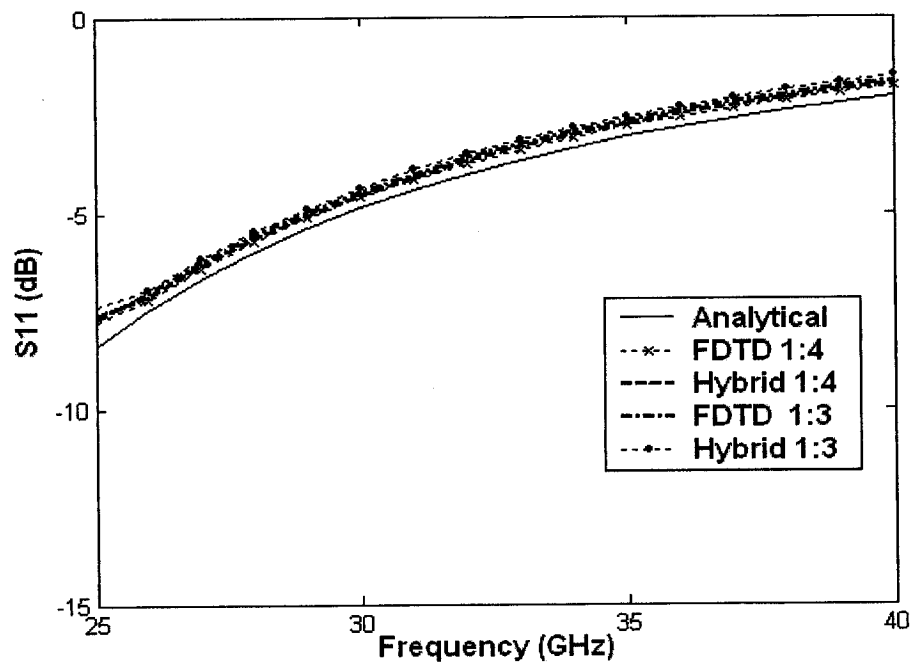
Fig. 4.5 Reflection coefficient S11 vs. frequency for waveguide
with the capacitive iris
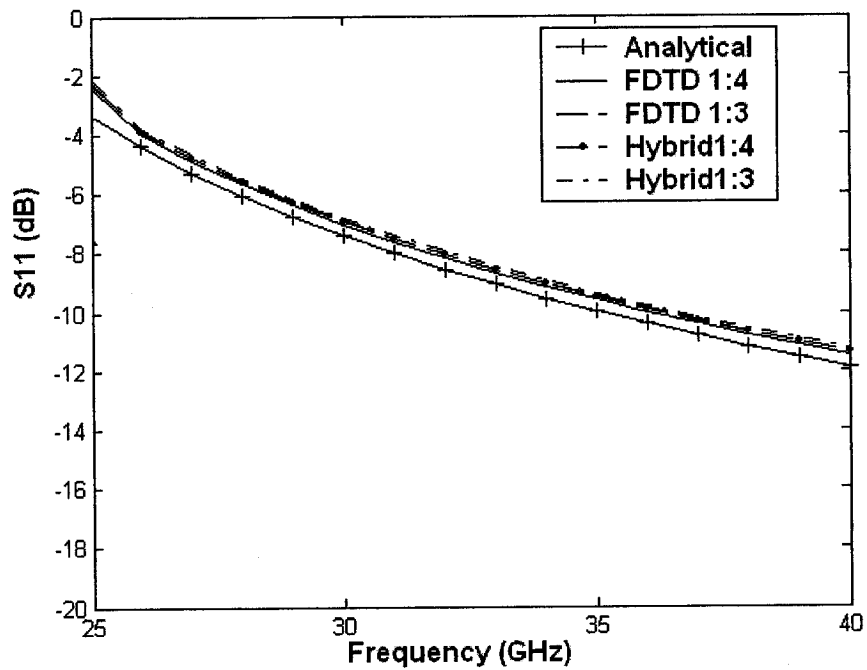
Fig. 4.6 Reflection coefficient S11 vs. frequency for waveguide
with the inductive iris

61

4.3.2   Optical Structure

FDTD method already has been applied to optical structures successfully [144-145]. In the previous section, the hybrid method was applied to RF/microwave structures; here it is applied to the optical structure. Equations in the previous section are modified for the optical structures. For simplicity electric and magnetic field equations are shown for FDTD and ADI-FDTD respectively.

FDTD equations

$$
E_x\Big|_{i+\frac{1}{2},j,k}^{n+1} = E_x\Big|_{i+\frac{1}{2},j,k}^{n} + \frac{\Delta t}{n^2 \varepsilon_0} \left[\frac{H_z\Big|_{i+\frac{1}{2},j+\frac{1}{2},k}^{n+\frac{1}{2}} - H_z\Big|_{i+\frac{1}{2},j-\frac{1}{2},k}^{n+\frac{1}{2}}}{\Delta y} \right]
$$

$$
- \frac{\Delta t}{n^2 \varepsilon_0} \left[\frac{H_y\Big|_{i+\frac{1}{2},j,k+\frac{1}{2}}^{n+\frac{1}{2}} - H_y\Big|_{i+\frac{1}{2},j,k-\frac{1}{2}}^{n+\frac{1}{2}}}{\Delta z} \right]
$$

(4.5a)

$$
H_x\Big|_{i,j+\frac{1}{2},k+\frac{1}{2}}^{n+\frac{1}{2}} = H_x\Big|_{i,j+\frac{1}{2},k+\frac{1}{2}}^{n-\frac{1}{2}} + \frac{\Delta t}{\mu} \left[\frac{E_y\Big|_{i,j+\frac{1}{2},k+1}^{n} - E_y\Big|_{i,j+\frac{1}{2},k}^{n}}{\Delta z} \right]
$$

$$
- \frac{\Delta t}{\mu} \left[\frac{E_z\Big|_{i,j+1,k+\frac{1}{2}}^{n} - E_z\Big|_{i,j,k+\frac{1}{2}}^{n}}{\Delta y} \right]
$$

(4.5b)

ADI-FDTD Equations

First time step:

$$
\frac{E_x\Big|_{i+\frac{1}{2},j,k}^{n+\frac{1}{2}} - E_x\Big|_{i+\frac{1}{2},j,k}^{n}}{\Delta t / 2}
$$

$$
= \frac{1}{n^2 \varepsilon_0} \left[\frac{H_z\Big|_{i+\frac{1}{2},j+\frac{1}{2},k}^{n+\frac{1}{2}} - H_z\Big|_{i+\frac{1}{2},j-\frac{1}{2},k}^{n+\frac{1}{2}}}{\Delta y} - \frac{H_y\Big|_{i+\frac{1}{2},j,k+\frac{1}{2}}^{n} - H_y\Big|_{i+\frac{1}{2},j,k-\frac{1}{2}}^{n}}{\Delta z} \right]
$$

(4.6a)

$$\frac{H_x\Big|_{i,j+\frac{1}{2},k+\frac{1}{2}}^{n+\frac{1}{2}} - H_x\Big|_{i,j+\frac{1}{2},k+\frac{1}{2}}^{n}}{\Delta t / 2}$$

$$= \frac{1}{\mu}\left[\frac{E_y\Big|_{i,j+\frac{1}{2},k+1}^{n+\frac{1}{2}} - E_y\Big|_{i,j+\frac{1}{2},k}^{n+\frac{1}{2}}}{\Delta z} - \frac{E_z\Big|_{i,j+1,k+\frac{1}{2}}^{n} - E_z\Big|_{i,j,k+\frac{1}{2}}^{n}}{\Delta y}\right] \qquad (4.6b)$$

<u>Second time step</u>

$$\frac{E_x\Big|_{i+\frac{1}{2},j,k}^{n+1} - E_x\Big|_{i+\frac{1}{2},j,k}^{n+\frac{1}{2}}}{\Delta t / 2}$$

$$= \frac{1}{n^2\varepsilon_0}\left[\frac{H_z\Big|_{i+\frac{1}{2},j+\frac{1}{2},k}^{n+\frac{1}{2}} - H_z\Big|_{i+\frac{1}{2},j-\frac{1}{2},k}^{n+\frac{1}{2}}}{\Delta y} - \frac{H_y\Big|_{i+\frac{1}{2},j,k+\frac{1}{2}}^{n+1} - H_y\Big|_{i+\frac{1}{2},j,k-\frac{1}{2}}^{n+1}}{\Delta z}\right] \qquad (4.7a)$$

$$\frac{H_x\Big|_{i,j+\frac{1}{2},k+\frac{1}{2}}^{n+1} - H_x\Big|_{i,j+\frac{1}{2},k+\frac{1}{2}}^{n+\frac{1}{2}}}{\Delta t / 2}$$

$$= \frac{1}{\mu}\left[\frac{E_y\Big|_{i,j+\frac{1}{2},k+1}^{n+\frac{1}{2}} - E_y\Big|_{i,j+\frac{1}{2},k}^{n+\frac{1}{2}}}{\Delta z} - \frac{E_z\Big|_{i,j+1,k+\frac{1}{2}}^{n+1} - E_z\Big|_{i,j,k+\frac{1}{2}}^{n+1}}{\Delta y}\right] \qquad (4.7b)$$

In above equations, n is the refractive index and $n = \sqrt{\dfrac{\varepsilon}{\varepsilon_0}} = \sqrt{\varepsilon_r} = \sqrt{1+\chi}$ with χ

being electric susceptibility and ε_r being the dielectric constant. The above equations now can be solved by using the tridiagonal matrix, similar to that discussed in the previous section.

An optical dielectric slab waveguide as shown in Fig 4.7 was considered and computed. To select the desired mode of propagation, wavelength λ and width d need to be selected carefully. The following are the steps for the determination of the wavelength λ and width d of a thin film layer:

Step 1: compute λ_0 with $c_0 = f\lambda_0$, $\lambda_0 = \dfrac{c_0}{f}$ and $c_0 = \dfrac{1}{\sqrt{\mu_0 \varepsilon_0}}$

Step 2: compute λ within the film

$$\lambda = \frac{\lambda_0}{n}$$

Step 3: compute "d" of the thin film or core for optical slab waveguide with the following

formula $d = \dfrac{m\lambda}{2\sqrt{n_1^2 - n_2^2}}$, where m is the mode number, λ is wavelength in

dielectric, n_1 is the refractive index of core, and n_2 is the refractive index of

cladding. To minimize the number of modes one can choose $\dfrac{d}{\lambda}$ small or n_2 close

to n_1. In our case, we selected parameters in such a way that only one mode was

allowed to propagate.

The dielectric slab waveguide (see Fig 4.7) has dimensions of $4.29 \times 2.96 \times 6.56 \mu m$. The

cross sectional view of this application is shown in Fig 4.8 with CPML as an absorbing

boundary condition. The width of the thin film layer was taken $0.686 \mu m$ while λ used

was $0.82 \mu m$. Refractive indexes for thin film layer and cladding were 3.6 and 3.55

respectively. These dimensions of the thin film for this structure allow only one mode for

propagation.

Cell sizes taken for FDTD were $\Delta x = 0.082\, um$, $\Delta y = 0.0683\, um$ and $\Delta z = 0.0729\, um$

while cell sizes taken for ADI-FDTD were,

$$\Delta x' = \frac{\Delta x (FDTD)}{2} \qquad \Delta y' = \frac{\Delta y (FDTD)}{2} \qquad \Delta z' = \frac{\Delta z (FDTD)}{2}$$

The propagation constant β was computed numerically with the following equation:

$$\beta = \frac{1}{h} img \left| \ln \frac{\Im(E(i,j,p2))}{\Im(E(i,j,P1))} \right| \qquad (4.8)$$

where $\Im$ represents Fourier transform, h is the distance between the source point "P1"

and the destination point "P2".

The phase velocity v_p is computed with $v_p = \dfrac{\omega}{\beta}$.

Fig. 4.9 shows the computed normalized propagation constant verses frequency. Fig 4.10 is shows normalized phase velocity versus frequency. It is obvious from these results that there is very good agreement between the FDTD and the proposed hybrid method for optical applications.
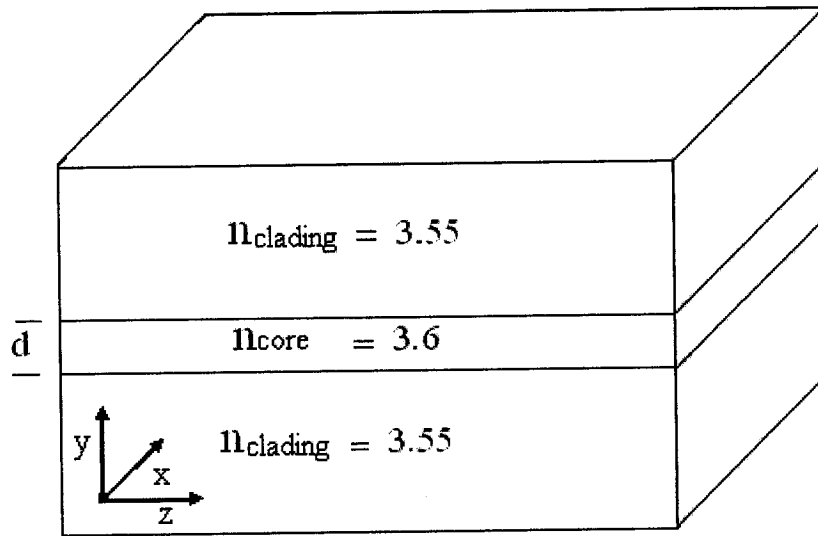
Fig. 4.7 3-D view of the optical dielectric slab waveguide
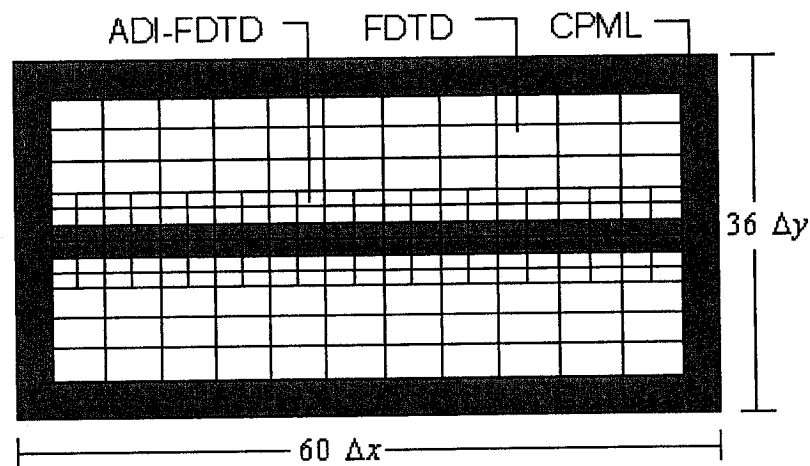
Fig. 4.8 The cross section of the rectangular optical slab waveguide
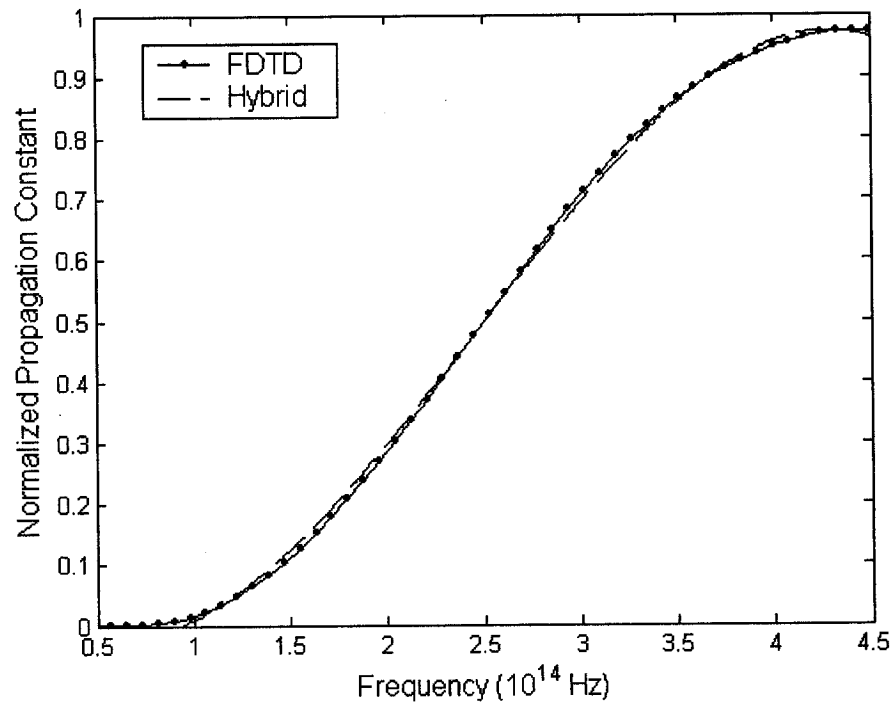
Fig 4.9 Normalized propagation constant vs. frequency
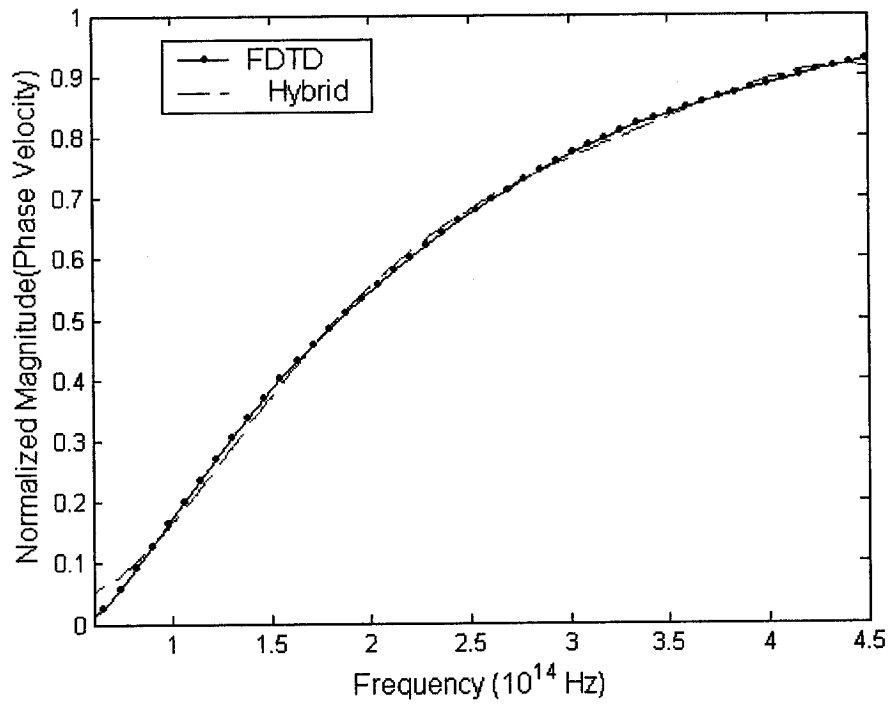
Fig. 4.10   Normalized phase velocity vs. frequency.

66

4.3.3　Applications of the Hybrid Method to Planar Circuit Structures

The planar structures are the most frequently used structures in RF and microwave electronics, in particularly, the coplanar structures. The coplanar structures feature in that their metal plates or films are deposited on the upper side of the substrate. Consequently, RF energy is concentrated on the plane surfaces and the active components can be mounted very easily. The easy mounting makes it very effective for microwave integrated circuit (MICs) and monolithic microwave integrated circuit fabrications. To further improve the RF efficiency, some coplanar structures have ground planes also at the bottom side of the substrate [146-149]. In this section, coplanar waveguide, coplanar strip line without ground planes at the bottom side and microstrip line are used as simulation examples.

In [150-151][153] the hybrid method was applied in such a way that a uniform fine mesh is applied around sharp varying field regions and coarse mesh in the rest of region. In this section the hybrid method was applied to the coplanar structure with a non-uniform mesh in the metallic region and a uniform mesh for the rest of the solution domain. Nonuniform mesh is very suitable for planar circuits and is applied in the regions of edges and corners of the strips. This is because fields concentrate around the metal surfaces and require finer numerical grids than the rest of the regions to resolve the fields. The ADI-FDTD method was employed in the nonuniform mesh region, and the conventional FDTD method was used for the rest of the region where there are no sharp changes of the fields.

The reason for the above arrangement is justified as follows: if the conventional FDTD is used in the nonuniform region, the time step is determined by the smallest spatial step in the nonuniform mesh region, as dictated by the CFL constraint; consequently, the time step may become very small and the CPU time becomes large. If a uniform mesh is used, the computational efficiency is reduced as a large number of cells are needed to resolve the sharp changes of the fields. The memory and CPU time will be significantly increased. With the above arrangement, the ADI-FDTD employed in the nonuniform mesh regions can have a larger time step as the ADI-FDTD does not have the CFL

constraint. At the same time, in the remaining coarse mesh region, the use of FDTD can ensure the minimum memory requirement and thus the uses of least CPU time. To terminate open solution domains, the convolutional perfectly matched layer (CPML) [142-143] was implemented.

The hybrid method was explained in detail earlier for 2-D and 3-D cases. The difference here is that a nonuniform mesh was used with the ADI-FDTD to resolve the fields around the edges of the metal strips. Due to the use of the nonuniform mesh, the circuit boundary can be modeled in a more conformal way than modeled with a uniform mesh. If a numerical grid is uniform but does not cover a boundary wall, we then have to reduce the cell size of the whole grid to better fit the boundary. This will increase computation expenditures. On the other hand, with a nonuniform mesh or grid, the boundary can be covered by changing the cell size only in the region near the boundary. This is the advantage of the hybrid method with a nonuniform grid. It should be pointed out that a nonuniform mesh is overall second-order accurate because it converges with higher order accuracy [3].

4.3.3.1 Simulation Results for Planar Structures

In [146], coplanar waveguides have been studied for various heights of the substrate. It was observed that the attenuation loss will be less with a reasonable height of substrate. In [147], results were observed for coplanar waveguide with different widths of ground metals while keeping the gap and centre strip widths constant.

In our case, the coplanar waveguide was studied with the hybrid method and FDTD method. The structure considered is shown in Fig 4.11 where w is the width of ground metal strips and both strips have the same size. s is the width of the signal line, and m is the width of the gap between the signal line and the ground strip, which is the same for both gaps. In our computations, the thickness of the strips was assumed to be zero, $w = 60 \mu m$, $s = 30 \mu m$ and $m = 20 \mu m$. The width, height and length of the structure are 250, 500 and 700 μm respectively.
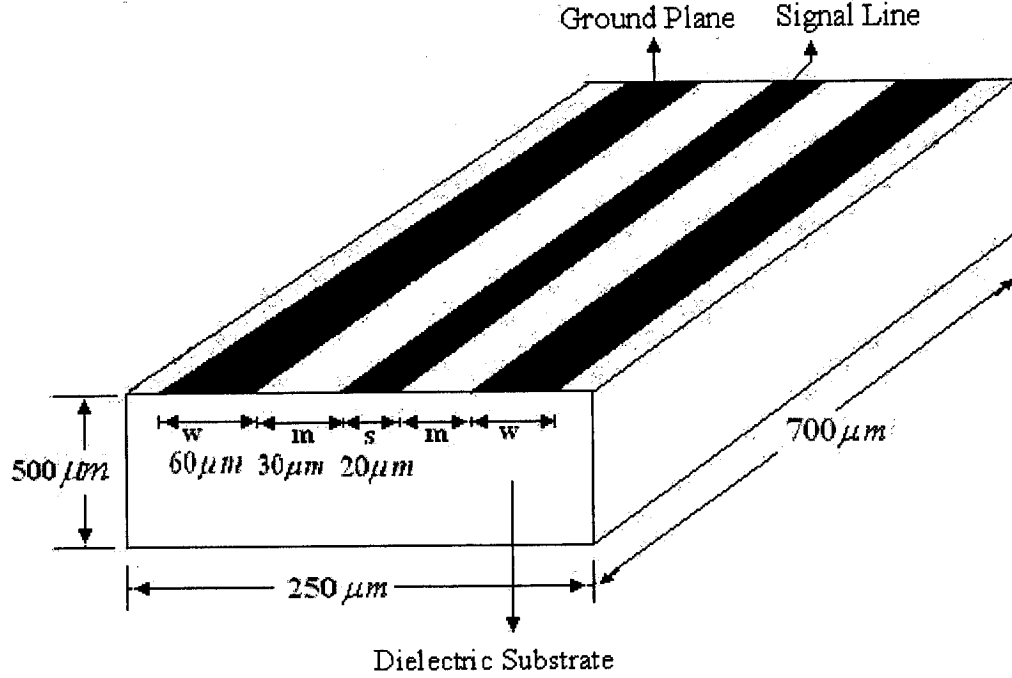
Fig 4.11 Coplanar waveguide structure with dimensions

Fig. 4.12 shows the cross sectional view of the structure used including CPML. Ten CPML layers were used on the top, sides and ends. In them,

$$\alpha = 0.05, \ k = 16, \quad \sigma_{opt} = \frac{m+1}{150\,\pi\sqrt{\varepsilon_r}\,\Delta l}\,|_{m=4}$$

The following cell sizes were used for simulations:

$$\Delta x_{min} = 5\mu m, \ \Delta x_{max} = 10\mu m, \ \Delta y_{min} = 2.5\,\mu m \ , \ \Delta y_{max} = 20\,\mu m \ \text{and} \ \Delta z = 10\,\mu m$$

The numbers of cells used were 66, 61 and 90 in x, y and z directions respectively. The height of the dielectric substrate was $500\,\mu m$ with dielectric constant being 9.4. Both the hybrid and the conventional FDTD were used to compute the structure. They were computed in three numerical grid arrangements: 1) a uniform coarse grid, 2) a uniform fine grid, and 3) a nonuniform grid.

69
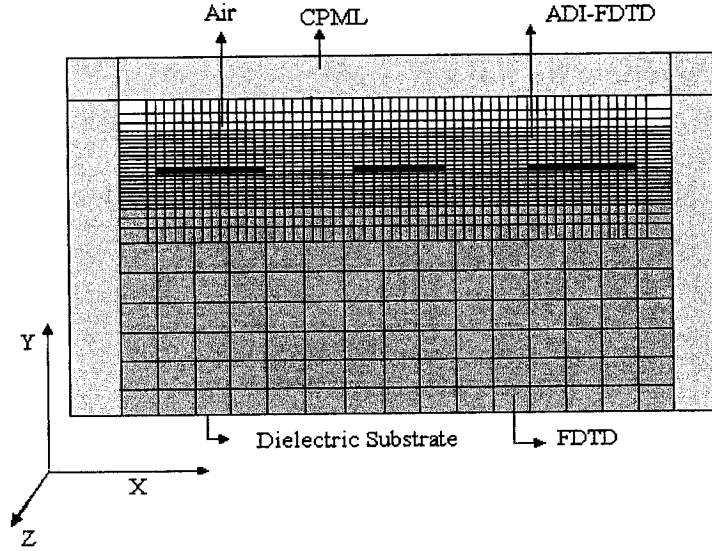
Fig 4.12 The cross sectional view of coplanar waveguide with CPML

However, in all cases, the time step Δt used with the hybrid method was chosen to be three times larger than that in the FDTD case. Thus the total number of iterations required with the hybrid method was one-third of that with the FDTD method. The advantage of the nonuniform mesh is that we can take cells of different sizes in each direction. With a variable mesh, cell size can be adjusted close to the desired area easily. It should be pointed out, that in a nonuniform mesh, the FDTD scheme appears to be first-order accurate. However, Monk proved that a nonuniform mesh is overall of second-order accuracy because it converges with higher-order accuracy [4].

Fig 4.13 shows the computed effective dielectric constant of the coplanar waveguide and its variations with frequency. Fig 4.14 shows the phase velocity. In these figures fine mesh means plot for the smallest cell size of nonuniform mesh for whole structure with the FDTD method. FDTD and ADI-FDTD coarse mesh means that the cell size selected for whole structure is equal to the largest cell in the nonuniform hybrid mesh, while the FDTD or Hybrid nonuniform mesh means variable mesh as shown in Fig. 4.12. The effective dielectric constant and the phase velocity were computed with the following formulas:

$$\varepsilon_{eff}(f) = \left(\frac{\beta(f)c}{2\pi f}\right)^2, \qquad V_p = \frac{2\pi f}{\beta(f)} \text{ or } V_p = \frac{c}{\sqrt{\varepsilon_{eff}(f)}}$$

70

where the phase shift constant $\beta(f)$ was computed numerically [152].

As can be seen, the effective dielectric constant is increased with the increase of frequency, while the phase velocity decreases. It is observed that the hybrid method with the nonuniform mesh agrees well with the FDTD method with a uniform fine mesh.
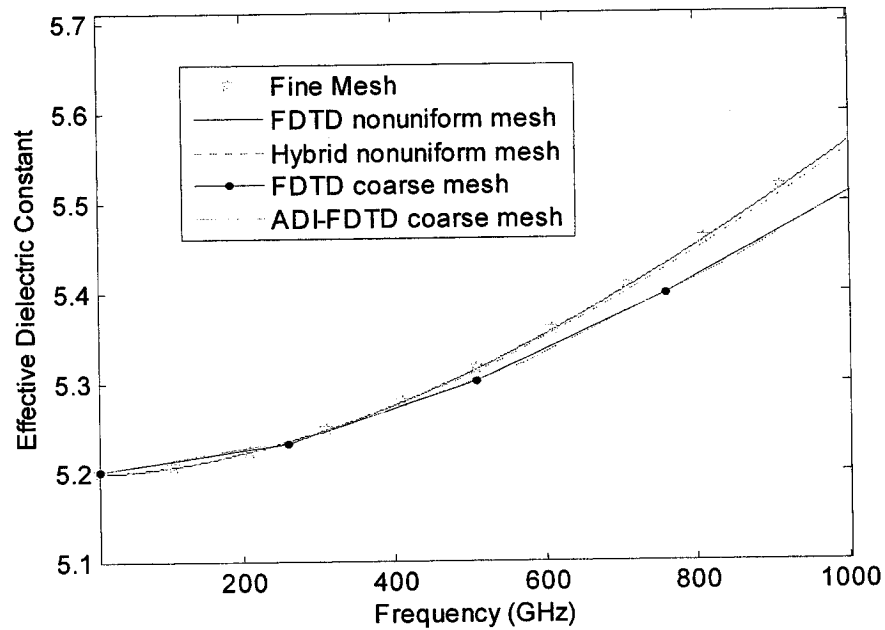
Fig. 4.13 Effective dielectric constant vs. frequency for coplanar waveguide
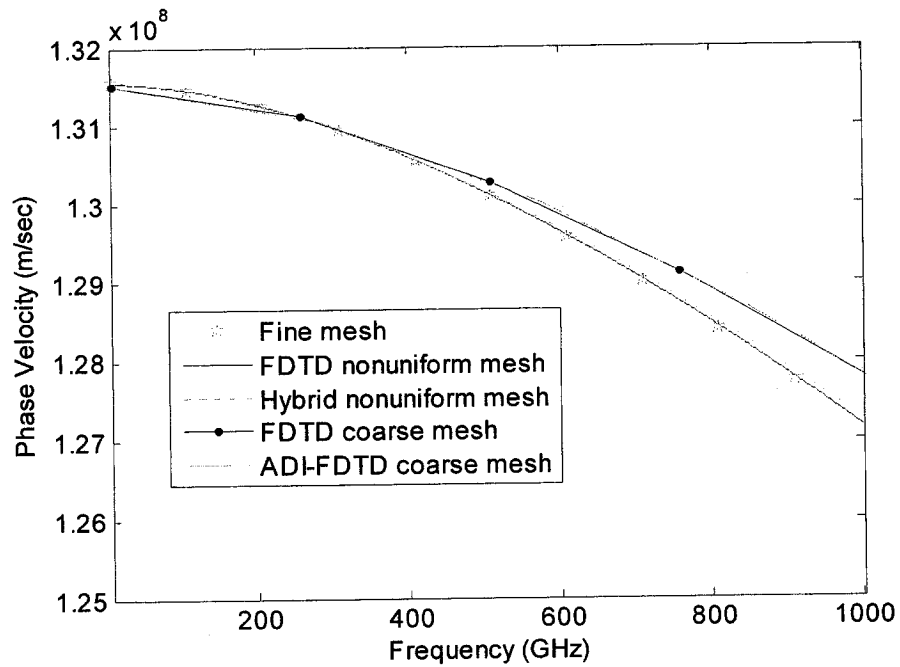
Fig. 4.14 Phase velocity vs. frequency for coplanar waveguide

However, the time and memory used by the hybrid method was 1510 seconds and 80.18 MB, respectively, while those used by the FDTD were 3157 seconds and 88.06 MB. Therefore, we can conclude that the hybrid method is more efficient than the FDTD, in particular in terms of CPU time. All the computations were performed on a PC Pentium IV with 512 RAM and a CPU of 2.4GHz.

In addition to the coplanar waveguide, coplanar strip line and microstrip line were also computed. Dimensions and cell sizes used for the coplanar strip line were exactly the same as those used for the coplanar waveguide, so the memory and the time used were also same. Its cross- sectional view is shown in Fig. 4.15. The computation results are shown in Fig. 4.16 and 4.17. As can be seen, the hybrid method is in very good agreement with other methods but with better efficiency in terms of the computer resources used which are the same as those for the coplanar waveguide.

Next application considered is the microstrip line [154]. Its crossectional view is shown in Fig. 4.18. In this case the cell ratio used for the coarse and fine mesh is 1:2; for the pure FDTD case, the whole domain was modeled with fine mesh. The effective dielectric constant used for this structure is shown in Fig. 4.19. It can be observed that there is a very good agreement between the proposed hybrid method and the FDTD method. However for the hybrid FDTD/ADI-FDTD, if permittivity of the substrate will change then to keep the same accuracy there is need to change the cell size in the substrate area, same is for the conventional FDTD method also. The cell size will decrease with the increase of substrate permittivity and vice versa.
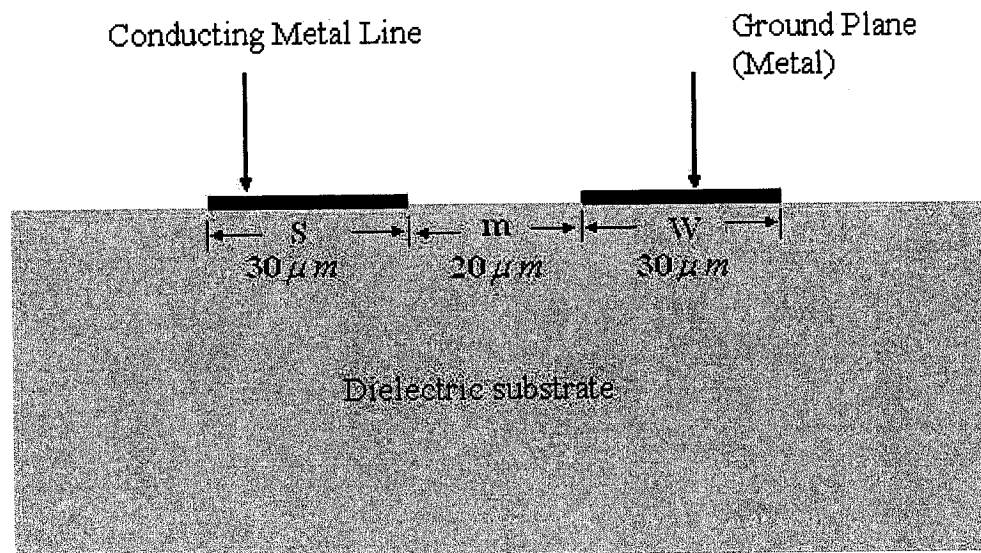
Fig. 4.15 Cross sectional view of the coplanar strip line
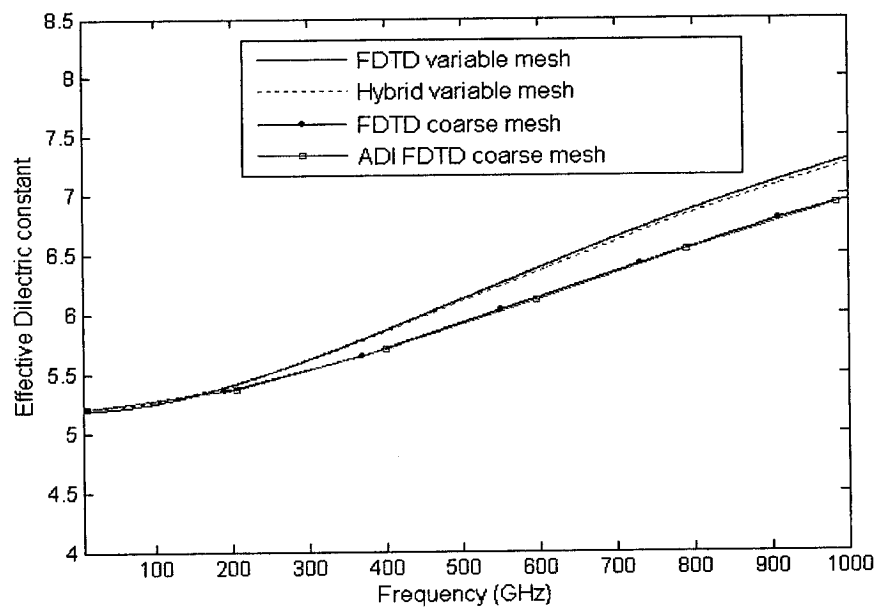
Fig. 4.16 Effective dielectric constant vs. frequency for coplanar strip line
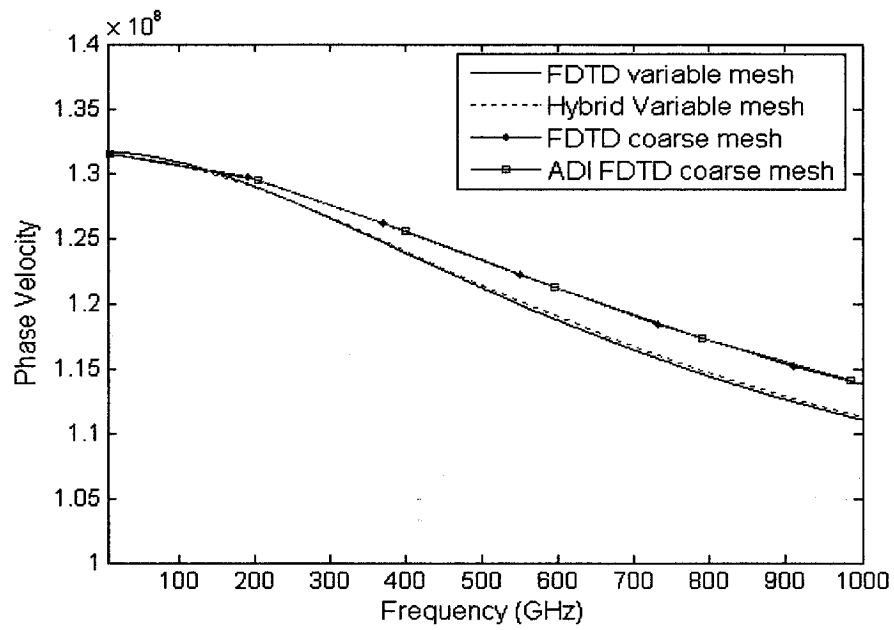
Fig. 4.17 Phase velocity vs. frequency for coplanar strip line
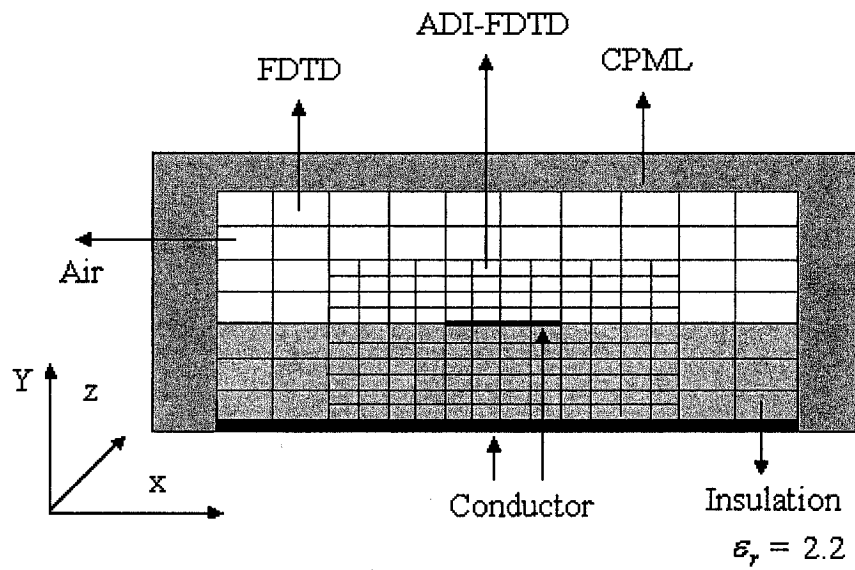
Fig. 4.18 Cross sectional view of microstrip line
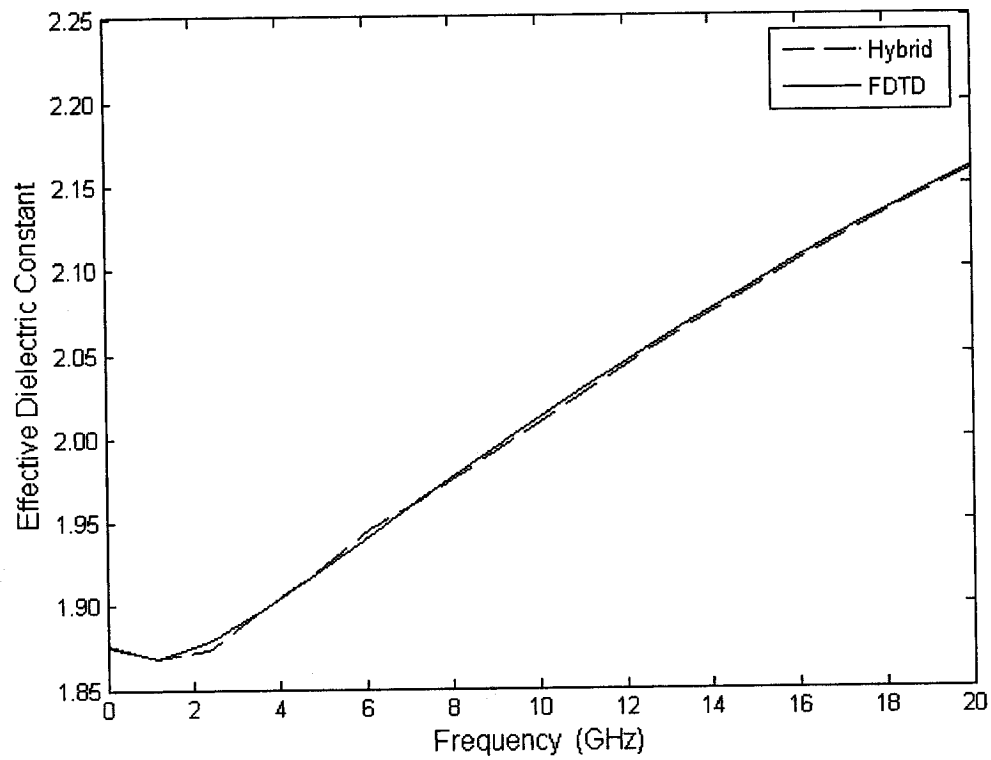
Fig. 4.19 Effective dielectric constant vs. frequency for the microstrip line

4.4 Conclusions

In this chapter, 3-D hybrid ADI-FDTD/FDTD technique has been described. It is found that the hybrid technique improves the computation efficiency in terms of both CPU time and memory for modeling RF/microwave and optical structures. In addition to the above applications, it has been applied to the planar structures. It shows that the hybrid method is faster in simulation time, with less memory requirement and the same accuracy level as that of the FDTD method.

Chapter 5   Error Reduced ADI-FDTD Methods

5.1   Introduction

Efficient numerical algorithms are required to solve complex and electrically large structures. The existing FDTD method plays an important role in the simulation of different structures [1-4], especially RF and microwave, photonics, and VLSI. Many commercial software packages currently available are based on the FDTD method, and many more are in development. In addition FDTD-based hardware accelerators [155] were also developed to increase the computation speed. However, the Courant-Friedrich-Levy (CFL) stability condition makes the explicit FDTD methods computationally expensive in applications where small cell sizes are needed to resolve high variations of fields. To solve this problem, a subgridding technique was introduced in the previous chapter. Many other techniques were also proposed [3-4] but CFL condition persists.

To remove this restriction, unconditionally stable ADI-FDTD method and Crank-Nicolson (CN) FDTD methods have been proposed recently [6-7][156-157]. Due to their unconditional stability, both methods have attracted much attention in recent years. It has been found that although the ADI-FDTD is computationally efficient, but it has large errors with large time steps [156]. Such a property compromises the uses of the ADI-FDTD with its unconditional stability. On the other hand, the CN-FDTD method is of much high accuracy, even with large time steps, but at the cost of much larger computational time [157-159]. Therefore, it will be desirable to develop a method that has the advantages of both methods.

In fact, further studies on the ADI-FDTD and the CN-FDTD methods have shown the ADI-FDTD method can be considered as the perturbed form of the CN method with the so-called splitting error term [156]. Based on it, an iterative method that solves the CN-FDTD method in an ADI-FDTD fashion was reported [158]. It embodies a loop of iterations at each FDTD marching time step. Consequently, it achieved much higher accuracy than that of the ADI-FDTD at the cost of more computation time. In this

chapter, the novel ADI-FDTD methods are proposed that are based on the CN-FDTD formulation but with the same computational efficiency as that of the conventional ADI-FDTD. Although the achieved accuracy may not be as high as that with the CN-FDTD method, it is sufficient for most of the large time step simulations without increasing computation expenditures. We name the methods as the error-reduced (ER) ADI-FDTD methods due to their less error at higher time steps as compared to the conventional ADI-FDTD method.

This chapter is divided into the following sections: in section 5.2, formulations and numerical results of the proposed methods for 2-D case are presented; in section 5.3 formulations and numerical results are extended to the 3-D case; and in section 5.4 conclusions are presented.

5.2   Formulations of the 2-D ER-ADI-FDTD

For simplicity, the TE-to-z wave is considered. The related Maxwell's equations in the matrix form are:

$$\frac{\partial}{\partial t}\begin{bmatrix} E_x \\ E_y \\ H_z \end{bmatrix} = \begin{bmatrix} 0 & 0 & \dfrac{\partial}{\varepsilon\partial y} \\ 0 & 0 & -\dfrac{\partial}{\varepsilon\partial x} \\ \dfrac{\partial}{\mu\partial y} & -\dfrac{\partial}{\mu\partial x} & 0 \end{bmatrix}\begin{bmatrix} E_x \\ E_y \\ H_z \end{bmatrix} \tag{5.1}$$

or

$$\frac{\partial U}{\partial t} = [C]U$$

where $[C] = \begin{bmatrix} 0 & 0 & \dfrac{\partial}{\varepsilon\partial y} \\ 0 & 0 & -\dfrac{\partial}{\varepsilon\partial x} \\ \dfrac{\partial}{\mu\partial y} & -\dfrac{\partial}{\mu\partial x} & 0 \end{bmatrix}$ and $U = \begin{bmatrix} E_x \\ E_y \\ H_z \end{bmatrix}$

77

[C] can be broken up into [A] and [B] such that:

$$\frac{\partial U}{\partial t} = [A]U + [B]U \tag{5.2}$$

with

$$[A] = \begin{bmatrix} 0 & 0 & \dfrac{\partial}{\varepsilon\,\partial y} \\ 0 & 0 & 0 \\ \dfrac{\partial}{\mu\,\partial y} & 0 & 0 \end{bmatrix} \quad \text{and } [B] = \begin{bmatrix} 0 & 0 & 0 \\ 0 & 0 & -\dfrac{\partial}{\varepsilon\,\partial x} \\ 0 & -\dfrac{\partial}{\mu\,\partial x} & 0 \end{bmatrix}$$

Replacement of the time derivative with central finite difference leads to

$$([I] - \frac{\Delta t}{2}[A])([I] - \frac{\Delta t}{2}[B])U^{n+1} = ([I] + \frac{\Delta t}{2}[A])([I] + \frac{\Delta t}{2}[B])U^n + \frac{\Delta t^2}{4}[A][B](U^{n+1} - U^n) \tag{5.3}$$

To compute (5.3), two ADI-FDTD-like steps can be taken:

Step 1

$$([I] - \frac{\Delta t}{2}[A])U^{n+\frac{1}{2}} = ([I] + \frac{\Delta t}{2}[B])U^n + \frac{\Delta t^2}{8}[A][B](U^{n+1} - U^n) \tag{5.4}$$

and

Step 2

$$([I] - \frac{\Delta t}{2}[B])U^{n+1} = ([I] + \frac{\Delta t}{2}[A])U^{n+\frac{1}{2}} + \frac{\Delta t^2}{8}[A][B](U^{n+1} - U^n) \tag{5.5}$$

However, the above two equations are both implicit: the right-hand sides contain the quantities to be found or updated. Although the iterative method [158] may be applied for solutions, it may increase the CPU time as iterative computations are involved at each time step. Therefore, efficient approaches need to be developed. In this paper, we propose the following two methods.

78

Method #1

To make the computation explicit on the right-hand sides of the above equations, the term

$$\frac{\Delta t^2}{8}[A][B](U^{n+1} - U^n) \tag{5.6}$$

is modified with the following approximating equations:

$$U^n = \frac{U^{n+\frac{1}{2}} + U^{n-\frac{1}{2}}}{2} \ , \ U^{n+\frac{1}{2}} = \frac{U^{n+1} + U^n}{2}$$

Then, the two ADI-FDTD steps are computed as:

Step 1

$$([I] - \frac{\Delta t}{2}[A])U^{n+\frac{1}{2}} = ([I] + \frac{\Delta t}{2}[B])U^n + \frac{\Delta t^2}{4}[A][B](U^n - U^{n-\frac{1}{2}}) \tag{5.7}$$

and

Step 2

$$([I] - \frac{\Delta t}{2}[B])U^{n+1} = ([I] + \frac{\Delta t}{2}[A])U^{n+\frac{1}{2}} + \frac{\Delta t^2}{4}[A][B](U^{n+\frac{1}{2}} - U^n) \tag{5.8}$$

More specifically, in the context of TE mode, the above equations become:

Step1

$$E_x^{n+\frac{1}{2}} = E_x^n + \frac{\Delta t}{2\varepsilon}\frac{\partial}{\partial y}H_z^{n+\frac{1}{2}} - \frac{\Delta t^2}{8\mu\varepsilon}\frac{\partial}{\partial x\partial y}(E_y^n - E_y^{n-\frac{1}{2}}) \tag{5.9}$$

$$E_y^{n+\frac{1}{2}} = E_y^n - \frac{\Delta t}{2\varepsilon}\frac{\partial}{\partial x}H_z^n \tag{5.10}$$

$$H_z^{n+\frac{1}{2}} = H_z^n + \frac{\Delta t}{2\mu}\frac{\partial}{\partial y}E_x^{n+\frac{1}{2}} - \frac{\Delta t}{2\mu}\frac{\partial}{\partial x}(E_y^n) \tag{5.11}$$

79

and

Step 2

$$E_x{}^{n+1} = E_x^{n+\frac{1}{2}} + \frac{\Delta t}{2\varepsilon}\frac{\partial}{\partial y}H_z^{n+\frac{1}{2}} - \frac{\Delta t^2}{8\mu\varepsilon}\frac{\partial}{\partial x\partial y}(E_y^{n+\frac{1}{2}} - E_y^n) \tag{5.12}$$

$$E_y^{n+1} = E_y^{n+\frac{1}{2}} - \frac{\Delta t}{2\varepsilon}\frac{\partial}{\partial x}H_z^{n+1} \tag{5.13}$$

$$H_z{}^{n+1} = H_z^{n+\frac{1}{2}} + \frac{\Delta t}{2\mu}\frac{\partial}{\partial y}E_x^{n+\frac{1}{2}} - \frac{\Delta t}{2\mu}\frac{\partial}{\partial x}(E_y^{n+1}) \tag{5.14}$$

The above equations are then discretized as follows:

Step 1

$$\begin{aligned}
E_x\Big|_{i+\frac{1}{2},j}^{n+\frac{1}{2}} = {} & E_x\Big|_{i+\frac{1}{2},j}^{n} + \frac{\Delta t}{2\varepsilon\Delta y}\left(H_z\Big|_{i+\frac{1}{2},j+\frac{1}{2}}^{n+\frac{1}{2}} - H\Big|_{i+\frac{1}{2},j-\frac{1}{2}}^{n+\frac{1}{2}} \right) \\
& - \frac{\Delta t^2}{8\mu\varepsilon\Delta x\Delta y}\left(\begin{array}{c} E_y\Big|_{i+1,j+\frac{1}{2}}^{n} - E_y\Big|_{i+1,j-\frac{1}{2}}^{n} - E_y\Big|_{i,j+\frac{1}{2}}^{n} + E_y\Big|_{i,j-\frac{1}{2}}^{n} \\ - E_y\Big|_{i+1,j+\frac{1}{2}}^{n-\frac{1}{2}} + E_y\Big|_{i+1,j-\frac{1}{2}}^{n-\frac{1}{2}} - E_y\Big|_{i,j+\frac{1}{2}}^{n-\frac{1}{2}} + E_y\Big|_{i,j-\frac{1}{2}}^{n-\frac{1}{2}} \end{array} \right)
\end{aligned} \tag{5.15}$$

$$E_y\Big|_{i,j+\frac{1}{2}}^{n+\frac{1}{2}} = E_y\Big|_{i+j+\frac{1}{2}}^{n} - \frac{\Delta t}{2\varepsilon\Delta x}\left(H_z\Big|_{i+\frac{1}{2},j+\frac{1}{2}}^{n} - H_z\Big|_{i-\frac{1}{2},j+\frac{1}{2}}^{n} \right) \tag{5.16}$$

$$H_z\Big|_{i+\frac{1}{2},j+\frac{1}{2}}^{n+\frac{1}{2}} = H_z\Big|_{i+\frac{1}{2},j+\frac{1}{2}}^{n} + \frac{\Delta t}{2\mu\Delta y}\left(E_x\Big|_{i+\frac{1}{2},j+1}^{n+\frac{1}{2}} - E_x\Big|_{i+\frac{1}{2},j}^{n+\frac{1}{2}} \right) - \frac{\Delta t}{2\mu\Delta x}\left(E_y\Big|_{i+1,j+\frac{1}{2}}^{n} - E_y\Big|_{i,j+\frac{1}{2}}^{n} \right) \tag{5.17}$$

and

Step 2

$$E_x\Big|_{i+\frac{1}{2},j}^{n+1} = E_x\Big|_{i+\frac{1}{2},j}^{n+\frac{1}{2}} + \frac{\Delta t}{2\varepsilon\Delta y}\left(H_z\Big|_{i+\frac{1}{2},j+\frac{1}{2}}^{n+\frac{1}{2}} - H\Big|_{i+\frac{1}{2},j-\frac{1}{2}}^{n+\frac{1}{2}}\right)$$
$$-\frac{\Delta t^2}{8\mu\varepsilon\Delta x\Delta y}\left(\begin{array}{c} E_y\Big|_{i+1,j+\frac{1}{2}}^{n+\frac{1}{2}} - E_y\Big|_{i+1,j-\frac{1}{2}}^{n+\frac{1}{2}} - E_y\Big|_{i,j+\frac{1}{2}}^{n+\frac{1}{2}} + E_y\Big|_{i,j-\frac{1}{2}}^{n+\frac{1}{2}} \\ - E_y\Big|_{i+1,j+\frac{1}{2}}^{n} + E_y\Big|_{i+1,j-\frac{1}{2}}^{n} - E_y\Big|_{i,j+\frac{1}{2}}^{n} + E_y\Big|_{i,j-\frac{1}{2}}^{n} \end{array}\right) \qquad (5.18)$$

$$E_y\Big|_{i,j+\frac{1}{2}}^{n+1} = E_y\Big|_{i+j+\frac{1}{2}}^{n+\frac{1}{2}} - \frac{\Delta t}{2\varepsilon\Delta x}\left(H_z\Big|_{i+\frac{1}{2},j+\frac{1}{2}}^{n+1} - H_z\Big|_{i-\frac{1}{2},j+\frac{1}{2}}^{n+1}\right) \qquad (5.19)$$

$$H_z\Big|_{i+\frac{1}{2},j+\frac{1}{2}}^{n+1} = H_z\Big|_{i+\frac{1}{2},j+\frac{1}{2}}^{n+\frac{1}{2}} + \frac{\Delta t}{2\mu\Delta y}\left(E_x\Big|_{i+\frac{1}{2},j+1}^{n+\frac{1}{2}} - E_x\Big|_{i+\frac{1}{2},j}^{n+\frac{1}{2}}\right) - \frac{\Delta t}{2\mu\Delta x}\left(E_y\Big|_{i+1,j+\frac{1}{2}}^{n+1} - E_y\Big|_{i,j+\frac{1}{2}}^{n+1}\right) \qquad (5.20)$$

Like the conventional ADI-FDTD method, these equations can be used for programming.

Method #2

In this method, the approximation $U^n = \dfrac{U^{n+1} + U^{n-1}}{2}$ is used in equation (5.6). The following two-steps are computed as follows:

Step 1

$$([I] - \frac{\Delta t}{2}[B])U^{n+1} = ([I] + \frac{\Delta t}{2}[A])U^n + \frac{\Delta t^2}{8}[A][B](U^n - U^{n-1}) \qquad (5.21)$$

and

81

Step 2

$$([I] - \frac{\Delta t}{2}[B])U^{n+2} = ([I] + \frac{\Delta t}{2}[A])U^{n+1} + \frac{\Delta t^2}{8}[A][B](U^{n+1} - U^n) \tag{5.22}$$

The equations above are different from the conventional ADI-FDTD formulations [6-7] in the addition of the terms on the right-hand sides that are proportional to the square of the time step [156]. The terms are related to the truncation errors and the additions of these in the computations are therefore expected to reduce the errors [158]. A numerical example is shown in the section below.

Similar procedure can be developed for a 2-D TM mode also.

5.2.1 Numerical Results

In this section, proposed Method # 1 and Method # 2 are applied, and their results are compared with the conventional ADI-FDTD and FDTD methods. It can be observed from equations (5.9) and (5.12) that in these two equations each contain one extra term as compared to the conventional ADI-FDTD method. These extra terms are proportional to the square of the time step and are responsible for the accuracy improvement of the methods.

A structure of two parallel plates of zero thickness in free space was considered and studied. The plates were $2m$ long and have a distance of $0.2m$ in between them. The geometry is shown in Fig. 5.1. To truncate the surrounding environment for simulation purpose, Perfect Magnetic Wall (PMW) was used on all four sides. The thickness of parallel plates considered was zero and Perfect Electric walls (PEC) were placed at these two lines. Cell size considered for both methods in each direction was $0.2m$. Basically this is the same structure used in [156] and was a very good example to examine the errors. The raised cosine waveform with frequency 750 kHz was used as a source. Fig 5.2 shows the computed electric field E_y along the x axis with different CFL factor "s" which is the ratio of time step to the CFL limit. It can be observed from this figure that

for $s \le 15$ results with the Method # 1 are the same as those with the conventional ADI-FDTD method at $s = 0.5$, while the results with Method # 2 are similar but have much larger errors. In Fig. 5.3 relative errors of the three methods, the conventional ADI-FDTD, Method # 1 and Method # 2 are plotted. The relative error is defined as:

$$\text{Relative error} = \frac{E_y^{meas} - E_y^{ref}}{E_y^{ref}}$$

where E_y^{meas} is a measured electric field, while E_y^{ref} is the reference field computed with the conventional FDTD method by using a CFL factor $s = 0.5$.

As can be seen, all the methods have similar errors at small $s \le 0.5$. With the increment of CFL factor, the error of the Method # 2 is increasing like the conventional ADI-FDTD method, but for $s \le 15$ Method # 1 has almost zero error. The Method # 1 also has error for $s \le 15$ but the error is so small that it is not visible for the scale of Fig. 5.3; this is the reason why it seems to be zero. Table 5.1 shows the computer resources used by the conventional ADI-FDTD and proposed error reduced methods. It is clear from there that simulation time used by Method # 1 and Method # 2 is approximately same as for the conventional ADI-FDTD with minor increment in memory for proposed methods. At $s \le 15$ Method # 1 is taking less than one second and has the same results as Method # 2, the conventional FDTD, and the conventional ADI-FDTD at $s = 0.5$.

Fig 5.4 shows computation time used by the proposed methods and the conventional ADI-FDTD method with different values of s. As can be seen, the computation time is almost the same for all the three methods. The memories used with three methods are 1.336MB (with the conventional ADI-FDTD), 1.344 MB (with Method #1) and 1.344 MB (with Method #2). The proposed two methods used slightly more memory but insignificantly.

y

10 m

2 m

0.2 m

PMC BOX

4 m

x
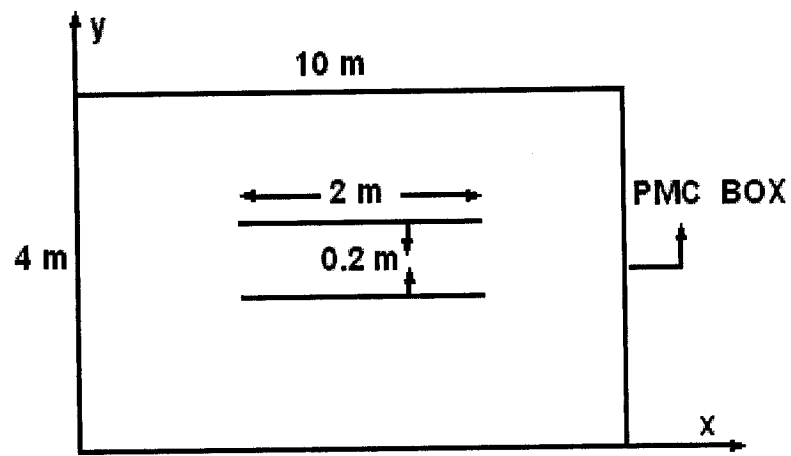
Fig. 5.1 Parallel conducting plates

Table 5.1 Computer resources used by the conventional ADI-FDTD and the proposed ADI-FDTD methods

Conventional ADI FDTD		New ADI-FDTD Method #1		New ADI-FDTD Method # 2		CFL factor "F"	No. of iterations
Time (sec)	Memory (MB)	Time (sec)	Memory (MB)	Time (sec)	Memory (MB)		
43	1.336	43	1.344	43	1.344	0.5	2000
4	1.336	4	1.344	4	1.344	5	200
1	1.336	1	1.344	1	1.344	10	100
<1	1.336	<1	1.344	<1	1.344	15	67
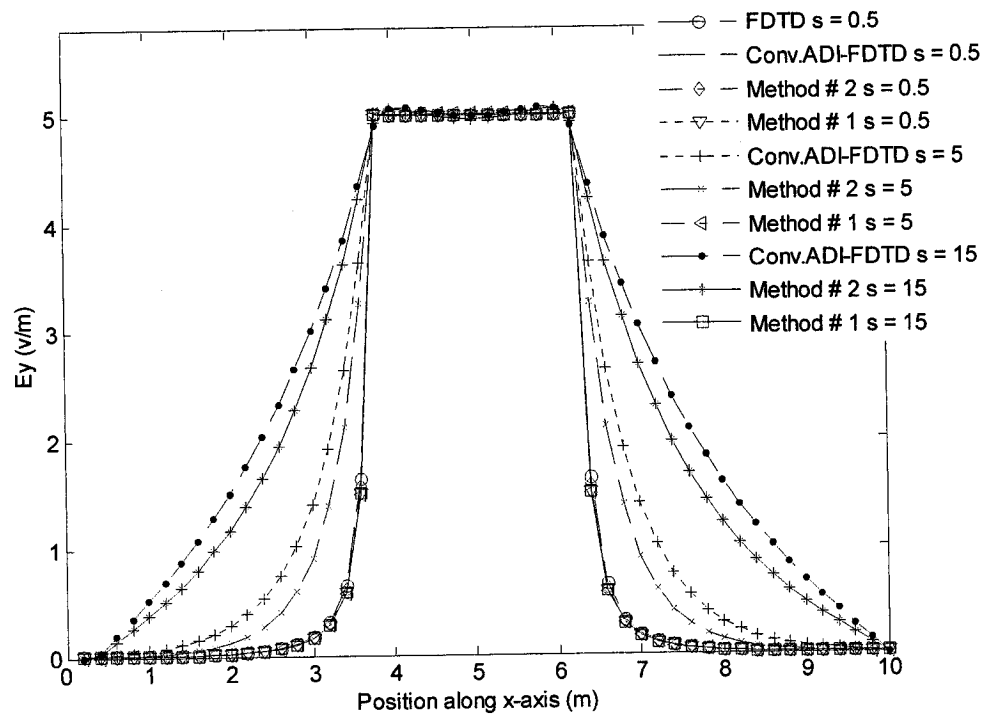
Fig. 5.2 Electric field Ey for FDTD, ADI-FDTD and proposed methods
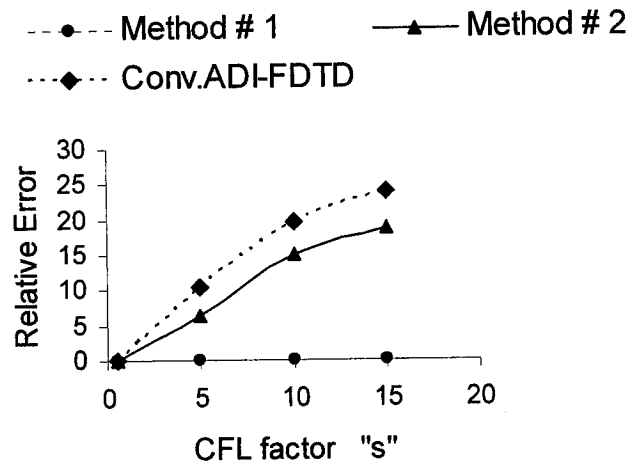
Fig 5.3 Relative error vs. CFL factor
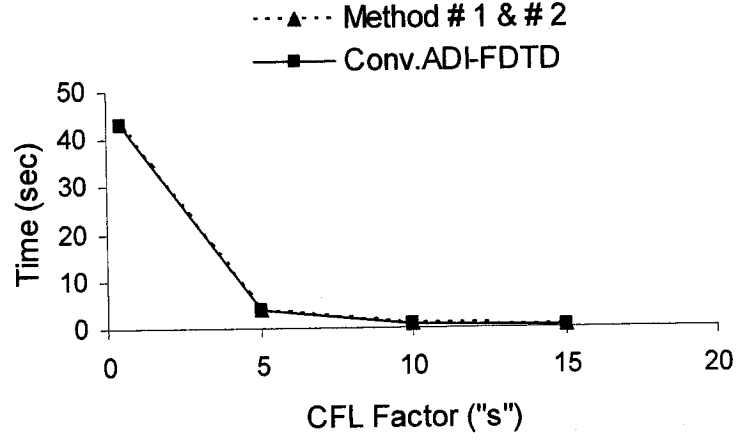
Fig. 5.4 Simulation time vs. CFL factor

5.3 Formulations of the 3-D ER-ADI-FDTD

Now the 2-D equations are extended to 3-D equations, and are written on the same pattern and are shown below:

$$
\frac{\partial}{\partial t}\begin{bmatrix} E_x \\ E_y \\ E_z \\ H_x \\ H_y \\ H_z \end{bmatrix} = \begin{bmatrix} 0 & 0 & 0 & 0 & -\dfrac{\partial}{\varepsilon\partial z} & \dfrac{\partial}{\varepsilon\partial y} \\ 0 & 0 & 0 & \dfrac{\partial}{\varepsilon\partial z} & 0 & -\dfrac{\partial}{\varepsilon\partial x} \\ 0 & 0 & 0 & -\dfrac{\partial}{\varepsilon\partial y} & \dfrac{\partial}{\varepsilon\partial x} & 0 \\ 0 & \dfrac{\partial}{\mu\partial z} & -\dfrac{\partial}{\mu\partial y} & 0 & 0 & 0 \\ -\dfrac{\partial}{\mu\partial z} & 0 & -\dfrac{\partial}{\mu\partial x} & 0 & 0 & 0 \\ \dfrac{\partial}{\mu\partial y} & -\dfrac{\partial}{\mu\partial x} & 0 & 0 & 0 & 0 \end{bmatrix}\begin{bmatrix} E_x \\ E_y \\ E_z \\ H_x \\ H_y \\ H_z \end{bmatrix}
\tag{5.23}
$$

This can be generalized as:

$$
\frac{\partial U_1}{\partial t} = [C_1]U_1
\tag{5.24}
$$

where

$$
U_1 = [E_x, E_y, E_{z,}H_x, H_y, H_z]^T \text{ and}
$$

86

$$[C_1] = \begin{bmatrix} 0 & 0 & 0 & 0 & -\dfrac{\partial}{\varepsilon\partial z} & \dfrac{\partial}{\varepsilon\partial y} \\[2mm] 0 & 0 & 0 & \dfrac{\partial}{\varepsilon\partial z} & 0 & -\dfrac{\partial}{\varepsilon\partial x} \\[2mm] 0 & 0 & 0 & -\dfrac{\partial}{\varepsilon\partial y} & \dfrac{\partial}{\varepsilon\partial x} & 0 \\[2mm] 0 & \dfrac{\partial}{\mu\partial z} & -\dfrac{\partial}{\mu\partial y} & 0 & 0 & 0 \\[2mm] -\dfrac{\partial}{\mu\partial z} & 0 & -\dfrac{\partial}{\mu\partial x} & 0 & 0 & 0 \\[2mm] \dfrac{\partial}{\mu\partial y} & -\dfrac{\partial}{\mu\partial x} & 0 & 0 & 0 & 0 \end{bmatrix}$$

Matrix $[C_1]$ is further divided into two matrices $[A_1]$ and $[B_1]$:

$$\frac{\partial U_1}{\partial t} = [A_1]U_1 + [B_1]U_1 \tag{5.25}$$

with

$$[A_1] = \begin{bmatrix} 0 & 0 & 0 & 0 & 0 & \dfrac{\partial}{\varepsilon\partial y} \\[2mm] 0 & 0 & 0 & \dfrac{\partial}{\varepsilon\partial z} & 0 & 0 \\[2mm] 0 & 0 & 0 & 0 & \dfrac{\partial}{\varepsilon\partial x} & 0 \\[2mm] 0 & \dfrac{\partial}{\mu\partial z} & 0 & 0 & 0 & 0 \\[2mm] 0 & 0 & \dfrac{\partial}{\mu\partial x} & 0 & 0 & 0 \\[2mm] \dfrac{\partial}{\mu\partial y} & 0 & 0 & 0 & 0 & 0 \end{bmatrix} \quad \text{and} \quad [B_1] = \begin{bmatrix} 0 & 0 & 0 & 0 & -\dfrac{\partial}{\varepsilon\partial z} & 0 \\[2mm] 0 & 0 & 0 & 0 & 0 & -\dfrac{\partial}{\varepsilon\partial x} \\[2mm] 0 & 0 & 0 & -\dfrac{\partial}{\varepsilon\partial y} & 0 & 0 \\[2mm] 0 & 0 & -\dfrac{\partial}{\mu\partial z} & 0 & 0 & 0 \\[2mm] -\dfrac{\partial}{\mu\partial z} & 0 & 0 & 0 & 0 & 0 \\[2mm] 0 & -\dfrac{\partial}{\mu\partial x} & 0 & 0 & 0 & 0 \end{bmatrix}$$

By using the following approximation

$$\frac{\partial U_1}{\partial t} = \frac{U_1^{n+1} + U_1^{n}}{2}$$

$U_1^{n+\frac{1}{2}} = \dfrac{U_1^{n+1} + U_1^n}{2}$ equation (5.25) becomes,

$$U_1^{n+1} - U_1^n = \frac{\Delta t}{2}[A_1](U_1^{n+1} + U_1^n) + \frac{\Delta t}{2}[B_1](U_1^{n+1} + U_1^n) \tag{5.26}$$

It can be rewritten as:

$$([I] - \frac{\Delta t}{2}[A_1])([I] - \frac{\Delta t}{2}[B_1])\,U_1^{n+1} = ([I] + \frac{\Delta t}{2}[A_1])([I] + \frac{\Delta t}{2}[B_1])U_1^n + \frac{\Delta t^2}{4}[A_1][B_1](U_1^{n+1} - U_1^n) \tag{5.27}$$

where $[I]$ is the identity matrix. To compute (5.27) in the ADI-FDTD fashion, two-step computation is applied with the introduction of an intermediate variable U_1^{tmp} :

Step 1

$$([I] - \frac{\Delta t}{2}[A_1])U_1^{tmp} = ([I] + \frac{\Delta t}{2}[B_1])U_1^n + \frac{\Delta t^2}{8}[A_1][B_1](U_1^{n+1} - U_1^n) \tag{5.28}$$

and

Step 2

$$([I] - \frac{\Delta t}{2}[B_1])U_1^{n+1} = ([I] + \frac{\Delta t}{2}[A_1])U_1^{tmp} + \frac{\Delta t^2}{8}[A_1][B_1](U_1^{n+1} - U_1^n) \tag{5.29}$$

The above equations are still implicit: the right hand sides contain the field quantities to be computed. Therefore, the approximations similar to the 2D case are applied. The final equation procedure for Method #1 and Method # 2 is given in Appendix A.

5.3.1   Numerical Results for 3-D ER-ADI-FDTD

A cavity of dimensions 9mm x 6mm x 15mm was computed. Its geometry is shown in Fig 5.5. The cell size used was equal to 0.6mm in all the three directions. Gaussian pulse was used as a source. The result obtained is shown in Fig. 5.6. It is clear from this result that the proposed methods for 3-D case unfortunately become unstable after few hundred

iterations.

In [160], a comparison has been made between the ADI and CN methods. It is shown that the ADI method is much computationally efficient than the CN method; however CN is more accurate than the ADI method. Efforts are continued to find some ways to make 3-D ER-ADI-FDTD methods stable so that the efficiency of the method is better than the conventional ADI-FDTD method and faster than the CN method.

5.4   Conclusions

In this chapter, error-reduced ADI-FDTD methods have been proposed. They not only retain the same numerical computational efficiency as the conventional ADI-FDTD method, but also achieve similar accuracy to that with the CN-FDTD. In particular, the first method presents superior performance with the large time steps. Therefore, the work presented in this chapter has laid the foundations for further studies and extensive applications of the ADI-FDTD method.

Unfortunately error reduced ADI-FDTD is unstable in the 3-D case, still reason of instability is not clear, we are trying to find some way for it , while it is stable for the 2-D case. The simulation time and the memory taken by both methods are approximately the same as those for the conventional ADI-FDTD method with only minor increase in memory.
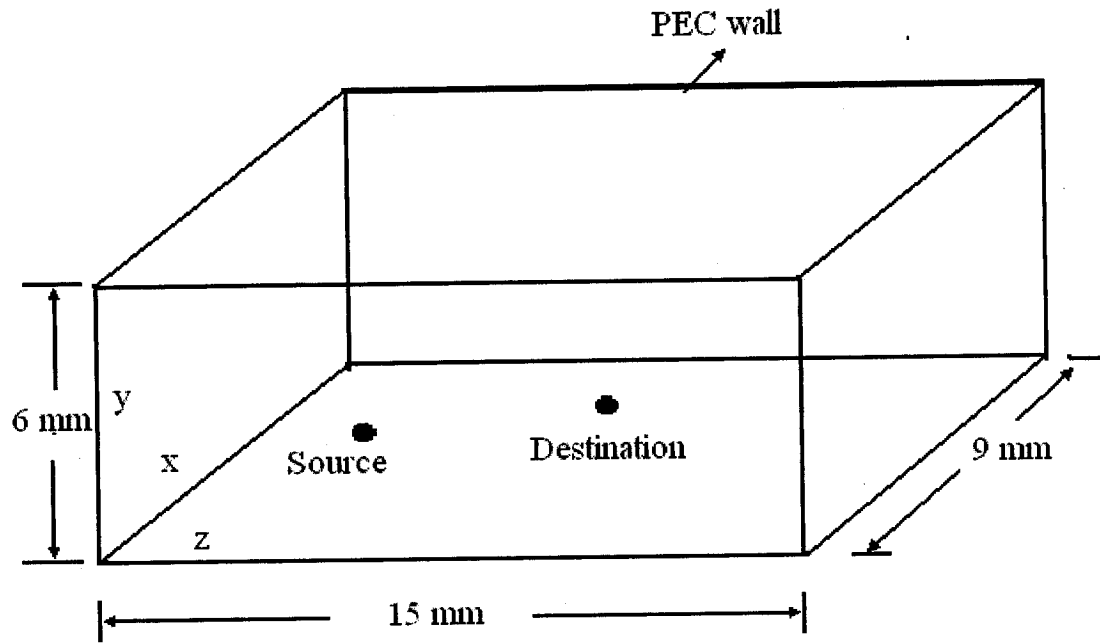
Fig. 5.5 Structure considered for 3-D case
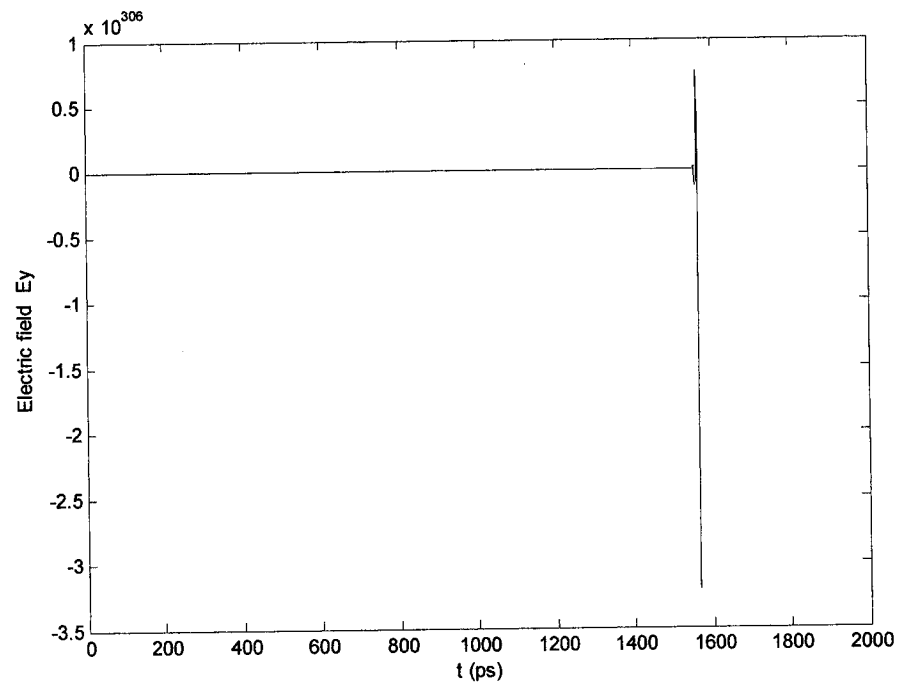
Fig. 5.6 3-D splitting error reduced ADI-FDTD

Chapter 6   Dispersion Optimized ADI-FDTD Methods

6.1   Introduction

Since Yee presented the FDTD method in 1966 [2], it has become such a mature technique [3-4] that many commercial software packages based on this algorithm have been developed and more are under way. However its CFL limit is still a limiting factor for electrically large and high Q structures. To compensate for this limit, unconditionally stable ADI-FDTD [6-7] method was presented and now is becoming an alternate to the FDTD method. Although ADI-FDTD is CFL free, it faces the problem of larger dispersion errors with bigger time steps. To get the real advantage of this unconditional stability, efforts have been put into controlling this dispersion problem [126][161-163]. In [161], dispersion reduction is presented for the two-dimensional case. In [162], higher order ADI-FDTD is introduced to reduce the dispersion but at the cost of simulation time and memory. In the previous chapter, error-reduced terms are added into the existing ADI-FDTD method to get the better results but instability problems still exist for the three-dimensional cases. In [164], improvement in dispersion is presented for the 2D ADI-FDTD method by introducing artificial anisotropy.

Similar to the FDTD method, the dispersion of the ADI-FDTD method is an inherent feature of the algorithm, which affects the overall accuracy. To circumvent this problem, reductions in cell size are needed and, as a result, increase the computation load. In this chapter, novel ways to minimize the numerical dispersion of the ADI-FDTD method are presented. In them, additional controlling parameters are introduced to reduce the dispersion error. These dispersion-optimized ADI-FDTD (DO-ADI-FDTD) methods improve accuracy in comparison with the original ADI-FDTD method but without additional computational complexity and loads. They are initially applied to one-dimensional ADI-FDTD and then extended to two and three-dimensional ADI-FDTD methods.

This chapter is divided into the following sections: in section 6.2, formulations of the 1-D

DO-ADI-FDTD method, its unconditional stability and dispersion are presented; in sections 6.3 and 6.4 this technique is extended to 2-D and 3-D cases respectively. Conclusions are presented in section 6.5. Note that the contents of this chapter have been published in [165].

6.2   Numerical Calculations for 1-D DO-ADI-FDTD

In a linear, lossless and isotropic medium, the differential form of Maxwell's equations is given as:

$$\nabla \times \vec{E} = -\mu \frac{\partial \vec{H}}{\partial t} \tag{6.1}$$

$$\nabla \times \vec{H} = \varepsilon \frac{\partial \vec{E}}{\partial t} \tag{6.2}$$

To control the dispersion, a controlling parameter B is introduced in the 1-D ADI-FDTD equations. Consider only E_z and H_y field components that travel in the x direction. Equations (6.1) and (6.2) become:

Step 1

$$E_z\Big|_i^{n+\frac{1}{2}} = E_z\Big|_i^{n} + B \frac{\Delta t}{2\varepsilon\Delta x}\left(H_y\Big|_{i+\frac{1}{2}}^{n+\frac{1}{2}} - H_y\Big|_{i-\frac{1}{2}}^{n+\frac{1}{2}} \right) \tag{6.3a}$$

$$H_y\Big|_{i+\frac{1}{2}}^{n+\frac{1}{2}} = H_y\Big|_{i+\frac{1}{2}}^{n} + B \frac{\Delta t}{2\mu\Delta x}\left(E_z\Big|_{i+1}^{n+\frac{1}{2}} - E_z\Big|_{i}^{n+\frac{1}{2}} \right) \tag{6.3b}$$

and
Step 2

$$E_z\Big|_i^{n+1} = E_z\Big|_i^{n+\frac{1}{2}} + B \frac{\Delta t}{2\varepsilon\Delta x}\left(H_y\Big|_{i+\frac{1}{2}}^{n+\frac{1}{2}} - H_y\Big|_{i-\frac{1}{2}}^{n+\frac{1}{2}} \right) \tag{6.4a}$$

$$H_y\big|_{i+\frac{1}{2}}^{n+1} = H_y\big|_{i+\frac{1}{2}}^{n+\frac{1}{2}} + B\frac{\Delta t}{2\mu\Delta x}\left(E_z\big|_{i+1}^{n+\frac{1}{2}} - E_z\big|_{i}^{n+\frac{1}{2}}\right)$$

(6.4b)

where Δt is the time increment and Δx space increment in x direction.

Equations (6.3) and (6.4) are basically same as the conventional 1-D ADI-FDTD formulations except a controlling parameter is introduced. It will be shown latter that B can lead to dispersion reduction. It is not easy to solve unknown field components in (6.3). For efficient computation, these equations should be decoupled. This decoupling is obtained by putting equation (6.3b) into (6.3a) and the resulting equation is (6.5a). There is no need of re-arrangement in equation (6.4) due to its explicit nature. The two-step computations then become:

<u>Step 1</u>

$$-(B\frac{\Delta t^2}{4\mu\varepsilon\Delta x^2})E_z\big|_{i+1}^{n+\frac{1}{2}} + (1+B\frac{\Delta t^2}{2\mu\varepsilon\Delta x^2})E_z\big|_{i}^{n+\frac{1}{2}} - (B\frac{\Delta t^2}{4\mu\varepsilon\Delta x^2})E_z\big|_{i-1}^{n+\frac{1}{2}}$$

$$= E_z\big|_{i}^{n} + B\frac{\Delta t}{2\varepsilon\Delta x}\left(H_y\big|_{i+\frac{1}{2}}^{n} - H_y\big|_{i-\frac{1}{2}}^{n}\right)$$

(6.5a)

$$-(B\frac{\Delta t^2}{4\mu\varepsilon\Delta x^2})H_y\big|_{i+\frac{3}{2}}^{n+\frac{1}{2}} + (1+B\frac{\Delta t^2}{2\mu\varepsilon\Delta x^2})H_y\big|_{i+\frac{1}{2}}^{n+\frac{1}{2}} - (B\frac{\Delta t^2}{4\mu\varepsilon\Delta x^2})H_y\big|_{i-\frac{1}{2}}^{n+\frac{1}{2}}$$

$$= H_y\big|_{i+\frac{1}{2}}^{n} + B\frac{\Delta t}{2\mu\Delta x}\left(E_z\big|_{i+1}^{n} - E_z\big|_{i}^{n}\right)$$

(6.5b)

and

<u>Step 2</u>

$$E_z\big|_{i}^{n+1} = E_z\big|_{i}^{n+\frac{1}{2}} + B\frac{\Delta t}{2\varepsilon\Delta x}\left(H_y\big|_{i+\frac{1}{2}}^{n+\frac{1}{2}} - H_y\big|_{i-\frac{1}{2}}^{n+\frac{1}{2}}\right)$$

(6.6a)

$$H_y\big|_{i+\frac{1}{2}}^{n+1} = H_y\big|_{i+\frac{1}{2}}^{n+\frac{1}{2}} + B\frac{\Delta t}{2\mu\Delta x}\left(E_z\big|_{i+1}^{n+\frac{1}{2}} - E_z\big|_{i}^{n+\frac{1}{2}}\right)$$

(6.6b)

In the following paragraphs, the above scheme will be shown to be unconditionally stable even with the parameter B. Assume that the spatial frequency is k_x along the x direction. The field components in the spatial spectral domain can be written as:

$$E_z \mid_i^n = E_z^n e^{-j(k_x i \Delta x)} \tag{6.7a}$$

$$H_y \mid_{i+\frac{1}{2}}^n = H_y^n e^{-j(k_x(i+\frac{1}{2})\Delta x)} \tag{6.7b}$$

Substitution of equations (6.7) into equation (6.5) leads to equations in the spatial spectral domain in terms of $k_x, \Delta t$ and Δx.

Step 1

$$(1 + B^2 \frac{\sin^2(\frac{k_x \Delta x}{2})\Delta t^2}{\mu \varepsilon \Delta x^2}) E_z^{n+\frac{1}{2}} = E_z^n - jB \frac{\sin(k_x \Delta x / 2)\Delta t}{\varepsilon \Delta x} H_y^n \tag{6.8a}$$

$$(1 + B^2 \frac{\sin^2(\frac{k_x \Delta x}{2})\Delta t^2}{\mu \varepsilon \Delta x^2}) H_y^{n+\frac{1}{2}} = H_y^n - jB \frac{\sin(k_x \Delta x / 2)\Delta t}{\varepsilon \Delta x} E_z^n \tag{6.8b}$$

or

$$\begin{bmatrix} E_z^{n+\frac{1}{2}} \\ H_y^{n+\frac{1}{2}} \end{bmatrix} = \begin{bmatrix} \dfrac{1}{R_x} & \dfrac{-jP_x}{\varepsilon R_x} \\ -\dfrac{jP_x}{\mu R_x} & \dfrac{1}{R_x} \end{bmatrix} \begin{bmatrix} E_z^n \\ H_y^n \end{bmatrix} \tag{6.9}$$

where $W_x = \dfrac{\Delta t}{\Delta x} \cdot \sin\left(\dfrac{k_x \Delta x}{2}\right), P_x = BW_x, R_x = 1 + \dfrac{P_x^2}{\mu \varepsilon}$

In compact form

$$\mathbf{F}^{n+\frac{1}{2}} = A_1 \mathbf{F}^n \tag{6.10}$$

94

where

$$\mathbf{F}^n = \begin{bmatrix} E_z^n \\ H_y^n \end{bmatrix}, \quad \mathbf{F}^{n+\frac{1}{2}} = \begin{bmatrix} E_z^{n+\frac{1}{2}} \\ H_y^{n+\frac{1}{2}} \end{bmatrix}$$

and

$$\Lambda_1 = \begin{bmatrix} \dfrac{1}{R_x} & \dfrac{-jP_x}{\varepsilon R_x} \\ -\dfrac{jP_x}{\mu R_x} & \dfrac{1}{R_x} \end{bmatrix}$$

Step 2

$$(1 + B^2 \frac{\sin^2(k_x \Delta x)\Delta t^2}{\mu \varepsilon \Delta x^2})E_z^{n+1} = E_z^{n+\frac{1}{2}} - jB \ \frac{\sin(k_x \Delta x / 2)\Delta t}{\varepsilon \Delta x} H_y^{n+\frac{1}{2}} \qquad (6.11a)$$

$$(1 + B^2 \frac{\sin^2(k_x \Delta x)\Delta t^2}{\mu \varepsilon \Delta x^2})H_y^{n+1} = H_y^{n+\frac{1}{2}} - jB \frac{\sin(k_x \Delta x / 2)\Delta t}{\varepsilon \Delta x} E_z^{n+\frac{1}{2}} \qquad (6.11b)$$

$$\begin{bmatrix} E_z^{n+1} \\ H_y^{n+1} \end{bmatrix} = \begin{bmatrix} 1 & \dfrac{-jP_x}{\varepsilon} \\ -\dfrac{jP_x}{\mu} & 1 \end{bmatrix} \begin{bmatrix} E_z^{n+\frac{1}{2}} \\ H_y^{n+\frac{1}{2}} \end{bmatrix},$$

In compact form,

$$\mathbf{F}^{n+1} = \Lambda_2 \mathbf{F}^{n+\frac{1}{2}} \qquad (6.11c)$$

where $\quad \mathbf{F}^{n+\frac{1}{2}} = \begin{bmatrix} E_z^{n+\frac{1}{2}} \\ H_y^{n+\frac{1}{2}} \end{bmatrix}, \quad \mathbf{F}^{n+1} = \begin{bmatrix} E_z^{n+1} \\ H_y^{n+1} \end{bmatrix}$

$$\Lambda_2 = \begin{bmatrix} 1 & \dfrac{-jP_x}{\varepsilon} \\ \\ -\dfrac{jP_x}{\mu} & 1 \end{bmatrix}$$

(6.12)

Now combination of (6.10) and (6.11c) reads

$$\mathbf{F}^{n+1} = \Lambda_2\Lambda_1\mathbf{F}^n = \Lambda\mathbf{F}^n$$

(6.13)

where

$$\Lambda = \frac{1}{R_x}\begin{bmatrix} 1-\dfrac{P_x^2}{\mu\varepsilon} & \dfrac{-j2P_x}{\varepsilon} \\ \\ -\dfrac{j2P_x}{\mu} & 1-\dfrac{P_x^2}{\mu\varepsilon} \end{bmatrix}$$

The eigenvalues of Λ can be found as:

$$\lambda_1 = \frac{\mu\varepsilon - P_x^2 + j2P_x\sqrt{\mu\varepsilon}}{\mu\varepsilon + P_x^2} \quad \text{and} \quad \lambda_2 = \frac{\mu\varepsilon - P_x^2 - j2P_x\sqrt{\mu\varepsilon}}{\mu\varepsilon + P_x^2}$$

or simply:

$$\lambda_1 = \frac{\sqrt{\mu\varepsilon} + jP_x}{\sqrt{\mu\varepsilon} - jP_x} \quad \text{and} \quad \lambda_2 = \frac{-\sqrt{\mu\varepsilon} + jP_x}{-\sqrt{\mu\varepsilon} - jP_x}$$

It is not difficult to see

$$|\lambda_1| = \sqrt{\frac{\left(\sqrt{\mu\varepsilon}\right)^2 + \left(P_x\right)^2}{\left(\sqrt{\mu\varepsilon}\right)^2 + \left(-P_x\right)^2}} = 1 \quad \text{and} \quad |\lambda_2| = \sqrt{\frac{\left(-\sqrt{\mu\varepsilon}\right)^2 + \left(P_x\right)^2}{\left(-\sqrt{\mu\varepsilon}\right)^2 + \left(-P_x\right)^2}} = 1$$

Therefore, the 1-D DO scheme is stable.

6.2.1   Numerical Dispersion

Numerical dispersion of (6.3)-(6.4) can be derived in the same way as that described in [126]. After some linear algebraic manipulations, the dispersion is found as:

$$(e^{j\omega\Delta t}\mathbf{I} - \Lambda)\mathbf{F} = 0 \tag{6.14}$$

Here I is a 2 by 2 identity matrix. To have a non-trivial solution of (6.14),

$$\det(e^{j\omega\Delta t}\mathbf{I} - \Lambda) = 0$$

or

$$\cos(\omega\Delta t) = \frac{\mu\varepsilon - P_x^2}{\mu\varepsilon + P_x^2} \tag{6.15}$$

since $1 + \cos(\omega\Delta t) = 1 + \dfrac{\mu\varepsilon - P_x^2}{\mu\varepsilon + P_x^2}$

$$\cos^2\left(\frac{\omega\Delta t}{2}\right) = \frac{\mu\varepsilon}{\mu\varepsilon + P_x^2} \tag{6.16}$$

Equation (6.16) can be further simplified (see Appendix # B) as:

$$\tilde{k} = \frac{2}{\Delta x}\sin^{-1}\left(\sqrt{\frac{\mu\varepsilon\Delta x^2}{B^2\Delta t^2}\left(\frac{1}{\cos^2\left(\frac{\omega\Delta t}{2}\right)} - 1\right)}\right) \tag{6.17}$$

By taking $\quad B = \dfrac{1}{\cos\left(\dfrac{\omega_\circ \Delta x}{2c}\right)} \qquad$ (see Appendix # C)

97

$$\tilde{k} = \frac{2}{\Delta x} \sin^{-1}\left(\sqrt{\frac{\mu \varepsilon \Delta x^2}{\Delta t^2}\left(\frac{1}{\cos^2(\frac{\omega \Delta t}{2})} - 1 \right)} \right) \qquad (6.18)$$

where ω_o is a chosen frequency at which the dispersion is sought to be minimized.

6.2.2 Numerical Results

In this section, optimization is discussed for the one-dimensional case. The optimization analysis is done at the frequency of interest. Fig 6.1 shows the results between normalized phase velocity and number of cells or points per wavelength. It is apparent from this figure that the dispersion results for both the proposed and the conventional methods become very close when the number of cells per wavelength increases. On the other hand, at lower number of cells per wavelength the proposed method is better than the conventional method. Fig. 6.2 shows values of the optimizing parameter B at different number of cells per wavelength. It is clear from this figure that the value of B decreases when the number of cells per wavelength increases and it is close to 1 above 90 cells per wavelength. This is the reason why normalized phase velocity of both methods is close to each other in Fig 6.1, when numbers of samples are above 90 per cell. It can be concluded from these results that when $B = 1$, then the proposed method reduces to the conventional ADI-FDTD method. Additionally, it also supports the corollary that when the number of cells per wavelength increases, it causes small cell size and, as a result both methods will approach to analytical results. In the next sections, 2D and 3D methods are explained with their numerical results.
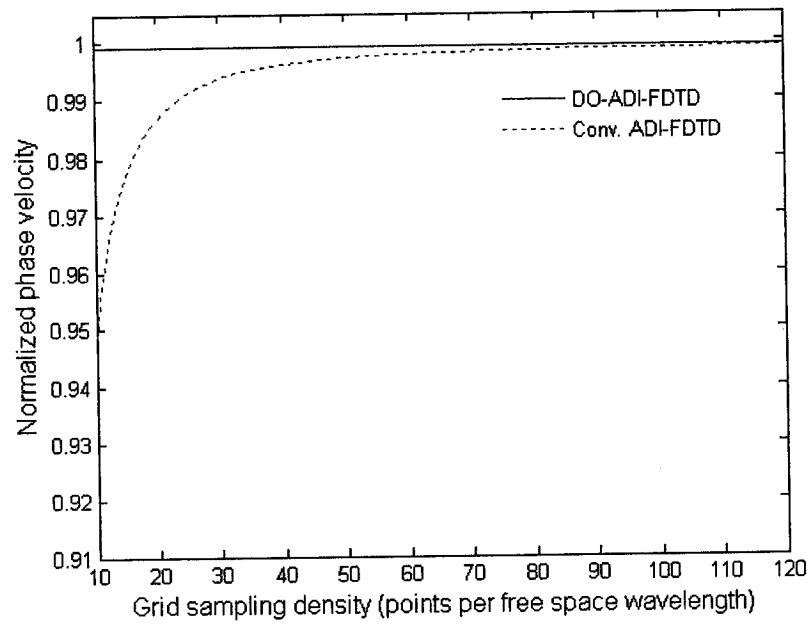
Fig. 6.1 Normalized phase velocity and numbers of cells per wavelength
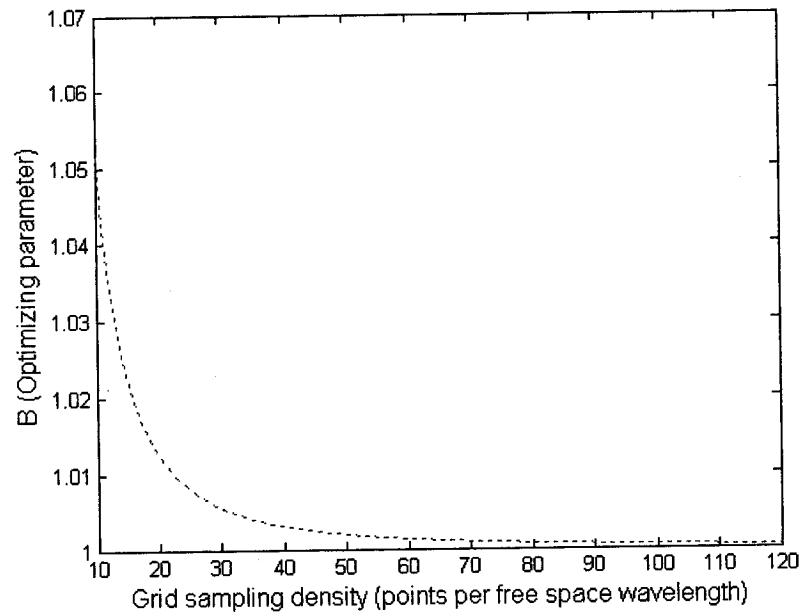
Fig. 6.2 The optimizing parameter B and the grid sampling density

6.3   Two-dimensional Dispersion-Optimized ADI-FDTD

For the two-dimensional electromagnetic structures, the procedure similar to that for the one-dimensional DO-ADI-FDTD method can be followed. In this section, 2-D equations for linear and lossless medium are considered for TE and TM modes. Maxwell's equations for 2-D TE case are:

$$\frac{\partial E_x}{\partial t} = \frac{1}{\varepsilon}\left(\frac{\partial H_z}{\partial y}\right) \tag{6.19a}$$

$$\frac{\partial E_y}{\partial t} = \frac{1}{\varepsilon}\left(-\frac{\partial H_z}{\partial x}\right) \tag{6.19b}$$

$$\frac{\partial H_z}{\partial t} = \frac{1}{\mu}\left(\frac{\partial E_x}{\partial y} - \frac{\partial E_y}{\partial x}\right) \tag{6.19c}$$

These equations in discretized form are given below in two DO-ADI-FDTD steps:

Step 1

$$\frac{E_x \big|_{i+\frac{1}{2},j}^{n+\frac{1}{2}} - E_x \big|_{i+\frac{1}{2},j}^{n}}{\Delta t / 2} = A\frac{1}{\varepsilon}\left(\frac{H_z \big|_{i+\frac{1}{2},j+\frac{1}{2}}^{n+\frac{1}{2}} - H_z \big|_{i+\frac{1}{2},j-\frac{1}{2}}^{n+\frac{1}{2}}}{\Delta y}\right) \tag{6.20a}$$

$$\frac{E_y \big|_{i,j+\frac{1}{2}}^{n+\frac{1}{2}} - E_y \big|_{i,j+\frac{1}{2}}^{n}}{\Delta t / 2} = B\frac{1}{\varepsilon}\left(-\frac{H_z \big|_{i+\frac{1}{2},j+\frac{1}{2}}^{n} - H_z \big|_{i-\frac{1}{2},j+\frac{1}{2}}^{n}}{\Delta x}\right) \tag{6.20b}$$

$$\frac{H_z\big|_{i+\frac{1}{2},j+\frac{1}{2}}^{n+\frac{1}{2}} - H_z\big|_{i+\frac{1}{2},j+\frac{1}{2}}^{n}}{\Delta t/2}$$

$$= \frac{1}{\mu}\left(A\frac{E_x\big|_{i+\frac{1}{2},j+1}^{n+\frac{1}{2}} - E_x\big|_{i+\frac{1}{2},j}^{n+\frac{1}{2}}}{\Delta y} - B\frac{E_y\big|_{i+1,j+\frac{1}{2}}^{n} - E_y\big|_{i,j+\frac{1}{2}}^{n}}{\Delta x}\right)$$
(6.20c)

Step 2

$$\frac{E_x\big|_{i+\frac{1}{2},j}^{n+1} - E_x\big|_{i+\frac{1}{2},j}^{n+\frac{1}{2}}}{\Delta t/2} = A\frac{1}{\varepsilon}\left(\frac{H_z\big|_{i+\frac{1}{2},j+\frac{1}{2}}^{n+\frac{1}{2}} - H_z\big|_{i+\frac{1}{2},j-\frac{1}{2}}^{n+\frac{1}{2}}}{\Delta y}\right)$$
(6.21a)

$$\frac{E_y\big|_{i,j+\frac{1}{2}}^{n+1} - E_y\big|_{i,j+\frac{1}{2}}^{n+\frac{1}{2}}}{\Delta t/2} = B\frac{1}{\varepsilon}\left(-\frac{H_z\big|_{i+\frac{1}{2},j+\frac{1}{2}}^{n+1} - H_z\big|_{i-\frac{1}{2},j+\frac{1}{2}}^{n+1}}{\Delta x}\right)$$
(6.21b)

$$\frac{H_z\big|_{i+\frac{1}{2},j+\frac{1}{2}}^{n+1} - H_z\big|_{i+\frac{1}{2},j+\frac{1}{2}}^{n+\frac{1}{2}}}{\Delta t/2}$$

$$= \frac{1}{\mu}\left(A\frac{E_x\big|_{i+\frac{1}{2},j+1}^{n+\frac{1}{2}} - E_x\big|_{i+\frac{1}{2},j}^{n+\frac{1}{2}}}{\Delta y} - B\frac{E_y\big|_{i+1,j+\frac{1}{2}}^{n+1} - E_y\big|_{i,j+\frac{1}{2}}^{n+1}}{\Delta x}\right)$$
(6.21c)

Similarly, Maxwell's equations for the 2-D TM case are written as:

$$\frac{\partial E_z}{\partial t} = \frac{1}{\varepsilon}\left(\frac{\partial H_y}{\partial x} - \frac{\partial H_x}{\partial y}\right)$$
(6.22a)

$$\frac{\partial H_x}{\partial t} = \frac{1}{\mu}\left(-\frac{\partial E_z}{\partial y}\right)$$
(6.22b)

101

$$\frac{\partial H_y}{\partial t} = \frac{1}{\mu}\left(\frac{\partial E_z}{\partial x}\right) \tag{6.22c}$$

These equations in discretized form are given below in two steps of DO-ADI-FDTD:

Step 1

$$\frac{E_z\big|_{i,j}^{n+\frac{1}{2}} - E_z\big|_{i,j}^{n}}{\Delta t/2}$$

$$= \frac{1}{\varepsilon}\left(B\frac{H_y\big|_{i+\frac{1}{2},j}^{n+\frac{1}{2}} - H_y\big|_{i-\frac{1}{2},j}^{n+\frac{1}{2}}}{\Delta x} - A\frac{H_x\big|_{i,j+\frac{1}{2}}^{n} - H_x\big|_{i,j-\frac{1}{2}}^{n}}{\Delta y}\right)$$

(6.23a)

$$\frac{H_x\big|_{i,j+\frac{1}{2}}^{n+\frac{1}{2}} - H_x\big|_{i,j+\frac{1}{2}}^{n}}{\Delta t/2} = \frac{1}{\mu}\left(-A\frac{E_z\big|_{i,j+1}^{n} - E_z\big|_{i,j}^{n}}{\Delta y}\right) \tag{6.23b}$$

$$\frac{H_y\big|_{i+\frac{1}{2},j}^{n+\frac{1}{2}} - H_y\big|_{i+\frac{1}{2},j}^{n}}{\Delta t/2} = B\frac{1}{\mu}\left(\frac{E_z\big|_{i+1,j}^{n+\frac{1}{2}} - E_z\big|_{i,j}^{n+\frac{1}{2}}}{\Delta x}\right) \tag{6.23c}$$

Step 2

$$\frac{E_z\big|_{i,j}^{n+1} - E_z\big|_{i,j}^{n+\frac{1}{2}}}{\Delta t/2} \tag{6.24a}$$

$$= \frac{1}{\varepsilon}\left(B\frac{H_y\big|_{i+\frac{1}{2},j}^{n+\frac{1}{2}} - H_y\big|_{i-\frac{1}{2},j}^{n+\frac{1}{2}}}{\Delta x} - A\frac{H_x\big|_{i,j+\frac{1}{2}}^{n+1} - H_x\big|_{i,j-\frac{1}{2}}^{n+1}}{\Delta y}\right)$$

102

$$\frac{H_x \big|_{i,j+\frac{1}{2}}^{n+1} - H_x \big|_{i,j+\frac{1}{2}}^{n+\frac{1}{2}}}{\Delta t / 2} = \frac{1}{\mu}\left(-A\,\frac{E_z \big|_{i,j+1}^{n+1} - E_z \big|_{i,j}^{n+1}}{\Delta y}\right) \qquad (6.24b)$$

$$\frac{H_y \big|_{i+\frac{1}{2},j}^{n+1} - H_y \big|_{i+\frac{1}{2},j}^{n+\frac{1}{2}}}{\Delta t / 2} = \frac{1}{\mu}\left(B\,\frac{E_z \big|_{i+1,j}^{n+\frac{1}{2}} - E_z \big|_{i,j}^{n+\frac{1}{2}}}{\Delta x}\right) \qquad (6.24c)$$

Now after decoupling the coupled equations in each step of both the TE and TM cases, these equations can be solved efficiently.

6.3.1 Numerical Stability of the Two-dimensional DO-ADI-FDTD

The stability analysis pattern is the same as for the 1-D DO-ADI-FDTD case; here, only results are presented for both TE and TM cases.

TE case

$$A_1 = \begin{bmatrix} \dfrac{1}{R_y} & \dfrac{P_x P_y}{\mu \varepsilon R_y} & \dfrac{-jP_y}{\varepsilon R_y} \\[2mm] 0 & 1 & \dfrac{jP_x}{\varepsilon} \\[2mm] \dfrac{-jP_y}{\mu R_y} & \dfrac{jP_x}{\mu R_y} & \dfrac{1}{R_y} \end{bmatrix} \qquad (6.25)$$

$$A_2 = \begin{bmatrix} 1 & 0 & -j\dfrac{P_y}{\varepsilon} \\[2mm] \dfrac{P_x P_y}{\mu \varepsilon R_x} & \dfrac{1}{R_x} & \dfrac{jP_x}{\varepsilon R_x} \\[2mm] \dfrac{-jP_y}{\mu R_x} & \dfrac{jP_x}{\mu R_x} & \dfrac{1}{R_x} \end{bmatrix} \qquad (6.26)$$

In short, the 2-D TE case equations in matrix form are shown below:

$$\mathbf{F}^{n+1} = \Lambda_2 \cdot \mathbf{F}^{n+\frac{1}{2}} = \Lambda_2 \Lambda_1 \mathbf{F}^n = \Lambda \mathbf{F}^n \qquad (6.27)$$

103

Here $\mathbf{F}^n$ contains 3 x 1 matrix.

$$\mathbf{F}^n = \begin{bmatrix} E_x^n \\ E_y^n \\ H_z^n \end{bmatrix}$$

(6.28)

and

$$\Lambda = \begin{bmatrix} \dfrac{\mu^2\varepsilon^2 + \mu\varepsilon(P_x^2 - P_y^2) + P_x^2 P_y^2}{\mu^2\varepsilon^2 R_x R_y} & \dfrac{2P_x P_y}{\mu\varepsilon R_x R_y} & \dfrac{-2jP_y}{\varepsilon R_x R_y} \\ \dfrac{2P_x P_y}{\mu\varepsilon R_x} & \dfrac{\mu\varepsilon - P_x^2}{\mu\varepsilon R_x} & \dfrac{2jP_x}{\varepsilon R_x} \\ \dfrac{-2jP_y}{\mu R_x R_y} & \dfrac{2jP_x}{\mu R_x R_y} & \dfrac{\mu^2\varepsilon^2 - \mu\varepsilon(P_x^2 + P_y^2) - P_x^2 P_y^2}{\mu^2\varepsilon^2 R_x R_y} \end{bmatrix}$$

(6.29)

$$P_\alpha = Q_\alpha \frac{\Delta t}{\Delta \alpha} \cdot \sin\left(\frac{k_\alpha \Delta \alpha}{2}\right), \quad \alpha = x, y$$

(6.30)

where $Q_x = B \quad Q_y = A \quad R_\alpha = 1 + \dfrac{P_\alpha^2}{\mu\varepsilon}, \quad \alpha = x, y$

(6.31)

The eigenvalues obtained after solving equation (6.29) are:

$$\lambda_1 = 1 \quad \lambda_2 = \frac{N_1 + jN_2}{N_3} \quad \lambda_3 = \frac{N_1 - jN_2}{N_3}$$

(6.32)

where

$$N_1 = \left(\mu\varepsilon + W_x^2\right)\left(\mu\varepsilon + W_y^2\right)$$

$$N_2 = \sqrt{4\mu^2\varepsilon^2\left(\mu\varepsilon P_x^2 + \mu\varepsilon P_y^2 + P_x^2 P_y^2\right)}$$

(6.33)

$$N_3 = \mu^2\varepsilon^2 - \mu\varepsilon P_x^2 - \mu\varepsilon P_y^2 - P_x^2 P_y^2$$

The magnitudes of the eigenvalues are then

$$|\lambda_2| = |\lambda_3| = \left|\frac{N_1 + jN_2}{N_3}\right| = \left|\frac{N_1 - jN_2}{N_3}\right| = \sqrt{\frac{N_1^2 + N_2^2}{N_3^2}} = 1$$

(6.34)

Therefore, the 2-D dispersion-optimized ADI-FDTD method is also unconditionally stable.

<u>TM case:</u>

The TM case is exactly like the 2-D TE case, except with different field components that are given as E_z, H_x and H_y instead of H_z, E_x and E_y.

In this case vector $\mathbf{F}^n$

$$\mathbf{F}^n = \begin{bmatrix} E_z^n \\ H_x^n \\ H_y^n \end{bmatrix}. \tag{6.35}$$

Λ_1, Λ_2 and Λ like TE case are given as:

$$\Lambda_1 = \begin{bmatrix} \dfrac{1}{R_x} & \dfrac{jP_y}{\varepsilon R_x} & -\dfrac{jP_x}{\varepsilon R_x} \\ \dfrac{jP_y}{\mu} & 1 & \dfrac{jP_x}{\varepsilon R_x} \\ -\dfrac{jP_x}{\mu R_x} & \dfrac{P_x P_y}{\mu \varepsilon R_x} & \dfrac{1}{R_x} \end{bmatrix} \tag{6.36}$$

$$\Lambda_2 = \begin{bmatrix} \dfrac{1}{R_y} & \dfrac{jP_y}{\varepsilon R_y} & -\dfrac{jP_x}{\varepsilon R_y} \\ \dfrac{jP_y}{\mu R_y} & \dfrac{1}{R_y} & \dfrac{P_x P_y}{\mu \varepsilon R_y} \\ -\dfrac{jP_x}{\mu} & 0 & 1 \end{bmatrix} \tag{6.37}$$

$$\Lambda = \begin{bmatrix} \dfrac{\mu^2 \varepsilon^2 - \mu \varepsilon (P_x^2 + P_y^2) - P_x^2 P_y^2}{\mu^2 \varepsilon^2 R_x R_y} & \dfrac{2jP_y}{\varepsilon R_x R_y} & -\dfrac{2jP_x}{\varepsilon R_x R_y} \\ \dfrac{2jP_y}{\mu R_x R_y} & \dfrac{\mu^2 \varepsilon^2 + \mu \varepsilon (P_x^2 - P_y^2) + P_x^2 P_y^2}{\mu^2 \varepsilon^2 R_x R_y} & \dfrac{2P_x P_y}{\mu \varepsilon R_x R_y} \\ -\dfrac{2jP_x}{\mu R_x} & \dfrac{2P_x P_y}{\mu \varepsilon R_x} & \dfrac{\mu \varepsilon - P_x^2}{\mu \varepsilon R_x} \end{bmatrix} \tag{6.38}$$

105

Here definitions of P_α and R_α are the same as given by equations (6.30) and (6.31), respectively.

The eigenvalues for the TM case are given below:

$$\lambda_1 = 1, \quad \lambda_2 = \frac{N_1 + jN_2}{N_3}, \lambda_3 = \frac{N_1 - jN_2}{N_3} \tag{6.39}$$

$$|\lambda_2| = |\lambda_3| = \left| \frac{N_1 + jN_2}{N_3} \right| = \left| \frac{N_1 - jN_2}{N_3} \right| = \sqrt{\frac{N_1^2 + N_2^2}{N_3^2}} = 1$$

Hence this case is also unconditionally stable.

6.3.2 Numerical Dispersion of 2-D TE and TM Case

After some linear algebraic manipulation, equation (6.27) is written in the form

$$(e^{j\omega\Delta t} I - \Lambda)F = 0 \tag{6.40}$$

Here Λ and I are 3 x 3 matrices, and dispersion relation in the form of eigenvalues is given as:

$$(e^{j\omega\Delta t} - \lambda_1)(e^{j\omega\Delta t} - \lambda_2)(e^{j\omega\Delta t} - \lambda_3) = 0 \tag{6.41}$$

λ_1, λ_2 and λ_3 are given in equations (6.32) and (6.34)

After solving of equation (6.41), two answers are obtained:

$$\omega = 0 \tag{6.42}$$

and

$$\sin^2(\omega\Delta t) = \frac{M^2}{L^2} = \frac{4\mu^2\varepsilon^2 \left(\mu\varepsilon P_x^2 + \mu\varepsilon P_y^2 + P_x^2 P_y^2 \right)}{\left(\mu\varepsilon + P_x^2 \right)^2 \left(\mu\varepsilon + P_y^2 \right)^2} \tag{6.43}$$

106

First solution in equation (6.42) indicates the non-propagating solution in the unconditionally stable DO-ADI-FDTD method, and the second solution (6.43) indicates the propagating solution.

The dispersion relation depends on the eigenvalues as is shown in equation (6.42). The eigenvalues found for the TM case are exactly the same as for the TE case; therefore dispersion relation for TE and TM mode is the same and is given as:

$$\sin^2(\omega\Delta t) = \frac{M^2}{L^2} = \frac{4\mu^2\varepsilon^2\left(\mu\varepsilon P_x^2 + \mu\varepsilon P_y^2 + P_x^2 P_y^2\right)}{\left(\mu\varepsilon + P_x^2\right)^2\left(\mu\varepsilon + P_y^2\right)^2} \tag{6.44}$$

This dispersion equation is further simplified by using a double angle formula:

$$\sin^2(\frac{\omega\Delta t}{2}) = \frac{\mu\varepsilon P_x^2 + \mu\varepsilon P_y^2 + P_x^2 P_y^2}{\left(\mu\varepsilon + P_x^2\right)\left(\mu\varepsilon + P_y^2\right)} \tag{6.45}$$

Equation (6.45) can also be written in the cosine form:

$$\cos^2(\frac{\omega\Delta t}{2}) = \frac{\mu^2\varepsilon^2}{\left(\mu\varepsilon + P_x^2\right)\left(\mu\varepsilon + P_y^2\right)} \tag{6.46}$$

By dividing equation (6.45) with equation (6.46), the resulting equation is:

$$\tan^2(\frac{\omega\Delta t}{2}) = \frac{\mu\varepsilon P_x^2 + \mu\varepsilon P_y^2 + P_x^2 P_y^2}{\mu^2\varepsilon^2} \tag{6.47}$$

6.3.3 Numerical Results for 2-D DO-ADI-FDTD

For the 2-D case, the dispersion analysis of DO-ADI-FDTD and the conventional ADI-FDTD methods are explained for four different options. The dispersion error can be minimized by varying the parameters A and B. In comparisons with the 1-D case, here are two dispersion optimizing parameters, A and B. By using different combination of these two parameters, dispersion error can be reduced. In the following, three combinations of A and B are considered.

Combination #1

$$A = \frac{\sqrt{\mu\varepsilon}\ \Delta y \tan\left(\frac{1}{2}c\,k\,\Delta t'\right)}{\sin\left(\frac{1}{2}k\,\Delta y\right)\Delta t'} \quad , \qquad B = \frac{\sqrt{\mu\varepsilon}\ \Delta x \tan\left(\frac{1}{2}c\,k\,\Delta t'\right)}{\sin\left(\frac{1}{2}k\,\Delta x\right)\Delta t'}$$

Here k is the numerical wavenumber, parameter A is obtained by setting $\phi = 90°$, while B is obtained by setting $\phi = 0°$ in equation (6.47) and then optimizing (6.47). Δx and Δy are cell sizes in x and y direction respectively. The CFL number (CFLN) is $CFLN = \frac{\Delta t}{\Delta t_{CFL}}$; where Δt_{CFL}, the CFL limit is:

$$\Delta t_{CFL} = \frac{1}{c\sqrt{\frac{1}{\Delta x^2} + \frac{1}{\Delta y^2}}}$$

Fig. 6.3 shows the dispersion with different time steps or CFL number. It is clear from this figure that the DO-ADI-FDTD is better than the conventional ADI-FDTD method, even with an increment in CFLN. The dispersion improvements are larger than 1%.

Combination #2

$$A = \frac{\sqrt{\mu\varepsilon}\ \Delta y \tan\left(\frac{1}{2}c\,k\,\Delta t'\right)}{\sin\left(\frac{1}{2}k\,\Delta y\right)\Delta t'} \quad , \qquad B = 1$$

In this option, A is the same as that in combination #1, while parameter B is intentionally taken as 1. This setting is chosen to examine the dispersion effect if the optimization is taken along the y direction only. Fig 6.4 shows the results obtained for this option.

108
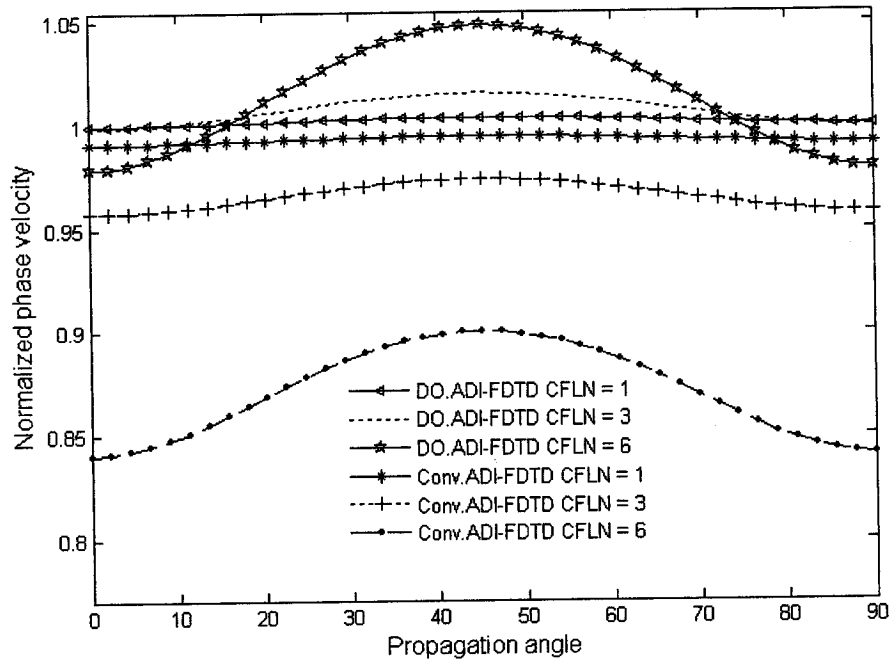
Fig. 6.3 Normalized phase velocity vs. propagation angle ϕ for different CFLN with combination 1
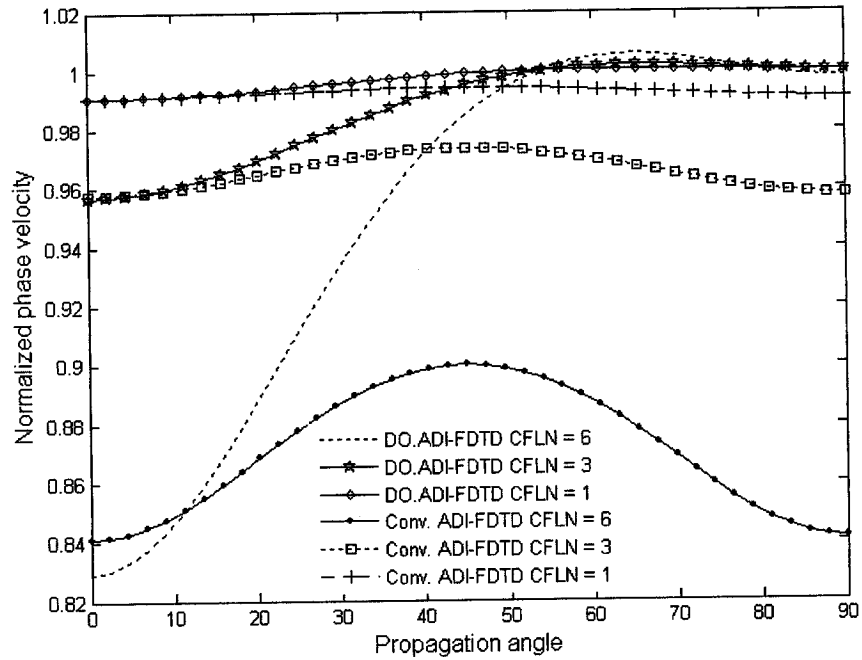
Fig. 6.4 Normalized phase velocity vs. propagation angle ϕ for different CFLN with combination 2

109

It demonstrates that when the propagation angle is small, then both methods have approximately the same dispersion errors. However, at an angle larger than $50°$, the DO-ADI-FDTD has much less dispersion error.

Combination #3

$$A=1 \qquad , \qquad B = \frac{\sqrt{\mu\varepsilon}\, \Delta x \tan\left(\frac{1}{2}c\,k\,\Delta t'\right)}{\sin\left(\frac{1}{2}k\,\Delta x\right)\Delta t'}$$

In this combination, B is the same as that in Combination #1, while A is taken as 1. The reason for this combination is to see the effect of dispersion when the optimization is taken along the x direction only. Fig 6.5 shows the results obtained for this combination are opposite to those obtained for Combination # 2. In this option, dispersion of the DO-ADI-FDTD is better than that of the conventional method at lower propagation angles but becomes almost the same beyond $50°$.
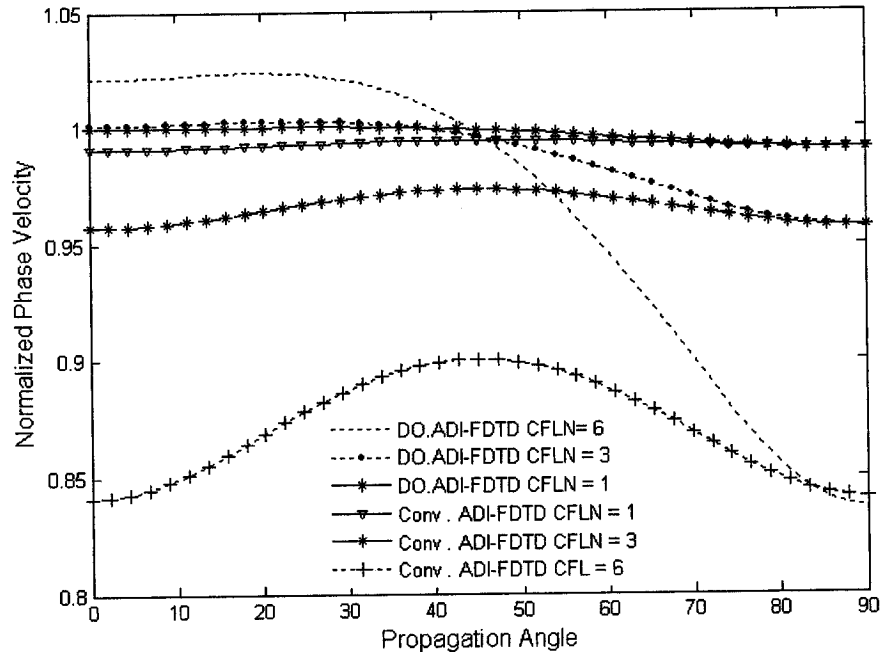
Fig. 6.5 Normalized phase velocity vs. propagation angle ϕ for different CFLN with combination 3

Combination #4

In this combination, A and B are the same as that in the 1-D case.

$$A = B = \left(\frac{1}{\cos(\frac{\omega_o \Delta t}{2})} \right)$$

ω_o is the frequency at which the dispersion is sought to be minimized. The dispersion is shown in Fig. 6.6. It is clear from this figure that the proposed combination has less dispersion than the conventional method. However, the improvements are above 0.6% and not as good as those with the other three combinations

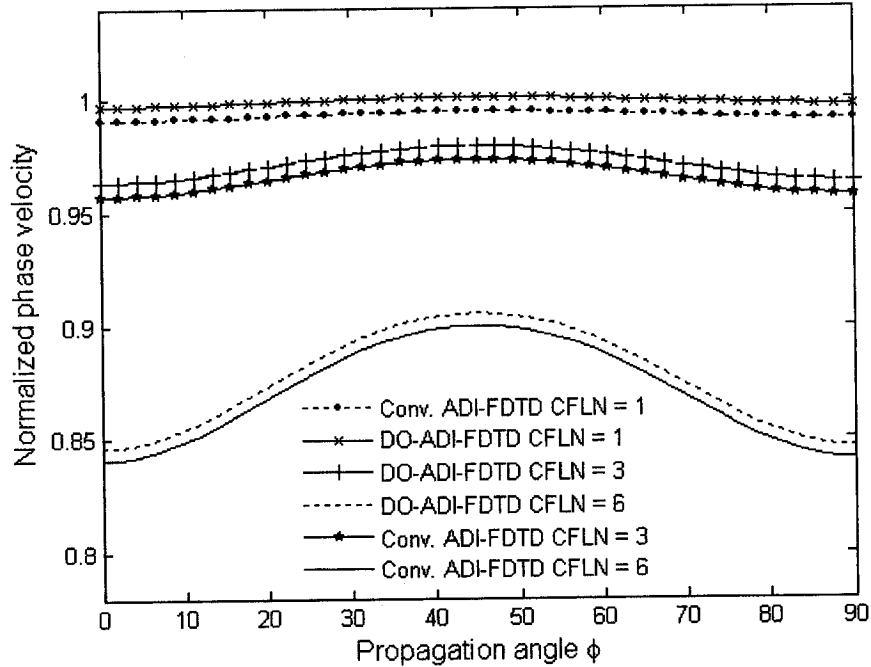Fig. 6.6 Normalized phase velocity vs. propagation angle ϕ for different CFLN with combination 4

6.4   Three-dimensional DO-ADI-FDTD

In the three-dimensional case, the same procedure as before can be followed. The Maxwell's equations to be solved are:

$$\frac{\partial E_x}{\partial t} = \frac{1}{\varepsilon}\left(\frac{\partial H_z}{\partial y} - \frac{\partial H_y}{\partial z}\right) \quad , \quad \frac{\partial E_y}{\partial t} = \frac{1}{\varepsilon}\left(\frac{\partial H_x}{\partial z} - \frac{\partial H_z}{\partial x}\right)$$

$$\frac{\partial E_z}{\partial t} = \frac{1}{\varepsilon}\left(\frac{\partial H_y}{\partial x} - \frac{\partial H_x}{\partial y}\right) \quad , \quad \frac{\partial H_x}{\partial t} = \frac{1}{\mu}\left(\frac{\partial E_y}{\partial z} - \frac{\partial E_z}{\partial y}\right)$$

$$\frac{\partial H_y}{\partial t} = \frac{1}{\mu}\left(\frac{\partial E_z}{\partial x} - \frac{\partial E_x}{\partial z}\right) \quad , \quad \frac{\partial H_z}{\partial t} = \frac{1}{\mu}\left(\frac{\partial E_x}{\partial y} - \frac{\partial E_y}{\partial x}\right)$$

The DO-ADI-FDTD formulations are then:

Step 1

$$E_x\Big|_{i+\frac{1}{2},j,k}^{n+\frac{1}{2}} = E_x\Big|_{i+\frac{1}{2},j,k}^{n} + A\frac{\Delta t}{2\varepsilon\Delta y}\left[H_z\Big|_{i+\frac{1}{2},j+\frac{1}{2},k}^{n+\frac{1}{2}} - H_z\Big|_{i+\frac{1}{2},j-\frac{1}{2},k}^{n+\frac{1}{2}}\right] - C\frac{\Delta t}{2\varepsilon\Delta z}\left[H_y\Big|_{i+\frac{1}{2},j,k+\frac{1}{2}}^{n} - H_y\Big|_{i+\frac{1}{2},j,k-\frac{1}{2}}^{n}\right] \qquad (6.48a)$$

$$E_y\Big|_{i,j+\frac{1}{2},k}^{n+\frac{1}{2}} = E_y\Big|_{i,j+\frac{1}{2},k}^{n} + C\frac{\Delta t}{2\varepsilon\Delta z}\left[H_x\Big|_{i,j+\frac{1}{2},k+\frac{1}{2}}^{n+\frac{1}{2}} - H_x\Big|_{i,j+\frac{1}{2},k-\frac{1}{2}}^{n+\frac{1}{2}}\right] - B\frac{\Delta t}{2\varepsilon\Delta x}\left[H_z\Big|_{i+\frac{1}{2},j+\frac{1}{2},k}^{n} - H_z\Big|_{i-\frac{1}{2},j+\frac{1}{2},k}^{n}\right] \qquad (6.48b)$$

$$E_z\Big|_{i,j,k+\frac{1}{2}}^{n+\frac{1}{2}} = E_z\Big|_{i,j,k+\frac{1}{2}}^{n} + B\frac{\Delta t}{2\varepsilon\Delta x}\left[H_y\Big|_{i+\frac{1}{2},j,k+\frac{1}{2}}^{n+\frac{1}{2}} - H_y\Big|_{i-\frac{1}{2},j,k+\frac{1}{2}}^{n+\frac{1}{2}}\right] - A\frac{\Delta t}{2\varepsilon\Delta y}\left[H_x\Big|_{i,j+\frac{1}{2},k+\frac{1}{2}}^{n} - H_x\Big|_{i,j-\frac{1}{2},k+\frac{1}{2}}^{n}\right] \qquad (6.48c)$$

$$H_x\Big|_{i,j+\frac{1}{2},k+\frac{1}{2}}^{n+\frac{1}{2}} = H_x\Big|_{i,j+\frac{1}{2},k+\frac{1}{2}}^{n} + C\frac{\Delta t}{2\mu\Delta z}\left[E_y\Big|_{i,j+\frac{1}{2},k+1}^{n+\frac{1}{2}} - E_y\Big|_{i,j+\frac{1}{2},k}^{n+\frac{1}{2}}\right] - A\frac{\Delta t}{2\mu\Delta y}\left[E_z\Big|_{i,j+1,k+\frac{1}{2}}^{n} - E_z\Big|_{i,j,k+\frac{1}{2}}^{n}\right] \qquad (6.48d)$$

$$H_y\Big|_{i+\frac{1}{2},j,k+\frac{1}{2}}^{n+\frac{1}{2}} = H_y\Big|_{i+\frac{1}{2},j,k+\frac{1}{2}}^{n} + B\frac{\Delta t}{2\mu\Delta x}\left[E_z\Big|_{i+1,j,k+\frac{1}{2}}^{n+\frac{1}{2}} - E_z\Big|_{i,j,k+\frac{1}{2}}^{n+\frac{1}{2}}\right] - C\frac{\Delta t}{2\mu\Delta z}\left[E_x\Big|_{i+\frac{1}{2},j,k+1}^{n} - E_x\Big|_{i+\frac{1}{2},j,k}^{n}\right] \qquad (6.48e)$$

112

$$H_z\Big|_{i+\frac{1}{2},j+\frac{1}{2},k}^{n+\frac{1}{2}} = H_z\Big|_{i+\frac{1}{2},j+\frac{1}{2},k}^{n} + A\frac{\Delta t}{2\mu\Delta y}\left[E_x\Big|_{i+\frac{1}{2},j+1,k}^{n+\frac{1}{2}} - E_x\Big|_{i+\frac{1}{2},j,k}^{n+\frac{1}{2}}\right] - B\frac{\Delta t}{2\mu\Delta x}\left[E_y\Big|_{i+1,j+\frac{1}{2},k}^{n} - E_y\Big|_{i,j+\frac{1}{2},k}^{n}\right] \qquad (6.48\text{f})$$

Step 2

$$E_x\Big|_{i+\frac{1}{2},j,k}^{n+1} = E_x\Big|_{i+\frac{1}{2},j,k}^{n+\frac{1}{2}} + A\frac{\Delta t}{2\varepsilon\Delta y}\left[H_z\Big|_{i+\frac{1}{2},j+\frac{1}{2},k}^{n+\frac{1}{2}} - H_z\Big|_{i+\frac{1}{2},j-\frac{1}{2},k}^{n+\frac{1}{2}}\right] - C\frac{\Delta t}{2\varepsilon\Delta z}\left[H_y\Big|_{i+\frac{1}{2},j,k+\frac{1}{2}}^{n+1} - H_y\Big|_{i+\frac{1}{2},j,k-\frac{1}{2}}^{n+1}\right] \qquad (6.49\text{a})$$

$$E_y\Big|_{i,j+\frac{1}{2},k}^{n+1} = E_y\Big|_{i,j+\frac{1}{2},k}^{n+\frac{1}{2}} + C\frac{\Delta t}{2\varepsilon\Delta z}\left[H_x\Big|_{i,j+\frac{1}{2},k+\frac{1}{2}}^{n+\frac{1}{2}} - H_x\Big|_{i,j+\frac{1}{2},k-\frac{1}{2}}^{n+\frac{1}{2}}\right] - B\frac{\Delta t}{2\varepsilon\Delta x}\left[H_z\Big|_{i+\frac{1}{2},j+\frac{1}{2},k}^{n+1} - H_z\Big|_{i-\frac{1}{2},j+\frac{1}{2},k}^{n+1}\right] \qquad (6.49\text{b})$$

$$E_z\Big|_{i,j,k+\frac{1}{2}}^{n+1} = E_z\Big|_{i,j,k+\frac{1}{2}}^{n+\frac{1}{2}} + B\frac{\Delta t}{2\varepsilon\Delta x}\left[H_y\Big|_{i+\frac{1}{2},j,k+\frac{1}{2}}^{n+\frac{1}{2}} - H_y\Big|_{i-\frac{1}{2},j,k+\frac{1}{2}}^{n+\frac{1}{2}}\right] - A\frac{\Delta t}{2\varepsilon\Delta y}\left[H_x\Big|_{i,j+\frac{1}{2},k+\frac{1}{2}}^{n+1} - H_x\Big|_{i,j-\frac{1}{2},k+\frac{1}{2}}^{n+1}\right] \qquad (6.49\text{c})$$

$$H_x\Big|_{i,j+\frac{1}{2},k+\frac{1}{2}}^{n+1} = H_x\Big|_{i,j+\frac{1}{2},k+\frac{1}{2}}^{n+\frac{1}{2}} + C\frac{\Delta t}{2\mu\Delta z}\left[E_y\Big|_{i,j+\frac{1}{2},k+1}^{n+\frac{1}{2}} - E_y\Big|_{i,j+\frac{1}{2},k}^{n+\frac{1}{2}}\right] - A\frac{\Delta t}{2\mu\Delta y}\left[E_z\Big|_{i,j+1,k+\frac{1}{2}}^{n+1} - E_z\Big|_{i,j,k+\frac{1}{2}}^{n+1}\right] \qquad (6.49\text{d})$$

$$H_y\Big|_{i+\frac{1}{2},j,k+\frac{1}{2}}^{n+1} = H_y\Big|_{i+\frac{1}{2},j,k+\frac{1}{2}}^{n+\frac{1}{2}} + B\frac{\Delta t}{2\mu\Delta x}\left[E_z\Big|_{i+1,j,k+\frac{1}{2}}^{n+\frac{1}{2}} - E_z\Big|_{i,j,k+\frac{1}{2}}^{n+\frac{1}{2}}\right] - C\frac{\Delta t}{2\mu\Delta z}\left[E_x\Big|_{i+\frac{1}{2},j,k+1}^{n+1} - E_x\Big|_{i+\frac{1}{2},j,k}^{n+1}\right] \qquad (6.49\text{e})$$

$$H_z\Big|_{i+\frac{1}{2},j+\frac{1}{2},k}^{n+1} = H_z\Big|_{i+\frac{1}{2},j+\frac{1}{2},k}^{n+\frac{1}{2}} + A\frac{\Delta t}{2\mu\Delta y}\left[E_x\Big|_{i+\frac{1}{2},j+1,k}^{n+\frac{1}{2}} - E_x\Big|_{i+\frac{1}{2},j,k}^{n+\frac{1}{2}}\right] - B\frac{\Delta t}{2\mu\Delta x}\left[E_y\Big|_{i+1,j+\frac{1}{2},k}^{n+1} - E_y\Big|_{i,j+\frac{1}{2},k}^{n+1}\right] \qquad (6.49\text{f})$$

It is not easy to handle unknown field components in equations (6.48a-6.48f) and (6.49a-6.49f). These equations can be re-arranged for efficient computation. For example, equation (6.48a) contains the unknown field components E_x and H_z. After substituting

113

equation (6.48d) into equation (6.48a), it becomes:

$$-(A^2\frac{\Delta t^2}{4\mu\varepsilon\Delta y^2})E_x\Big|_{i+\frac{1}{2},j+1,k}^{n+\frac{1}{2}} + (1+A^2\frac{\Delta t^2}{2\mu\varepsilon\Delta y^2})E_x\Big|_{i+\frac{1}{2},j,k}^{n+\frac{1}{2}} - (A^2\frac{\Delta t^2}{4\mu\varepsilon\Delta y^2})E_x\Big|_{i+\frac{1}{2},j-1,k}^{n+\frac{1}{2}}$$

$$= E_x\Big|_{i+\frac{1}{2},j,k}^{n} - AB\frac{\Delta t^2}{4\mu\varepsilon\Delta y\Delta x}\left(E_y\Big|_{i+1,j+\frac{1}{2},k}^{n} - E_y\Big|_{i,j+\frac{1}{2},k}^{n} - E_y\Big|_{i+1,j-\frac{1}{2},k}^{n} + E_y\Big|_{i,j-\frac{1}{2},k}^{n}\right)$$

$$+ A\frac{\Delta t}{2\varepsilon\Delta y}\left(H_z\Big|_{i+\frac{1}{2},j+\frac{1}{2},k}^{n} - H_z\Big|_{i+\frac{1}{2},j-\frac{1}{2},k}^{n}\right) - C\frac{\Delta t}{2\varepsilon\Delta z}\left(H_y\Big|_{i+\frac{1}{2},j,k+\frac{1}{2}}^{n} - H_y\Big|_{i+\frac{1}{2},j,k-\frac{1}{2}}^{n}\right)$$

Here three constants A, B and C are introduced to minimize the dispersion errors. By writing (6.48 – 6.49) in the spectral domain one can obtain:

$$\mathbf{F}^{n+1} = \mathbf{\Lambda}\mathbf{F}^{n} \tag{6.50}$$

where $\mathbf{\Lambda}$ was obtained by using Maple 9.0 and is given as:

$$\mathbf{\Lambda} = \begin{bmatrix} \dfrac{E_1+F_1}{R_xR_yR_z} & \dfrac{2\mu\varepsilon P_xP_y}{R_xR_y} & \dfrac{2\mu\varepsilon P_xP_z}{R_yR_z} & \dfrac{-2j\mu T}{R_xR_y} & \dfrac{2j\mu^2\varepsilon P_z}{R_yR_z} & \dfrac{2j\mu D_1}{R_xR_yR_z} \\[2mm] \dfrac{2\mu\varepsilon P_yP_x}{R_zR_x} & \dfrac{E_2+F_2}{R_xR_yR_z} & \dfrac{2\mu\varepsilon P_yP_z}{R_yR_z} & \dfrac{2j\mu D_2}{R_xR_yR_z} & \dfrac{-2j\mu T}{R_yR_z} & \dfrac{2j\mu^2\varepsilon P_x}{R_zR_x} \\[2mm] \dfrac{2\mu\varepsilon P_zP_x}{R_zR_x} & \dfrac{2\mu\varepsilon P_zP_y}{R_xR_y} & \dfrac{E_3+F_3}{R_xR_yR_z} & \dfrac{2j\mu^2\varepsilon P_y}{R_xR_y} & \dfrac{2j\mu D_3}{R_xR_yR_z} & \dfrac{-2j\mu T}{R_zR_x} \\[2mm] \dfrac{-2j\varepsilon T}{R_xR_z} & \dfrac{2j\varepsilon D_2}{R_xR_yR_z} & \dfrac{2j\mu\varepsilon^2 P_y}{R_yR_z} & \dfrac{E_1+F_3}{R_xR_yR_z} & \dfrac{2\mu\varepsilon P_xP_y}{R_yR_z} & \dfrac{2\mu\varepsilon P_zP_x}{R_zR_x} \\[2mm] \dfrac{2j\mu\varepsilon^2 P_z}{R_zR_x} & \dfrac{-2j\varepsilon T}{R_yR_x} & \dfrac{2j\varepsilon D_3}{R_xR_yR_z} & \dfrac{2\mu\varepsilon P_xP_y}{R_xR_y} & \dfrac{E_2+F_1}{R_xR_yR_z} & \dfrac{2\mu\varepsilon P_yP_z}{R_zR_x} \\[2mm] \dfrac{2j\varepsilon D_1}{R_xR_yR_z} & \dfrac{2j\mu\varepsilon^2 P_x}{R_xR_y} & \dfrac{-2j\varepsilon T}{R_zR_y} & \dfrac{2\mu\varepsilon P_zP_x}{R_xR_y} & \dfrac{2\mu\varepsilon P_yP_z}{R_yR_z} & \dfrac{E_3+F_2}{R_xR_yR_z} \end{bmatrix}$$

where

$$P_\alpha = Q_\alpha\frac{\Delta t}{\Delta\alpha}\cdot\sin\left(\frac{k_\alpha\Delta\alpha}{2}\right), \quad \alpha=x,y,z, \quad W_\alpha = \frac{\Delta t}{\Delta\alpha}\cdot\sin\left(\frac{k_\alpha\Delta\alpha}{2}\right), \quad \alpha=x,y,z$$

$$R_\alpha = 1 + Q_\alpha^2 \frac{W_\alpha^2}{\mu\varepsilon}, \quad \alpha = x, y, z, \quad Q_x^2 = B^2, \quad Q_y^2 = A^2, \quad Q_z^2 = C^2$$

$$R_x = 1 + \frac{P_x^2}{\mu\varepsilon}, \qquad R_y = 1 + \frac{P_y^2}{\mu\varepsilon}, \qquad R_z = 1 + \frac{P_z^2}{\mu\varepsilon}, \quad , \quad T = P_x P_y P_z$$

$$P_x = B \frac{\Delta t}{\Delta x} \sin(\frac{k \sin\theta \sin\phi \Delta x}{2}), \quad P_y = A \frac{\Delta t}{\Delta y} \sin(\frac{k \sin\theta \cos\phi \Delta y}{2}), \quad P_z = C \frac{\Delta t}{\Delta z} \sin(\frac{k \cos\theta \Delta z}{2})$$

$$E_1 = \mu^3 \varepsilon^3 + \mu^2 \varepsilon^2 (P_x^2 - P_y^2 - P_z^2) + T^2, \quad E_2 = \mu^3 \varepsilon^3 + \mu^2 \varepsilon^2 (P_y^2 - P_z^2 - P_x^2) + T^2$$

$$E_3 = \mu^3 \varepsilon^3 + \mu^2 \varepsilon^2 (P_z^2 - P_x^2 - P_y^2) + T^2, \quad F_1 = \mu\varepsilon (P_x^2 P_y^2 - P_y^2 P_z^2 - P_z^2 P_x^2)$$

$$F_2 = \mu\varepsilon (P_y^2 P_z^2 - P_z^2 P_x^2 - P_x^2 P_y^2), \quad F_3 = \mu\varepsilon (P_z^2 P_x^2 - P_x^2 P_y^2 - P_y^2 P_z^2)$$

$$D_1 = P_x P_z T - \mu^2 \varepsilon^2 P_y, \quad D_2 = P_y P_x T - \mu^2 \varepsilon^2 P_z, \quad D_3 = P_z P_y T - \mu^2 \varepsilon^2 P_x$$

The eigenvalues of Λ can be found as:

$$\lambda_1 = \lambda_2 = 1, \quad \lambda_3 = \lambda_5 = \frac{M_1 + jM_2}{M_3}, \quad \lambda_4 = \lambda_6 = \lambda_3 = \frac{M_1 - jM_2}{M_3}$$

where

$$M_1 = \mu^3 \varepsilon^3 - \mu\varepsilon \left(\mu\varepsilon P_x^2 + \mu\varepsilon P_y^2 + \mu\varepsilon P_z^2 + P_x^2 P_y^2 + P_y^2 P_z^2 + P_z^2 P_x^2 \right) + P_x^2 P_y^2 P_z^2$$

$$M_2 = \sqrt{4\mu\varepsilon \left(\mu\varepsilon P_x^2 + \mu\varepsilon P_y^2 + \mu\varepsilon P_z^2 + P_x^2 P_y^2 + P_y^2 P_z^2 + P_z^2 P_x^2 \right)\left(\mu^3 \varepsilon^3 + P_x^2 P_y^2 P_z^2 \right)}$$

and

$$M_3 = \left(\mu\varepsilon + P_x^2 \right)\left(\mu\varepsilon + P_y^2 \right)\left(\mu\varepsilon + P_z^2 \right)$$

The magnitudes of the eigenvalues are:

115

$$|\lambda_3| = |\lambda_4| = |\lambda_5| = |\lambda_6| = \left| \frac{M1 + jM2}{M3} \right| = \left| \frac{M1 - jM2}{M3} \right|$$

$$= \sqrt{\frac{M1^2 + M2^2}{M3^2}} = 1$$

Therefore, the 3D dispersion-optimized ADI-FDTD is unconditionally stable.
The numerical dispersion can be obtained from equation (6.50)

$$(e^{j\omega\Delta t}\mathbf{I} - \mathbf{\Lambda})\mathbf{F} = 0$$

which can be simplified to:

$$\sin^2(\omega\Delta t) = \frac{4\mu\varepsilon\left(\mu\varepsilon P_x^2 + \mu\varepsilon P_y^2 + \mu\varepsilon P_z^2 + P_x^2 P_y^2 + P_y^2 P_z^2 + P_z^2 P_x^2\right)\left(\mu^3\varepsilon^3 + P_x^2 P_y^2 P_z^2\right)}{\left(\mu\varepsilon + P_x^2\right)^2\left(\mu\varepsilon + P_y^2\right)^2\left(\mu\varepsilon + P_z^2\right)^2} \tag{6.51}$$

Equation (6.51) indicates the propagating mode of the DO-ADI-FDTD method. The dispersion relation for the conventional ADI-FDTD method is

$$\sin^2(\omega\Delta t) = \frac{4\mu\varepsilon\left(\mu\varepsilon W_x^2 + \mu\varepsilon W_y^2 + \mu\varepsilon W_z^2 + W_x^2 W_y^2 + W_y^2 W_z^2 + W_z^2 W_x^2\right)\left(\mu^3\varepsilon^3 + W_x^2 W_y^2 W_z^2\right)}{\left(\mu\varepsilon + W_x^2\right)^2\left(\mu\varepsilon + W_y^2\right)^2\left(\mu\varepsilon + W_z^2\right)^2} \tag{6.52}$$

Calculating the dispersion error from equation (6.51) is complex, and can be simplified by using the double angle formula,

$$\sin^2(\omega\Delta t) = 4\sin^2\left(\frac{\omega\Delta t}{2}\right)\cos^2\left(\frac{\omega\Delta t}{2}\right) = 4\sin^2\left(\frac{\omega\Delta t}{2}\right) - 4\sin^4\left(\frac{\omega\Delta t}{2}\right) \tag{6.53}$$

By comparing equations (6.51) and (6.53), the following equation is obtained,

$$-\sin^2\left(\frac{\omega\Delta t}{2}\right) + \sin^4\left(\frac{\omega\Delta t}{2}\right) + \frac{JG}{(J+G)^2} = 0 \tag{6.54}$$

where

116

$$J = \varepsilon\mu\left(\varepsilon\mu P_x^2 + \varepsilon\mu P_y^2 + \varepsilon\mu P_z^2 + P_x^2 P_y^2 + P_y^2 P_z^2 + P_x^2 P_z^2\right), \quad G = \varepsilon^3 \mu^3 + P_x^2 P_y^2 P_z^2$$

Now equation (6.54) is further simplified as:

$$
\sin^2(\frac{\omega \Delta t}{2}) = \frac{\mu\varepsilon\left(\mu\varepsilon P_x^2 + \mu\varepsilon P_y^2 + \mu\varepsilon P_z^2 + P_x^2 P_y^2 + P_y^2 P_z^2 + P_z^2 P_x^2\right)}{\left(\mu\varepsilon + P_x^2\right)\left(\mu\varepsilon + P_y^2\right)\left(\mu\varepsilon + P_z^2\right)}
\tag{6.55}
$$

Equation (6.55) can be written in cosine form,

$$
\cos^2(\frac{\omega \Delta t}{2}) = \frac{\left(\mu^3 \varepsilon^3 + P_x^2 P_y^2 P_z^2\right)}{\left(\mu\varepsilon + P_x^2\right)\left(\mu\varepsilon + P_y^2\right)\left(\mu\varepsilon + P_z^2\right)}
\tag{6.56}
$$

After dividing equation (6.55) by (6.56), the dispersion equation in tangent form is

$$
\tan^2(\frac{\omega \Delta t}{2}) = \frac{\mu\varepsilon\left(\mu\varepsilon\, P_x^2 + \mu\varepsilon\, P_y^2 + \mu\varepsilon\, P_z^2 + P_x^2 P_y^2 + P_y^2 P_z^2 + P_z^2 P_x^2\right)}{\left(\mu^3 \varepsilon^3 + P_x^2 P_y^2 P_z^2\right)}
\tag{6.57}
$$

Now equations (6.55)-(6.57) are more simplified as compared to equation (6.51) and are easy to handle for dispersion analyses. Any of the equations (6.55-6.57) can be used for dispersion analyses by using Newton's iterative method.

6.4.1 Numerical Results for Three-dimensional DO-ADI-FDTD

In the three-dimensional case, three controlling parameters A, B and C are introduced. Different combinations of A, B and C will lead to different dispersion characteristics. In the following, four combinations are considered.

Combination #1

In this option, A and B are taken as one, C is obtained by setting $\theta = 0°$ and $\phi = 90°$ in equation (6.57) and then optimized it.

$$A=1, \quad B=1, \quad C = \frac{\sqrt{\mu\varepsilon}\, \Delta z \tan\left(\frac{1}{2}c\,k\,\Delta t\right)}{\sin\left(\frac{1}{2}k\,\Delta z\right)\Delta t}$$

CFLN is the CFL number equal to $\frac{\Delta t}{\Delta t_{CFL}}$ with Δt_{CFL} being the CFL time step limit.

Fig 6.7 shows the dispersion characteristics. It can be seen that the DO-ADI-FDTD has less dispersion than the conventional ADI-FDTD for $\theta < 50°$.
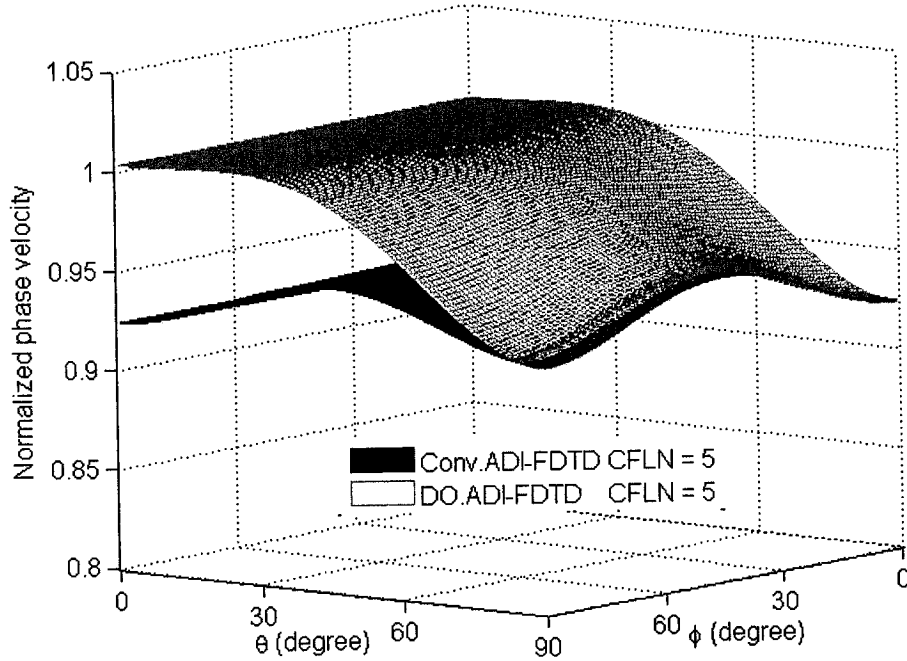
Fig. 6.7 Numerical dispersion for combination 1 and the conventional ADI-FDTD method

Combination #2

$$A = 1, \quad B = \frac{\sqrt{\mu\varepsilon}\,\Delta x\tan\left(\dfrac{1}{2}c\,k\,\Delta t\right)}{\sin\left(\dfrac{1}{2}k\,\Delta x\right)\Delta t}, \quad C = 1$$

In this combination, parameter B is obtained by setting $\theta = 90°$ and $\phi = 90°$ in equation (6.57) and optimizing it. The parameters A and C are set to 1 in order to examine the dispersion characteristics due to the optimization in the x- direction only. The results obtained are shown in Fig 6.8. The DO-ADI-FDTD method has better dispersion characteristics than that of the ADI-FDTD method when $\theta > 50°$.
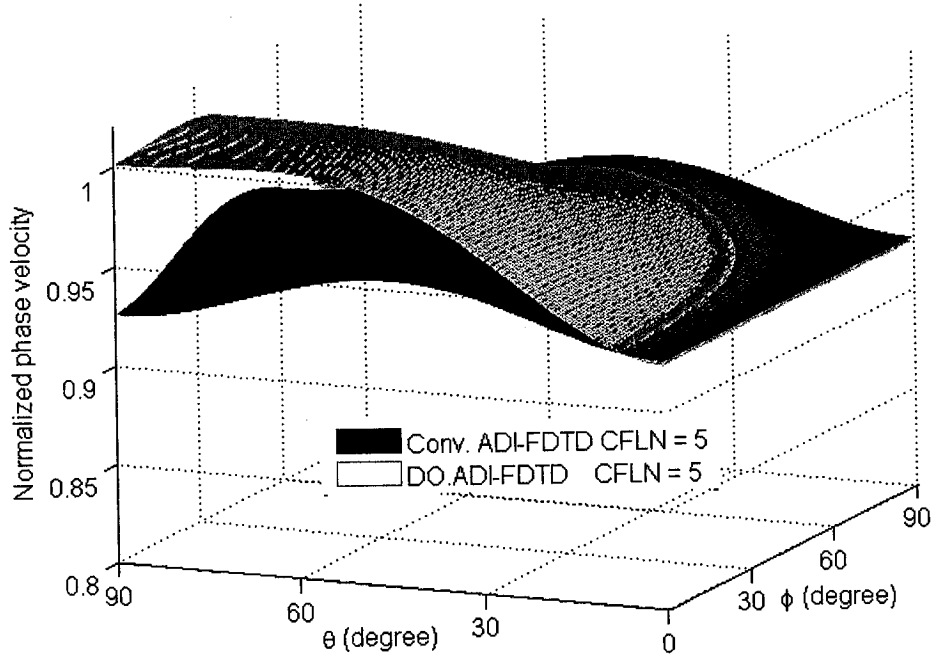
Fig. 6.8 Numerical dispersion for combination 2 and the conventional ADI-FDTD method

Combination #3

$$A = \frac{\sqrt{\mu\varepsilon} \, \Delta y \tan\left(\frac{1}{2} c \, k \, \Delta t\right)}{\sin\left(\frac{1}{2} k \, \Delta y\right) \Delta t}, \quad B = 1, \quad C = 1$$

The parameter setting for this combination is set to see the effect on dispersion characteristics by optimization only in the y direction. A is obtained by setting $\theta = 90°$ and $\phi = 0°$ in equation (6.57) and then optimizing it. The dispersion characteristic is shown in Fig 6.9.

Fig. 6.9 Numerical dispersion for combination 3 and the conventional ADI-FDTD method

Combination #4

In this combination, the setting is used to see the dispersion characteristics when optimization is made in all three directions (x, y and z).

120

$$A = \frac{\sqrt{\mu\varepsilon}\,\Delta y \tan\left(\frac{1}{2}c\,k\,\Delta t'\right)}{\sin\left(\frac{1}{2}k\,\Delta y\right)\Delta t'} \; , \; B = \frac{\sqrt{\mu\varepsilon}\,\Delta x \tan\left(\frac{1}{2}c\,k\,\Delta t'\right)}{\sin\left(\frac{1}{2}k\,\Delta x\right)\Delta t'} \; , \; C = \frac{\sqrt{\mu\varepsilon}\,\Delta z \tan\left(\frac{1}{2}c\,k\,\Delta t'\right)}{\sin\left(\frac{1}{2}k\,\Delta z\right)\Delta t'}$$

Fig 6.10 shows the numerical dispersion for this combination with CFL factor equal to 5 and it demonstrates that the DO-ADI-FDTD is better than the conventional method.
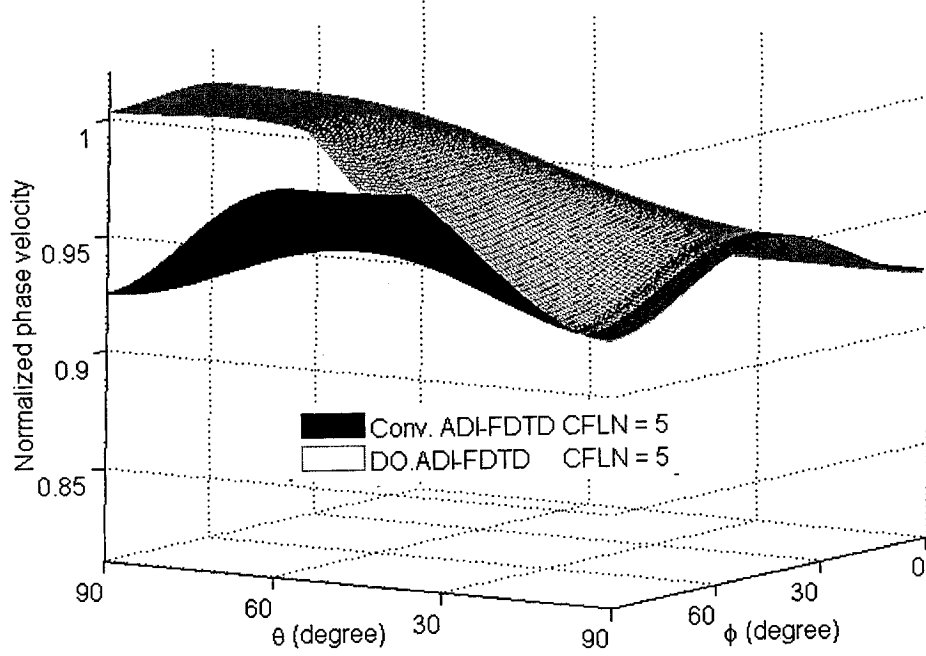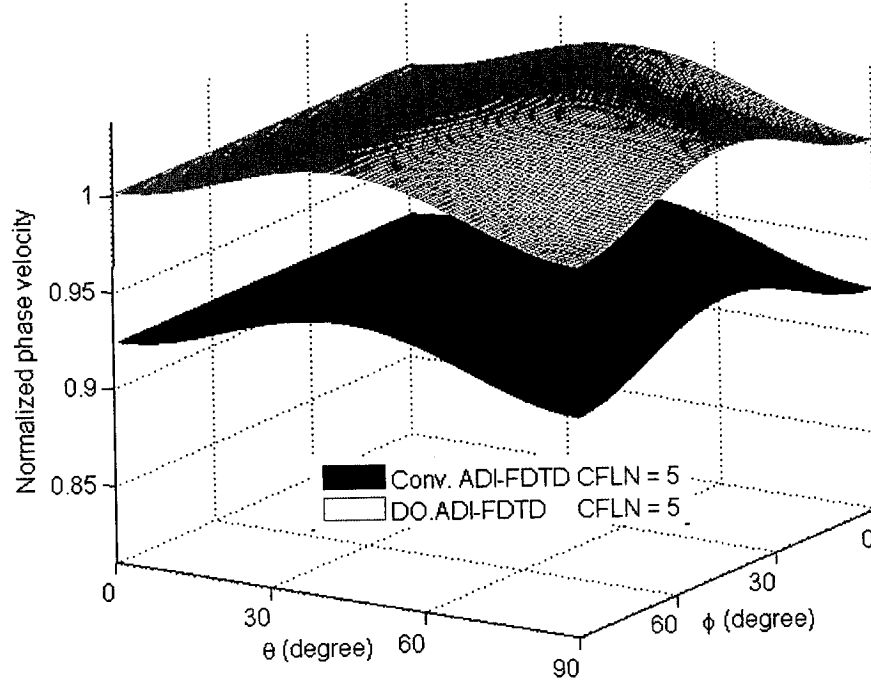

Fig. 6.10 Numerical dispersion for combination 4 and the conventional ADI-FDTD method

Combination #5

In this combination A, B and C are taken the same as those for the one dimensional case.

$$A = B = C = \left(\frac{1}{\cos(\frac{\omega_o \Delta t}{2})}\right)$$

ω_o is the frequency at which the dispersion error is to be minimized. Fig 6.11 shows the

121

normalized phase velocity vs. wave propagation angles θ and ϕ for this combination, while the cell size $= \frac{\lambda}{20}$ and the $CFLN = 1$. Fig 6.12 shows the results of the normalized phase velocity vs. propagation angle for different cell sizes with the CFL number (ratio of time step to CFL time step limit) equal to 5. It is clear from these figures that the proposed combination is better than that of the conventional method. The improvement, however, is rather moderate, about 0.4%.
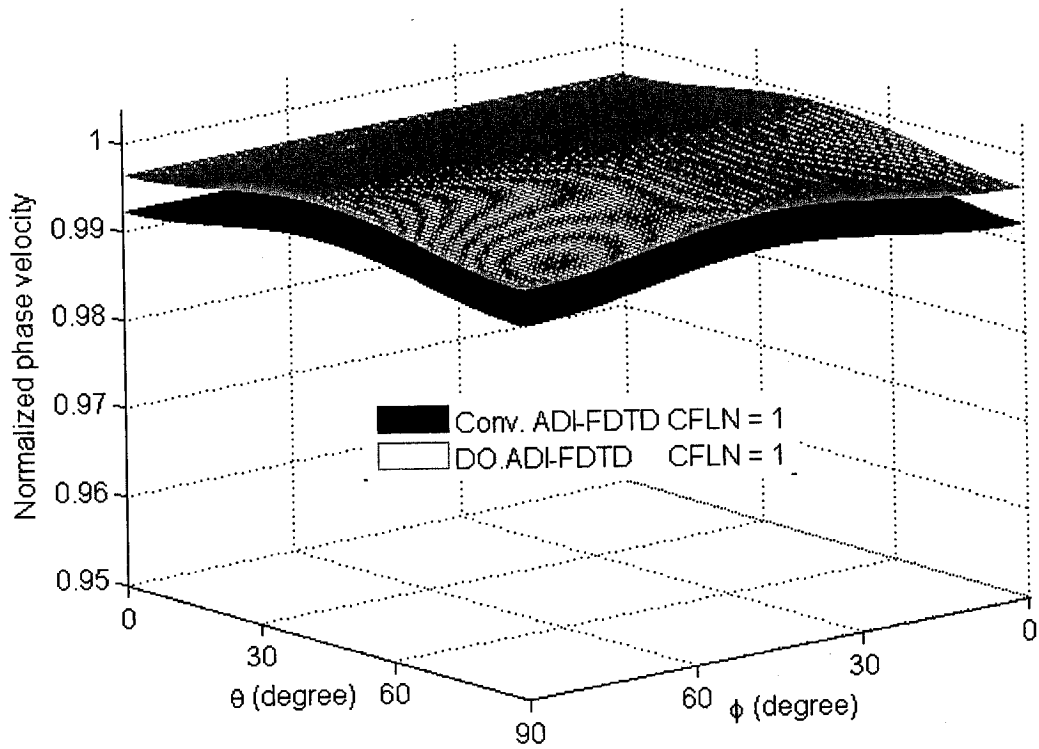
Fig. 6.11 Numerical dispersion for the combination 5 and the conventional ADI-FDTD method

Fig 6.13 shows the absolute error versus the CFL number, where absolute error is indicated in percentage. To calculate the percentage absolute error FDTD at CFLN = 0.5 was used as a reference. The DO-ADI-FDTD method shows less dispersion than that of the conventional ADI-FDTD method. These results are obtained by using Combination

#3 as an example. Similar results can be obtained for other four combinations.
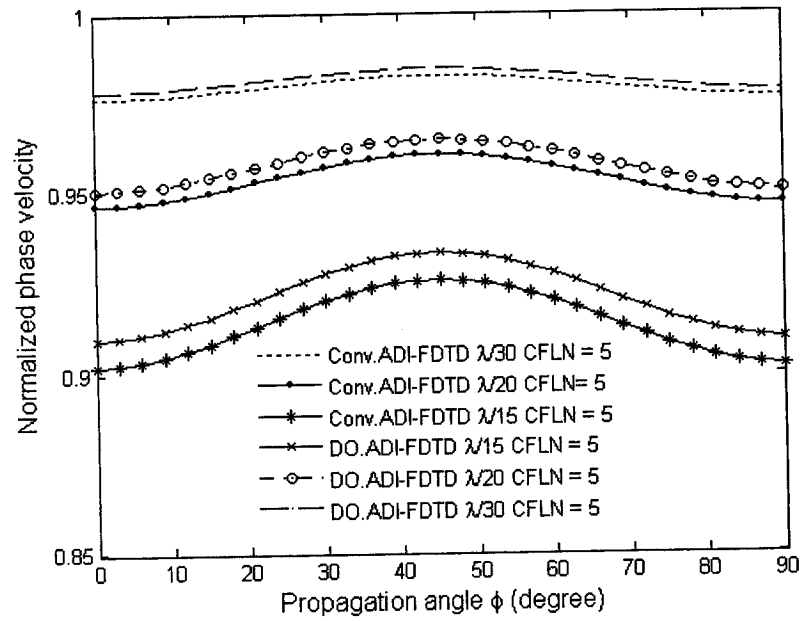
Fig. 6. 12 Normalized phase velocity vs. propagation angle for different cell sizes with combination 5
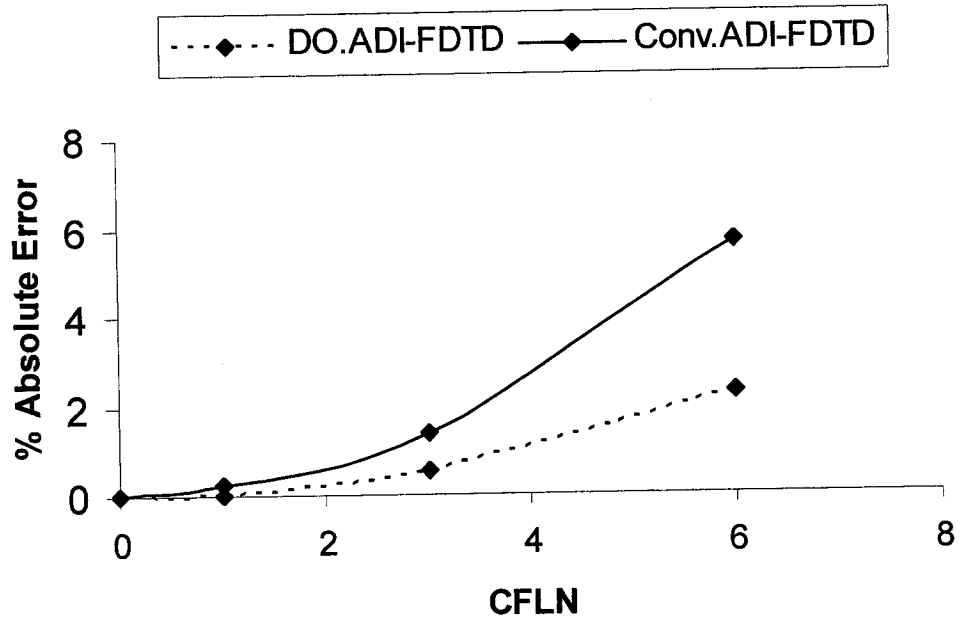
Fig. 6.13 Absolute error vs. CFLN with combination 3

To confirm the above analysis, a homogeneous cavity of dimensions 9*mm* x 6*mm* x 15*mm*

was simulated. The numbers of cells in the x, y and z directions were 16, 10, and 26 respectively. A Gaussian pulse was excited for TE_{101} mode and was positioned at (8, 5, 8) and measurement was made at (8, 8, 13). The measured frequency with DO-ADI-FDTD was 19.50 GHz and 19.27 GHz with the conventional ADI-FDTD. The analytical frequency is 19.42 GHz and is the frequency at which optimization is required. To find the value of control parameters normally the frequency used in the control parameter equations is the frequency at which optimization is required. The relative error for the conventional ADI-FDTD method is 0.77% and for the DO-ADI-FDTD method is 0.41%. The electric field measured vs. frequency is shown in Fig 6.14. These results are obtained by using the Combination # 3 as an example. The value of A used is 1.0304, while the simulation time and memory used are the same, i.e. 11 seconds and 1.648MB for the proposed method and the conventional ADI-FDTD method.
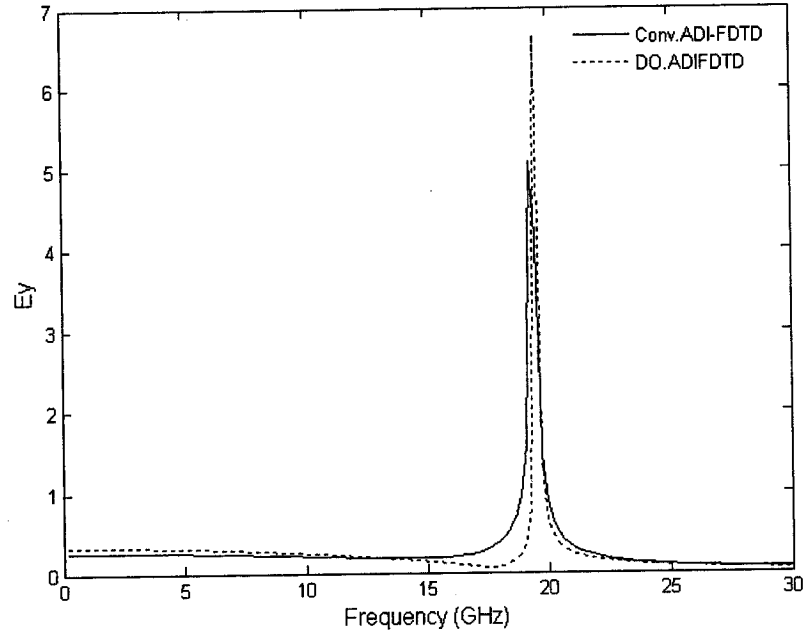
Fig. 6.14 Measured electric field E_y vs. frequency

6.5 Conclusions

In this chapter, to reduce the dispersion error associated with the unconditionally stable ADI-FDTD method, dispersion-improved ADI-FDTD algorithms are proposed with the

introduction of dispersion controlling parameters. Thorough studies of the improved versions of the ADI-FDTD method are presented in one-, two- and three-dimensional cases. Choices of different controlling parameters are investigated. From these detailed analyses of all the cases, we conclude that the proposed methods are in general better than the conventional ADI-FDTD method; however, the controlling parameters need to be chosen optimally to lead to better dispersion error reductions.

Chapter 7   Conclusions and Future Work

7.1   Summary

In this thesis, different numerical algorithms have been developed and implemented to increase the efficiency and accuracy of the existing time domain algorithms. This improvement is necessary due to the complexity of the modern circuit structures. Therefore, efficient algorithms are very important for accurate and efficient designs. In this thesis, efficient methods are presented that are better for electromagnetic structures design and simulations. These efficient methods are time domain methods and are very useful for wide frequency spectrum solutions as compared to frequency domain methods. Approaches presented in this thesis are more efficient and provide a competitive edge over the methods developed before.

In Chapter 1, a brief review of time and frequency domain methods was presented. In Chapter 2, FDTD and ADI-FDTD methods were described, that provided the basis for all the remaining chapters in this thesis. In Chapter 3, a hybrid FDTD and ADI-FDTD method for two-dimensional cases was proposed. In it, the FDTD and ADI-FDTD interfacing scheme was given, and then numerical experiments were run. This hybrid approach was found better than the FDTD and ADI-FDTD methods alone in terms of simulation time and memory usage. In Chapter 4, the hybrid technique was extended to three-dimensional cases. This technique was applied to different examples including RF/microwave and optical structures. Again the results were found better than the FDTD and ADI-FDTD alone in both time and memory usage. To reduce the splitting error of ADI-FDTD method, novel error reduced ADI-FDTD methods were proposed in Chapter 5. They made the ADI-FDTD method more promising in terms of modeling accuracy and efficiency. In Chapter 6, new dispersion-optimized ADI-FDTD methods were proposed to mitigate the problem of larger dispersion errors with larger time steps. These approaches were applied to the 1-D, 2-D and 3-D cases. It is concluded from the results that proposed novel optimization techniques improve the dispersion of the ADI-FDTD method, while using the same simulation time and memory as the conventional ADI-FDTD. Thus these

126

novel approaches provide better results without increasing the use of computation resources.

In brief, methods proposed in this thesis improve the computation time and memory as well as accuracy for the FDTD and ADI-FDTD methods.

7.2 Future Directions

In previous chapters, novel numerical approaches were proposed and used for different applications. The results obtained are very promising. These methods can be applied to many other problems that are affecting the efficiency of FDTD and ADI-FDTD methods individually. However, there are still a number of issues that need to be addressed. These are discussed briefly below:

Hybrid with FEM and MoM

FEM is effective for irregular boundaries as compared to both FDTD and ADI-FDTD methods; on the other hand, FEM is not as efficient as the hybrid FDTD and ADI-FDTD method. In these situations, the hybrid FDTD/ADI-FDTD/FEM can be very useful. Therefore, FEM can be applied to the region containing irregular boundaries, while hybrid FDTD and ADI-FDTD methods to rest of the region.

MoM is effective for computing the homogeneous and layered dielectrics. It is difficult to apply MoM to nonlinear and non-homogeneous structures, while the hybrid FDTD and ADI-FDTD can be applied to these structures relatively easily. In structures having layered dielectrics and non-linear characteristics, the hybrid FDTD/ADI-FDTD/MoM can be applied efficiently.

Hybrid with other numerical methods

Error reduced ADI-FDTD method that is more accurate than the conventional ADI-

FDTD method can be used with FDTD to make a hybrid FDTD/ER-ADI-FDTD method instead of the hybrid FDTD/conventional ADI-FDTD that has been used in this thesis.

ABC for error reduced ADI-FDTD

ABCs have not been developed for error reduced ADI-FDTD methods. Therefore, ABCs can be used with error reduced ADI-FDTD methods for further applications of these methods.

3-D error reduced ADI-FDTD

The error reduced ADI-FDTD method is unconditionally stable for 2-D cases, but is found unstable for 3D cases. Further studies are needed on the issue so that unconditional stability may be achieved for 3-D structures. If unconditional stability becomes possible, the splitting error of the conventional 3-D ADI-FDTD method can be reduced and the error-reduced techniques become more useful.

References

[1] Swanson, D. G., and Hofer, W. J. R., *Microwave circuit modeling using electromagnetic field simulation*, Artech House Inc. Norwood MA USA 2003

[2] Yee, K. S., "Numerical solution of initial boundary value problems involving Maxwell's equations in isotropic media," *IEEE Trans. on Antennas Propagation*, vol. AP-14, May 1966, PP. 302–307

[3] Taflove, A., *Computational Electrodynamics: The Finite-Difference Time-Domain Method*, Boston: Artech House, 1995

[4] Taflove, A., *Computational Electrodynamics: The Finite-Difference Time-Domain Method*, Boston: Artech House, 2000.

[5] Sadiku, M. N. O., *"Numerical Techniques in Electromagnetics"*, Second Edition Boca Raton: CRC Press, 2001

[6] Namiki, T., "A new FDTD algorithm based on Alternating Direction Implicit Method," *IEEE Trans. on Microwave Theory and Techniques*, vol. 47, No.10, Oct. 1999. PP.2003-2007

[7] Zheng, F., Chen Z., and Zhang, J., "Toward the development of a three-Dimensional unconditionally stable finite-difference time domain method," *IEEE Trans. on Microwave Theory and Techniques*, vol. 48, No.9, September 2000, PP. 1550-1558

[8] Lee, H-B., and Itoh, T., "A systematic optimum design of waveguide-to-microstrip transition," *IEEE Trans. Microwave Theory and Techniques*. Vol. 45, No. 5, May 1997, PP. 803-809

[9] Aoyagi, S., and Tal, Y. C., "Development of surface micromachinable capacitive accelerator using fringe electrical field," *12th International Conference on solid State Sensors, Aaualors and micmsystems*. Boston, Vol. 2, 8-12 June 2003, PP.1383 - 1386

[10] Grise, W. R., and Zargari, A., "Delamination and cracking failures in high-voltage stator winding coatings," *IEEE Elect. Insulation Confer. 1997 and Elect. Manufac. & Coil Winding Confer. Proceedings*, Rosemont, IL USA, 22-25 Sept. 1997, PP. 835 – 839

[11] Swanson, D. G., "Application notes: what's my impedance?," *IEEE Microwave*

Magazine, Dec. 2001, Vol. 2, Issue 4, PP. 72-82

[12] Makkonen, T., Holappa, A., Ella, J., and Salomaa, M. M., "Finite Element simulations of thin-film composite BAW resonators," *IEEE Trans. on Ultrasonic, Ferroelectrics and frequency control,* Vol. 48, No. 5, Sept. 2001, PP. 1241-1258

[13] Sadiku, M. N. O., *elements of electromagnetics,* third edition, Oxford University press Inc. New York

[14] Meyer, F. J. C., and Davidson, D. B., "Adaptive-mesh refinement of finite-element solutions for two-dimensional electromagnetic problems," *IEEE Antennas and Propagation Magazine,* vol. 38, Issue 5, Oct. 1996, PP. 77-83

[15] Fernandez, F. A., Yong, Y. C., and Ettinger, R. D., "A simple adaptive mesh generator for 2-D finite element calculation", *IEEE Trans. on Magnetics,* vol. 29, Mar. 1991, PP. 1882–1885

[16] Schrik, E., Dewilde, P. M., and Meijis, N. P., "Theoretical and practical validation of combined BEM/FEM substrate resistance modelling," *IEEE/ACM International Conference on Computer Aided Design,* Nov. 2002, PP. 10-15

[17] Harrington, R. F., *Field computation by moment methods,* New York, 1968

[18] Rautio, J. C., and Harrington, R. F., "An electromagnetic time harmonic analysis of shielded microstrip circuits," *IEEE Trans. on Microwave Theories and Techniques* Vol. 35, No. 8, Aug 1987, PP. 726-730

[19] Sainati, R. A., *CAD of microstrip antennas for wireless applications,* Artech House, Inc. Norwood, MA, USA 1996

[20] Devereux, R. W., Bruce, A., and Fuller, G. L., "Assessment of analytical codes for use in modeling aircraft onboard EMI threats," *IEEE Digital Avionics Systems Conference,* 1997. 16th DASC. AIAA 1997, vol.1, PP. 4.3 - 17-24

[21] Agilent Technologies. June 2001. Momentum, accessed on January 12, 2006 http://eesof.tm.agilent.com/products/momentum,

[22] Ansoft Corporation, December 2002, Ensemble TM essentials, accessed on January 12, 2006 http://www.ansoft.com/workshops/hfworkshop02/ Ensemble.

[23] Sonnet Software. March, 1983. Sonnet Lite, accessed on January 12, 2006 http://www.sonnetusa.com/products/lite

[24] Zeland software. May, 1997. http://www.linmic.com/zeland.htm , accessed on January 15, 2006

[25] Applied Wave Research, Inc. January, 2006. Cell size definition in microwave office design suite's EMSight, accessed on January 15 2006 http://www.appwave.com/src/news/articles/AR0409a.pdf.

[26] Sun, W., and Balanis, C. A., 'Edge-Based FEM Solution of Scattering from Inhomogeneous and Anisotropic Objects," *IEEE Trans. on Antennas and Propagations,* Vol. 42, No. 5, May 1994, PP. 627- 632

[27] Sarma, M. S., "potential functions in electromagnetic field problems," *IEEE Trans. on Magnetics.* Vol.6, No.3 1970, PP.513-518

[28] Ryff, P., Biringer, P., and Burke, P., "Calculation Methods for Current Distribution in Single-Turn Coils of Arbitrary Cross Section," *IEEE Trans. on Power Apparatus and Systems,* vol. PAS-89, no. 2, Feb. 1970, PP. 228-232

[29] Mur, G., "A Finite Difference Method for the solution of electromagnetic waveguide discontinuity problems", *IEEE Trans. Microwave Theory and Techniques"* Jan. 1974, Vol. 22, PP. 54- 57

[30] Schweig, E., and Bridges, W. B., "Computer analysis of dielectric waveguides: A Finite-Difference Method," *IEEE Trans. on Microwave Theory and Techniques,* Vol. 32, No. 5, May 1984, PP. 531- 541

[31] Smith, G. D., *Numerical solution of partial differential equations,* Oxford University press, Inc. New York, 1985

[32] Jin, H., and Vahldieck, R., "The frequency-domain transmission line matrix method-a new concept," *IEEE Trans. on Microwave Theory Techniques,* vol. 40, Dec.1992, PP. 2207–2218

[33] Johns, P. B., "A Symmetrical Condensed Node for the TLM Method," *IEEE Trans. on Microwave Theory and Techniques,* Vol. 4, Apr. 1987, PP. 370-377

[34] Huang, J., "Frequency domain transmission line matrix method and its applications to electromagnetic analysis," Ph.D. dissertation, Univ. of Victoria, Victoria, Canada, 1995

[35] Hesselbarth, J., and Vahldieck, R., "Accuracy of the frequency-domain TLM method and its application to microwave circuits," *International J. of Numerical*

Modelling Electronic networks, devices and fields, May 2002, PP. 371-383

[36]   Pasalic, D., Bornemann, J., and Vahldieck, R., "Absorbing boundary conditions in the Frequency-Domain TLM method and their application to planar circuits," *IEEE Trans. on Microwave Theory and Techniques,* Vol. 49, No. 8, Aug. 2001, PP. 1469 – 1476

[37]   Sadiku, M. N. O., and Garcia, R. C., "Method of Lines solution of axisymmetric problems," *Southeastcon Proceedings of the IEEE,* Apr 2000, PP.527-530

[38]   Zafarullah, A., "Application of the method of lines to parabolic partial differential equations with error estimates," *Jour. ACM,* vol. 17, No. 2, Apr. 1970, PP. 294-302

[39]   Schiesser, W. E., *The Numerical Method of Lines,* San Diego: Academic Press, 1991

[40]   Pregla, R., "Method of lines for the analysis of multilayered gyrotropic waveguide structures," *IEE Proc. on Microwaves, Antennas and Propagation,* Vol. 140, No. 3, June 1993, PP. 183 -192

[41]   Wu, K., and Vahldieck, R., "The method of lines applied to planar transmission lines in circular and elliptical waveguides," *IEEE Trans. on Microwave Theory and Techniques,* vol. 37, No. 12, Dec. 1989, PP. 1958-1963

[42]   Ma, J. G., and Chen, Z., "Application of the method of lines to the laplace equation," *Micro. Opt. Tech. Lett.,* vol. 14, no. 6, 1997 PP.330-333

[43]   Sadiku, M. N. O., *Numerical Techniques in Electromagnetics,* Boca Raton, FL: CRC Press, 1992, PP. 48

[44]   Lee, H. F., and Chen, W., *Advances in microstrip and printed antennas,* John Wiley & Sons, Inc. USA, 1997

[45]   Itoh, T., and Mittra, R., "Spectral-Domain Approach for calculating the dispersion Characteristics of Microstrip Lines," *IEEE Trans. on Microwave Theory and Techniques,* July 1973, PP.496 - 499

[46]   Jansen, R. H., "The Spectral-Domain Approach for Microwave Integrated Circuits" *IEEE Trans. on Microwave Theory and Techniques,* Vol. MTT 33, No.10, Oct.1985, PP. 1043 – 1056.

[47]   Montisci, G., and Mazzarella, G., "Full-Wave Analysis of a Waveguide Printed

Slot," *IEEE Trans. on antennas and Propagation*, Vol. 52, No. 8, Aug. 2004 PP. 2168-2171

[48] Kythe, P. K., *An introduction to boundary element methods*, Boca Raton, CRC Press, 1995

[49] Beer, G., and Watson, J. O., *Introduction to finite and boundary element methods for engineers*, John Wiley & Sons, Inc. Toronto 1992

[50] Wang, X. Y., Lou, J. J., Lu, C., Shum, P., Zhao, C. L., Chaudhuri, P. R., and Yan, M., " Full- vector analysis of photonic crystal fibers using the boundary element method," *Information, Communications and Signal Processing, 2003 and the Fourth Pacific Rim Conference on Multimedia. Proceedings of the 2003 Joint Conference of the Fourth International Conference on*, Vol. 2, Dec. 2003 PP. 1293 - 1297

[51] Hirayama, K., and Koshiba, M., "Numerical analysis of arbitrarily shaped discontinuities between planar dielectric waveguides with different thicknesses," *IEEE Trans. on Microwave Theory and Techniques*, Vol. 38, No. 3, March 1990, PP. 260 - 264

[52] Tsuboi, H., Tanaka, H., and Fujita, M., "Electromagnetic field analysis of the wire antenna in the presence of a dielectric with three-dimensional shape," *IEEE Trans. on Magnetics*, Vol. 25, No. 5, Sept. 1989, PP. 3602-3604

[53] Itoh, T., *Numerical techniques for microwave and millimeter wave passive structures*, John Wiley & Sons, Inc. USA, 1989.

[54] Mansour, R.R., and Macphie, R. H., "An Improved Transmission Matrix Formulation of Cascaded Discontinuities and its Application to E-Plane Circuits," *IEEE Trans. on Microwave Theory and Techniques*, Vol. MTT-34, No 12, Dec. 1986, PP. 1490-1498

[55] Bogelsack, F., and Wolf, I., "Application of a Projection Method to a Mode-Matching Solution for Microstrip Lines with Finite Metallization Thickness," *IEEE Trans. Microwave Theory and Techniques*, Vol. 35, No. 10, Oct 1987, PP. 918- 921

[56] Prkna, L., Hubalek, M., and Ctyroky, J., "Field Modeling of Circular Microresonators by Film Mode Matching," *IEEE Journal of selected topics in*

quantum electronics, Vol.11, No. 1, January/February 2005, PP. 217-223

[57]   Wells, C. G., and Ball, J. R., "Mode-Matching Analysis of a Shielded Rectangular Dielectric-Rod Waveguide," *IEEE Trans. Microwave Theory and Techniques* Accepted for future publication 2005

[58]   Advanced EM, July, 2004. http://advancedem.com/semcad.html, accessed on January 18, 2006

[59]   Zeland software. May, 1997, Fidelity: FDTD based simulator, accessed on January 18, 2006, http://www.zeland.com.

[60]   Johns, P. B., "A Symmetrical Condensed Node for the TLM Method", *IEEE Trans. on Microwave Theory and Techniques*, Vol. No. 4, Apr. 1987, PP. 370-377

[61]   Chen, Z., Ney, M. M., and Hoefer, W.J. R., "A new finite difference time domain formulation and its equivalence with the TLM symmetrical condensed node," *IEEE Trans. on Microwave Theory and Techniques*, vol. 39, No.12, Dec. 1991, PP. 2160-2169

[62]   Krumpholz, M., and Russer, P., "Discrete time domain Green's functions for three dimensional TLM modelling of the radiating boundary conditions," *ACES*, Mar. 1993, Monterey, CA, USA, PP. 458-466

[63]   Chen, Z., "Modelling of absorbing boundary conditions with TLM," *First international workshop on Transmission Line Matrix modeling-theory and Application* Victoria B.C., Canada, Aug. 1-3 1995, PP. 63 - 72

[64]   Faustus Scientific Corporation, September 1998. http://www.faustcorp.com, accessed on January 16, 2006

[65]   Namiki, T., "A new FDTD algorithm free from the CFL condition restraint for a 2D-TE wave," *IEEE Antennas and Propagation Society International Symp.*, Vol. 1, July 1999, PP.192-195

[66]   Zheng, F., and Chen, Z., "Development of a three-dimensional Unconditionally Stable Finite-Difference Time-Domain Method", *IEEE International RFIC/Microwave Symposium*, Boston, June 11-16, 2000, PP. 1117-1120

[67]   On the real-world performance of ADI-FDTD, http://advancedem.com/semcad /ADI_FDTD_poster.pdf, accessed on December 15, 2005

[68] Krumpholz, M., and Katehi, L. P. B., "New prospects for time domain analysis,"
IEEE Microwave Guided Wave Lett. Vol. 5, No. 11, Nov. 1995, PP. 382–384

[69] Krumpholz, M., and Katehi, L. P. B., "MRTD: New time domain schemes based
on multiresolution analysis," *IEEE Trans. on Microwave Theory and
Techniques*, Vol. 44, No. 4, Apr. 1996, PP. 555–571

[70] Chen, Y., Mittra, R., and Cao, Q., *Multiresolution Time Domain Scheme for
Electromagnetic Engineering*, John Wiley & sons Canada Ltd, 2005

[71] Bushyager, N. A., and Tentzeris, M. M., "RF MEMS: development of design
rules" *The Pacific RIM/International, Intersociety, Electronic Packaging
Technical/Business Conference & Exhibition* July 8–13, 2001, PP.1-4

[72] Chen, Z., and Zhang, J., "An efficient eigen-based spatial-MRTD method for
computing resonant structures *IEEE Microwave and Guided Wave Letters*, Vol.
9, No. 9, Sept. 1999, PP. 333- 335

[73] Chen, Z., and Zhang, J., "An unconditionally stable 3-D ADI-MRTD method
free of the CFL stability Condition," *IEEE Microwave and Wireless components
Letters*, Vol. 11, No. 8, Aug. 2001, PP. 349-351

[74] Sarris, C. D., and Katehi, L. P. B., "An efficient numerical interface between
FDTD and Haar MRTD—formulation and applications" *IEEE Trans. on
Microwave Theory Techniques*, Vol. 51, No. 4, Apr. 2003, PP. 1146-1156.

[75] Liu, Q. H., "The PSTD-algorithm: a time-domain method requiring only two
cells per wavelength" *Microwave and Optical Technology Letters*, Vol. 15, No.
3, June 1997, PP. 158-165

[76] Berenger, J. P., "A Perfectly Matched Layer for the Absorption of
Electromagnetic Waves," *J. Comput. Phys.*, Vol. 114, 1994, PP. 185-200

[77] Liu, Q. H., and Zhao, G., "Review of PSTD methods for transient
electromagnetics," *International J. of Numerical Modelling Electronic networks,
devices and fields,"* 2004, No.17, PP. 299–323

[78] Liu, Q. H., Millard, X. M., Tian, B., and Zhang, Z. Q., "Applications of
nonuniform fast transform algorithms in numerical solutions of differential and
integral equations," *IEEE Transactions on Geoscience and Remote Sensing*
2000, Vol. 38, No.4, PP.1551 - 1560

[79]   Leung, W. K., and Chan, C. H., "Combining the FDTD and PSTD methods," *Microwave and Optical Technology Letters,* 1999, Vol.23, No.4, PP. 249–254

[80]   Tian, B., and Liu, Q. H., "Nonuniform fast cosine transform and Chebyshev PSTD algorithm," *Progress in Electromagnetics Research* 2000, Vol. 28, PP.259 - 279

[81]   Zhao, G., Zeng, Y. Q., and Liu, Q. H., "The 3-D multinomial pseudospectral time-domain method for wideband simulation", *IEEE Microwave and Wireless Component Letters* 2003, Vol. 13, No.5, PP. 184 - 186

[82]   Zhao, G., and Liu, Q. H. "The unconditionally stable multidomain pseudospectral time- domain method", *IEEE Microwave and Wireless Components Letters* 2003, Vol. 13, No. 11, PP. 475 – 477

[83]   Rautio, J. C., and Harrington, R. F., "An electromagnetic time harmonic analysis of shielded microstrip circuits", *IEEE Trans. on Microwave Theory and Techniques,* Vol. 35, No. 8, Aug. 1987 PP. 726-730

[84]   Martin, R.G., Salinas, A., and Bretones, A.R., "Time-domain integral equation methods for transient analysis," *IEEE Antennas and Propagation Magazine* Vol. 34, No.3, June 1992, PP. 15 - 23

[85]   Bretones, A. R., Martin, R. G., and Mittra, R., "A new hybrid method combination of the Finite Difference Time Domain (FDTD) and the Method of Moments in the Time Domain (MoMTD)," *IEEE International Sympo. Electromagnetic Compatibility* Vol. 1, Aug. 1998, PP. 194-195

[86]   Martín, R. G., Rubio, R. G., García, S. G., Pantoja, M. F., and Bretones, A. R., "Simulation of ground penetrating radar using an ADI-FDTD/MOMTD hybrid method," *URSI EMTS,* 2004, PP. 203-205

[87]   Guillouard, K., M. Wong, F., and Hanna, V. F., "A new global time domain electromagnetic simulator of microwave circuits including lumped elements based on finite-element method," *IEEE MTT-S Int. Microwave Symp. Digest,* Denver, CO, June 1997, PP. 1239–1242

[88]   Gedney, S. D., and Navsariwala, U., "A comparison of the performance of the FDTD, FETD, and planar generalized Yee algorithms on high performance parallel computers," *Int. J. Numerical Modeling,* Vol. 8, May–Aug. 1995, PP.

265–276

[89]   Gedney, A. D., and Navsariwala, U., "An unconditionally stable finite element time-domain solution of the vector wave equation," *IEEE Microwave Guided Wave Lett.*, Vol. 5, Oct. 1995, PP. 332–334

[90]   Koh, D., Lee, H., and Itoh, T., "A hybrid full-wave analysis of via hole grounds using Finite Difference and Finite Element Time Domain methods," *IEEE MTT-S Digest* 1997, PP. 89- 92

[91]   Chang, S. H., Coccioli, R., Qian, Y., and Itoh, T., "A global finite-element time domain analysis of active nonlinear microwave," *IEEE Trans. on Microwave Theory and Techniques*, Vol. 47, Dec. 1999, PP. 2410–2416

[92]   Tsai, H. P., Wang, Y., and Itoh, T., "An Unconditionally Stable Extended (USE) Finite-Element Time-Domain Solution of Active Nonlinear Microwave Circuits Using Perfectly Matched Layers," *IEEE Trans. on Microwave Theory and Techniques*, Vol. 50, No. 10, Oct. 2002, PP. 2226 -2232

[93]   Monorchio, A., Bretones, A. R., Mittra, R., Manara, G., and Martín, R.G., "A Hybrid Time-Domain Technique that combines the Finite Element, Finite Difference and   method of Moment Techniques to solve complex electromagnetic problems," *IEEE Trans. on Antennas and Propagation*, Vol. 52, No. 10, Oct. 2004, PP. 2666- 2676

[94]   Edelvik, F., "A survey of Finite Volume Time Domain methods for solving Maxwell's equations," *Parallel and Scientific Computing Institute Royal Institute of Technology and Uppsala University*, Report No. 98:07

[95]   Schiavoni, D., Cappio, M. B., Giunta, M., Pompani, R., De Leo, R., and Pierucci, G., "Finite volume time domain technique for evaluation of scattering in GHz-TEM cell: model, comparison with measurements and literature references," *IEEE International Sympo. Electromagnetic Compatibility*, Aug. 1997, PP.602 - 607

[96]   Fumeaux, C., Baumann, D., Leuchtmann, P., and Vahldieck, R., "A generalized local time-step scheme for the FVTD method for efficient simulation of microwave antennas," *33rd European Microwave Conference* - Munich 2003, PP.467- 470

[97] Riley, D. G., and Turner, C. D., "Interfacing unstructured tetrahedron grids to structured grid FDTD," *IEEE Microwave Guided Wave Lett.,* Vol. 2, 1992, PP. 284 – 286.

[98] Riley, G., and Turner, C. D., "A solid model based transient volumetric Maxwell's solver using hybrid grids," *IEEE Antenna Propagat. Magazine,* Vol. 39, 1997, PP. 20 – 33

[99] Pursel, J. D., and Goggans, P. M., "A Finite-Difference Time-Domain Method for solving electromagnetic problems with bandpass limited sources," *IEEE Trans. Antennas and Propagation,* Vol. 47, No.1, PP. 9-15, Jan. 1999.

[100] Trakadas, P. T., Kouveliotis, N. K., and Capsalis, C. N., "Advantageous properties of the Complex-Envelope Finite-Difference Time-Domain technique," *2ndinternational workshop on biological effects of electromagnetic fields* 7-11Oct. 2002, Rhodes Greece.

[101] Ma, C., and Chen, Z., "Stability Analysis of the CE-FDTD Method," IEEE Microwave and Wireless components letters, Vol. 14, No. 5, May 2004, PP. 243-245

[102] Ma, C., and Chen, Z., "Stability and Numerical Dispersion Analysis of CE-FDTD Method," *IEEE Trans. on antennas and propagation,* Vol. 53, No. 1, Jan. 2005, PP. 332- 338.

[103] Ma, C., and Chen, Z., "Dispersion analysis of the three dimensional Complex Envelope ADI-FDTD method," *IEEE Trans. on antennas and propagation,* Vol. 53, No. 3, Mar. 2005, PP. 971- 976.

[104] Penney, C. W., Luebbers, R. J., and Schuster, J.W., "Scattering from coated targets using a frequency-dependent, surface impedance boundary condition in FDTD," *IEEE Trans. Antennas and Propagation,* Vol. 44 , No. 4, Apr. 1996, PP.434-443

[105] Taflove, A., and Brodwin, M. E., "Numerical solution of steady-state electromagnetic Scattering problems using the time-dependent Maxwell's equations," *IEEE Trans. on Microwave Theory and Techniques,* Aug. 1975, Vol. 23, No. 8 PP. 623- 630

[106] Scarlatti, A., and Holloway, C. L., "An equivalent transmission-line model

containing dispersion for high-speed digital lines-with an FDTD implementation," *IEEE Trans. on Electromagnetic Compatibility*, Vol. 43 , No. 4, Nov. 2001, PP. 504 - 514

[107] Ibrahim, T. S., R. Lee, Baertlein, B. A., and Robitaille, P. M. L., "Design of radiofrequency coils for magnetic resonance imaging applications at high fields: technological and physical feasibility issues," *IEEE International Symposium Antennas and Propagation Society*, Vol. 1, July 2001, PP. 370-373

[108] Colpitts, B. G., "Optical versus radar roughness in agricultural tillage," *International Geosciences and Remote Sensing Symposium*, Vol. 4, May 1996, PP. 2189 – 2191

[109] Lizhuang, M., Paul, D. L., Pothecary, N., Railton, C., Bows, J., Barratt, L., Mullin, J., and Simons, D., "Experimental validation of a combined electromagnetic and thermal FDTD model of a microwave heating process," *IEEE Trans. on Microwave Theory and Techniques*, Vol. 43, Issue. 11, Nov. 1995, PP. 2565 - 2572

[110] Bassen, H., and Casamento, J., "High resolution computations and measurements of potential EMI with models of medical implants and radiating sources," *International Symposium on Electromagnetic Compatibility (EMC)*, Vol. 1, 2004, PP. 75 - 80

[111] Shlager, K. L., and Schneider, J. B., "Comparison of the dispersion properties of several low-dispersion finite-difference time-domain algorithms," *IEEE Trans. on Antennas and Propagation*, Vol. 51, Issue. 3, Mar. 2003, PP. 642 - 653

[112] Wang, S., and Teixeira, F. L., "Dispersion-Relation-Preserving FDTD Algorithms for Large-Scale Three-Dimensional Problems," *IEEE Trans. on Antennas and Propagation*, Vol. 51, No. 8 Aug. 2003, PP. 1818 – 1828.

[113] Kim, I. S., and Hoefer, W. J. R., "Numerical dispersion characteristics and stability factor for the TD-FD method," *Electronic letters*, vol. 27, Mar. 1990, PP. 485-487.

[114] Pereda, J. A., Garcia, O., Vegas, A., and Prieto, A., "Numerical dispersion and stability of the FDTD Technique in lossy dielectrics," *IEEE Microwave and Guided Wave Letters*, Vol. 8, No. 7, July, 1998, PP. 245 – 247

[115] Naishadham, K., "Stability considerations in the application of PML absorbing boundary condition to FDTD simulation of microwave circuits," *IEEE MTT-S International Microwave Symposium Digest,* Vol. 2, June 1996 PP. 581 - 584

[116] Min, X., Sun, W., and Chen, K. M., "Stability analysis of the finite difference time domain method applied to unbounded electromagnetic problems," *International Symposium Antennas and Propagation Society,* Vol.4, May 1990, PP. 1640 - 1643

[117] Ramahi, O. M., "Stability of absorbing boundary conditions," *IEEE Trans. on Antennas and Propagation,* Vol. 47, Issue. 4, Apr. 1999, PP. 593 - 599

[118] Saitoh, I., and Takahashi, N., "Stability of symplectic finite-difference time-domain methods," *IEEE Trans. on Magnetics,* Vol. 38, No.2, Mar. 2002, PP. 665-668

[119] Zhang, Y., and Wang, W., "The studies of the stability of FDTD with Mur's absorbing boundary condition of second order in 3-D scattering problems," *IEEE Microwave and Guided Wave Letters,* Vol. 6, Issue: 3, Mar. 1996, PP. 120 - 122

[120] Costen, F., "Analysis and improvement of Liao ABC for FDTD," *IEEE Antennas and Propagation Society International Sympos.,* Vol. 1, June 2003, PP. 341 – 344

[121] Berenger, J. P., "A perfectly matched layer for the absorption of electromagnetic waves," *Journal of Computational Physics,* Vol. 114, 1994, PP. 195-200

[122] Jiang, H., and Tsunekawa, K., "Proposal of non-uniform mesh FDTD with Uniaxial PML (UPML)" *IEEE Topical Conference on Wireless Communication Technology,* Oct. 2003, PP. 412 - 415

[123] Roden, J. A., and Gedney, S. D., "Convolutional PML (CPML): An efficient FDTD implementation of the CFS-PML for arbitrary media," *Microwave Opt. Technology Lett.,* Vol. 27, Dec. 5, 2000, PP. 334–339

[124] Jiayuan, F., and Zhonghua, W., "Generalized perfectly matched layer-an extension of Berenger's perfectly matched layer boundary condition," *IEEE Microwave and Guided Wave Letters* Vol. 5, Issue: 12, Dec. 1995, PP. 451 - 453

[125] Thomas, J. W., *Numerical partial differential equations finite difference*

methods, Springer-Verlag, New York, Inc. 1995

[126] Zheng, F., and Chen, Z., "Numerical dispersion analysis of the unconditionally stable 3D ADI-FDTD method," *IEEE Trans. Microwave Theory and Techniques*, Vol. 49 2001, PP.1006–1009

[127] Liu, Q.H., "The pseudospectral time domain (PSTD): A new algorithm for solution of Maxwell's equations," *IEEE International Sympo. Antennas and Propagation Society*, Vol.1, July 1997, PP. 122–125

[128] Craddock, I. J., and Railton, C. J., "A new technique for the stable of static field solutions in the FDTD method for the analysis of thin wire and narrow," *IEEE Trans. Microwave Theory and Techniques*, Vol. 46, No.8, Aug. 1998, PP. 1091-1096

[129] Tardioli, G., Cascio, L., Righi, M., and Hoefer, W. J. R., "Special 3D-TLM corner nodes for singular field regions," Digest of 1997 *IEEE International Microwave Symposium*, Vol. 1, June 8-11, 1997, PP. 317 -320

[130] Kim, I. S., and Hoefer, W. J. R., "A local mesh refinement algorithm for the time-domain finite- difference method using Maxwell's Curl Equations," *IEEE Trans. on Microwave Theory and Techniques*, Vol. 38, No.6, June 1990, PP. 812-815

[131] Krishnaiah, K. M., and Railton, Chris J., "A Stable subgridding algorithm and its application to eigen value problems," *IEEE Trans. on Microwave Theory and Techniques*, Vol. 47, No.5, May 1999, PP. 620-628

[132] Thoma, P., and Weiland, T., "Numerical stability of finite difference time domain methods", *IEEE Transactions on Magnetics*, Vol. 34, No.5, Sept. 1998. PP. 2740-2743

[133] Shih, Y., and Hoefer, W. J. R., "The accuracy of TLM analysis of finned rectangular waveguide." *IEEE Trans. on Microwave Theo. Tech.*, vol. MTT 28, No.7, July 1980. PP. 743-746

[134] Shih, Y. C., and Hoefer, W. J. R., "Dominant and second-order mode cutoff frequencies in fin lines calculated with a two-dimensional TLM program," *IEEE Trans. on Microwave Theo. Tech.*, vol. MTT 28, December 1980. PP. 1443-1448

[135] Eswarappa, C., and Hoefer, W. J. R., "A hybrid 3D TLM-FDTD model of microwave fields," Digest of 1996 *IEEE International Microwave Symposium,* Vol.2, June 1996. PP. 1063-1066

[136] Marrocco, G., Fari, S., and Bardati, F., "A hybrid FDTD-MOM procedure for the modeling of electromagnetic radiation from cavity backed apertures," *IEEE International Sympo. Antennas and Propagation Society,* Vol. 4, July 2001, PP. 302-305

[137] Wang, B., Wang, Y., Yu, W., and Mittra, R., "A hybrid 2-D ADI-FDTD subgridding scheme for modeling on-chip Interconnects," *IEEE Trans. Advanced Packaging,* Vol. 24, No. 4, Nov. 2001 PP. 528-533.

[138] Ahmed, I., and Chen, Z., "A hybrid FDTD and ADI-FDTD scheme for RF/Microwave structure simulation," *19th Annual Review of Progress in Applied Computational Electromagnetics, Monterey, CA,* Mar. 24-28, 2003 PP. 408 - 412.

[139] Kashiwa, T. U., Uchiya, M., and Suzuki, K. K., "FDTD analysis of microwave circuits using edge condition," *IEEE Trans. on Magnetics,* Vol, 38, NO.2, Mar. 2002, pp 705-708

[140] Marcuvitz, N., *Waveguide Handbook,* McGraw-Hill Book Company Inc, 1951

[141] Craddock, I. J., Paul, D. L., Railton, C. J., Fletcher, P. N., and Dean, M., "Applications of single mode extraction from finite difference time domain data," *IEE Proc. Microwave and Antennas Propagation,* Vol. 146, No.2, Apr. 1999, PP. 160-162.

[142] Roden, J. A., and Gedney, S. D., "Convolutional PML (CPML): An Efficient FDTD implementation of the CFS-PML for arbitrary media," *Microwave and Optical Technology Letters,* Vol. 25, No. 5, Dec. 2000, PP. 334-339.

[143] Gedney, S. D., Liu, G., Roden, A., and Zhu, A., "Perfectly matched layer media with CFS for an unconditionally stable ADI-FDTD Method," *IEEE Trans. Antennas and propagation,* Vol.49, No.11, Nov 2001, PP. 1554-1559

[144] Shibayama, J., Takahashi, T., Yamauchi, J., and Nakano, H., "Efficient time-domain finite-difference beam propagation methods for the analysis of slab and circularly symmetric waveguides," *IEEE J. Light wave Technology,* vol.18,

No.3, Mar. 2000, PP. 437-442

[145] Reuter, C. E., Joseph, R. M., Thiele, E. T., Katz, D. S., and Taflove, A., "Ultrawideband absorbing boundary condition for termination of waveguiding structures in FD-TD simulations," *IEEE Microwave and Guided Wave Lett.,* Vol. 4, No.10, Oct. 1994, PP. 344-346

[146] Frankel, M. Y., Gupta, S., Valdmanis, J. A., and Mourou, G. A., "Terahertz attenuation and dispersion characteristics of coplanar transmission lines," *IEEE Trans. on Microwave Theory and Techniques,* Vol. 39, No.6, June 1991, PP. 910-916

[147] Hotta, M., Qian, Y., and Itoh, T., "Efficient analysis of conductor backed CPW's with reduced leakage loss," *IEEE Trans. on Microwave Theory and Techniques,* Vol. 47, No.8, Aug. 1999, PP. 1585-1587

[148] Huynh, N-H., and Wolfgang, H., "FDTD analysis of submillimeter-wave CPW with finite width ground metallization," *IEEE Microwave and guided wave letters,* Vol.7, No.12, Dec. 1997, PP. 414-416

[149] Tsuji, M., Yahata, N., and Shigesawa, H., "Significant contribution of improper real solution to fields excited by practical source in printed circuit transmission lines," *IEEE Trans. on Microwave Theory and Techniques,* Vol. 47, No.12, Dec. 1999, PP. 2487-2492

[150] Ahmed, I., and Chen, Z., "A hybrid FDTD and ADI-FDTD scheme for RF/Microwave structure simulation," *19th Annual Review of progress in Applied Computational Electromagnetics,* Monterey CA, Mar. 24-28 2003, PP. 408-412

[151] Chen, Z., and Ahmed, I., "3D hybrid ADI-FDTD/FDTD subgridding scheme applied to RF/Microwave and optical structures," *IEEE international sympo. Antennas and propagation Society* vol. 2, June 2004, PP. 1684-1687

[152] Namiki, T., and Itoh, K., "Investigation of Numerical Errors of the two-dimensional ADI-FDTD method," *IEEE Trans. on Microwave Theory and Techniques,* Vol. 48, No.11, Nov. 2000, PP. 1950-1956

[153] Ahmed, I., and Chen, Z., "A hybrid ADI-FDTD subgridding scheme for efficient electromagnetic computation," *International J. of Numerical Modelling Electronic networks, devices and fields,* vol.17, Jan. 2004, PP.237-249

143

[154] Sheen, D. M., Ali, S. M., Abouzahra, M. D., and Kong, J. A., "Application of the three-dimensional finite-difference time-domain method to the analysis of planar microstrip circuits," *IEEE Trans. on Microwave Theory and Techniques*, Vol. 38, No. 7, July 1990, PP. 849 - 857

[155] Schneider, R. N., Okoniewski, M. M., and Turner, L. E., "A software-coupled 2D FDTD hardware accelerator [electromagnetic simulation]," *IEEE International Sympo. Antennas and Propagation Society*, Vol. 2, June 2004, PP. 1692 - 1695

[156] Garcia, S. G., Lee, T-W., and Hagness, S. C., "On the accuracy of the ADI-FDTD method," *IEEE Antennas and Wireless Propagation Lett.*, Vol.1, 2002, PP.31-34

[157] Sun, G., and Trueman, C.W. "Approximate Crank–Nicolson schemes for the 2-D finite difference time domain method for TEz waves," *IEEE Trans. Antennas Propagation*, Vol. 52, No. 11, Nov. 2004, PP. 2963-2972

[158] Wang, S., Teixeira, F. L., and Chen, J., "An iterative ADI-FDTD with reduced splitting error," *IEEE Microwave and Wireless Component Lett.*, Vol. 15, No. 2, Feb. 2005, PP. 92-94

[159] Wang, S., "On the current source implementation for the ADI-FDTD method," *IEEE Microwave and Wireless Comp. Lett.*, Vol. 14, No. 11, Nov. 2004, PP. 513-515

[160] Wang, T.Y., and Chen, C.C.P., "Thermal-ADI: a linear-time chip-level dynamic thermal simulation algorithm based on alternating-direction-implicit (ADI) method," *International Symposium on Physical Design*, Sonoma, California, U.S, 2001, PP. 238 - 243

[161] Wang, M., Wang, Z., and Chen, J., "A parameter optimized ADI-FDTD method," *IEEE Antennas and propaga. letters*, vol. 2, 2003, PP. 118-121

[162] Fu, W., and Tan, E. L., "Stability and Dispersion Analysis for Higher Order 3-D ADI-FDTD Method", *IEEE Trans. Antennas and Propagation*, Vol. 53, No. 11, Nov. 2005, PP. 3691-3696

[163] Ahmed, I., and Chen, Z., "Error Reduced ADI-FDTD Methods," *IEEE Antennas and Wireless Propagation Lett.* Vol. 4, 2005, PP. 323 – 325

[164] Ping, A., "Improvement on the numerical dispersion of 2-D ADI-FDTD with

artificial anisotropy," *IEEE Microwave and Wireless Components Lett.* Vol. 14, No. 6, June 2004, PP. 292 – 294

[165]   Ahmed, I., and Chen, Z., "Dispersion-error optimized ADI-FDTD", *IEEE MTT-S Int. Microwave Symp. Digest*, San-Francisco USA, June 2006

APPENDICES

Appendix # A   Simplification of 3-D ER-ADI-FDTD Equations

In 3-D case, as can be seen from equations (5.25) to (5.29) there are approximately same steps as for the 2-D case, but with the difference that matrices are 6 x 6 instead of 3 x 3 for the 2-D case. From equations (A-3) and (A-4) in this Appendix, it can be observed that all the 12 terms in both steps have one extra term, and this extra term is the difference between two consecutive time steps. These terms are modified for both proposed methods by using the same approximate modifications as used for the 2-D case. After replacing the extra terms with approximate terms these equations run like the conventional ADI-FDTD method.

In this appendix equations for Method # 1 of 3-D ER-ADI-FDTD method are simplified that are obtained on the same pattern as for 2D case.

Method # 1

Step 1

$$([I]-\frac{\Delta t}{2}[A_1])U_1^{n+\frac{1}{2}} =([I]+\frac{\Delta t}{2}[B_1])U_1^{n} +\frac{\Delta t^2}{4}[A_1][B_1](U_1^{n} -U_1^{n-\frac{1}{2}}) \qquad (A-1)$$

Step 2

$$([I]-\frac{\Delta t}{2}[A_1])U_1^{n+1} =([I]+\frac{\Delta t}{2}[B_1])U_1^{n} +\frac{\Delta t^2}{4}[A_1][B_1](U_1^{n+\frac{1}{2}} -U^{n}) \qquad (A-2)$$

After putting values of $[I],[A_1]$, $[B_1]$ and U_1 in equation (A-1)

$$\left(\begin{bmatrix}1&0&0&0&0&0\\0&1&0&0&0&0\\0&0&1&0&0&0\\0&0&0&1&0&0\\0&0&0&0&1&0\\0&0&0&0&0&1\end{bmatrix} - \frac{\Delta t}{2}\begin{bmatrix} 0&0&0&0&0&\dfrac{\partial}{\varepsilon\,\partial y}\\[4pt] 0&0&0&\dfrac{\partial}{\varepsilon\,\partial z}&0&0\\[4pt] 0&0&0&0&\dfrac{\partial}{\varepsilon\,\partial x}&0\\[4pt] 0&\dfrac{\partial}{\mu\,\partial z}&0&0&0&0\\[4pt] 0&0&\dfrac{\partial}{\mu\,\partial x}&0&0&0\\[4pt] \dfrac{\partial}{\mu\,\partial y}&0&0&0&0&0\end{bmatrix}\right)\begin{bmatrix}E_x\\E_y\\E_z\\H_x\\H_y\\H_z\end{bmatrix}^{n+\frac12} =$$

$$\left(\begin{bmatrix}1&0&0&0&0&0\\0&1&0&0&0&0\\0&0&1&0&0&0\\0&0&0&1&0&0\\0&0&0&0&1&0\\0&0&0&0&0&1\end{bmatrix} + \frac{\Delta t}{2}\begin{bmatrix} 0&0&0&0&-\dfrac{\partial}{\varepsilon\,\partial z}&0\\[4pt] 0&0&0&0&0&-\dfrac{\partial}{\varepsilon\,\partial x}\\[4pt] 0&0&0&-\dfrac{\partial}{\varepsilon\,\partial y}&0&0\\[4pt] 0&0&-\dfrac{\partial}{\mu\,\partial y}&0&0&0\\[4pt] -\dfrac{\partial}{\mu\,\partial z}&0&0&0&0&0\\[4pt] 0&-\dfrac{\partial}{\mu\,\partial x}&0&0&0&0\end{bmatrix}\right)\begin{bmatrix}E_x\\E_y\\E_z\\H_x\\H_y\\H_z\end{bmatrix}^{n} +$$

$$\frac{\Delta t^2}{4}\begin{bmatrix} 0&0&0&0&0&\dfrac{\partial}{\varepsilon\,\partial y}\\[4pt] 0&0&0&\dfrac{\partial}{\varepsilon\,\partial z}&0&0\\[4pt] 0&0&0&0&\dfrac{\partial}{\varepsilon\,\partial x}&0\\[4pt] 0&\dfrac{\partial}{\mu\,\partial z}&0&0&0&0\\[4pt] 0&0&\dfrac{\partial}{\mu\,\partial x}&0&0&0\\[4pt] \dfrac{\partial}{\mu\,\partial y}&0&0&0&0&0\end{bmatrix}\begin{bmatrix} 0&0&0&0&-\dfrac{\partial}{\varepsilon\,\partial z}&0\\[4pt] 0&0&0&0&0&-\dfrac{\partial}{\varepsilon\,\partial x}\\[4pt] 0&0&0&-\dfrac{\partial}{\varepsilon\,\partial y}&0&0\\[4pt] 0&0&-\dfrac{\partial}{\mu\,\partial y}&0&0&0\\[4pt] -\dfrac{\partial}{\mu\,\partial z}&0&0&0&0&0\\[4pt] 0&-\dfrac{\partial}{\mu\,\partial x}&0&0&0&0\end{bmatrix}\left(\begin{bmatrix}E_x\\E_y\\E_z\\H_x\\H_y\\H_z\end{bmatrix}^{n} - \begin{bmatrix}E_x\\E_y\\E_z\\H_x\\H_y\\H_z\end{bmatrix}^{n-\frac12}\right)$$

After solving this matrix, following equations are obtained:

Step 1

$$E_x^{n+\frac{1}{2}} = E_x^n + \frac{\Delta t}{2\varepsilon}\frac{\partial H_z^{n+\frac{1}{2}}}{\partial y} - \frac{\Delta t}{2\varepsilon}\frac{\partial H_y^n}{\partial z} - \frac{\Delta t^2}{4\mu\varepsilon}\frac{\partial^2}{\partial x \partial y}(E_y^n - E_y^{n-\frac{1}{2}})$$

(A3-a)

$$E_y^{n+\frac{1}{2}} = E_y^n + \frac{\Delta t}{2\varepsilon}\frac{\partial H_x^{n+\frac{1}{2}}}{\partial z} - \frac{\Delta t}{2\varepsilon}\frac{\partial H_z^n}{\partial x} - \frac{\Delta t^2}{4\mu\varepsilon}\frac{\partial^2}{\partial y \partial z}(E_z^n - E_z^{n-\frac{1}{2}})$$

(A3-b)

$$E_z^{n+\frac{1}{2}} = E_z^n + \frac{\Delta t}{2\varepsilon}\frac{\partial H_y^{n+\frac{1}{2}}}{\partial x} - \frac{\Delta t}{2\varepsilon}\frac{\partial H_x^{n+\frac{1}{2}}}{\partial y} - \frac{\Delta t^2}{4\mu\varepsilon}\frac{\partial^2}{\partial x \partial z}(E_x^n - E_x^{n-\frac{1}{2}})$$

(A3-c)

$$H_x^{n+\frac{1}{2}} = H_x^n + \frac{\Delta t}{2\mu}\frac{\partial E_y^{n+\frac{1}{2}}}{\partial z} - \frac{\Delta t}{2\mu}\frac{\partial E_z^n}{\partial y} - \frac{\Delta t^2}{4\mu\varepsilon}\frac{\partial^2}{\partial x \partial z}(H_z^n - H_z^{n-\frac{1}{2}})$$

(A3-d)

$$H_y^{n+\frac{1}{2}} = H_y^n + \frac{\Delta t}{2\mu}\frac{\partial E_z^{n+\frac{1}{2}}}{\partial x} - \frac{\Delta t}{2\mu}\frac{\partial E_x^n}{\partial z} - \frac{\Delta t^2}{4\mu\varepsilon}\frac{\partial^2}{\partial x \partial y}(H_x^n - H_x^{n-\frac{1}{2}})$$

(A3-e)

$$H_z^{n+\frac{1}{2}} = H_z^n + \frac{\Delta t}{2\mu}\frac{\partial E_x^{n+\frac{1}{2}}}{\partial y} - \frac{\Delta t}{2\mu}\frac{\partial E_y^n}{\partial x} - \frac{\Delta t^2}{4\mu\varepsilon}\frac{\partial^2}{\partial y \partial z}(H_y^n - H_y^{n-\frac{1}{2}})$$

(A3-f)

Similarly

Step 2

$$E_x^{n+1} = E_x^{n+\frac{1}{2}} + \frac{\Delta t}{2\varepsilon}\frac{\partial H_z^{n+\frac{1}{2}}}{\partial y} - \frac{\Delta t}{2\varepsilon}\frac{\partial H_y^{n+1}}{\partial z} - \frac{\Delta t^2}{4\mu\varepsilon}\frac{\partial^2}{\partial x \partial y}(E_y^{n+\frac{1}{2}} - E_y^n)$$

(A4-a)

$$E_y^{n+1} = E_y^{n+\frac{1}{2}} + \frac{\Delta t}{2\varepsilon} \frac{\partial H_x^{n+\frac{1}{2}}}{\partial z} - \frac{\Delta t}{2\varepsilon} \frac{\partial H_z^{n+1}}{\partial x} - \frac{\Delta t^2}{4\mu\varepsilon} \frac{\partial^2}{\partial y \partial z} (E_z^{n+\frac{1}{2}} - E_z^n) \qquad \text{(A4-b)}$$

$$E_z^{n+1} = E_z^{n+\frac{1}{2}} + \frac{\Delta t}{2\varepsilon} \frac{\partial H_y^{n+\frac{1}{2}}}{\partial x} - \frac{\Delta t}{2\varepsilon} \frac{\partial H_x^{n+1}}{\partial y} - \frac{\Delta t^2}{4\mu\varepsilon} \frac{\partial^2}{\partial x \partial z} (E_x^{n+\frac{1}{2}} - E_x^n) \qquad \text{(A4-c)}$$

$$H_x^{n+1} = H_x^{n+\frac{1}{2}} + \frac{\Delta t}{2\mu} \frac{\partial E_y^{n+\frac{1}{2}}}{\partial z} - \frac{\Delta t}{2\mu} \frac{\partial E_z^{n+1}}{\partial y} - \frac{\Delta t^2}{4\mu\varepsilon} \frac{\partial^2}{\partial x \partial z} (H_z^{n+\frac{1}{2}} - H_z^n) \qquad \text{(A4-d)}$$

$$H_y^{n+1} = H_y^{n+\frac{1}{2}} + \frac{\Delta t}{2\mu} \frac{\partial E_z^{n+\frac{1}{2}}}{\partial x} - \frac{\Delta t}{2\mu} \frac{\partial E_x^{n+1}}{\partial z} - \frac{\Delta t^2}{4\mu\varepsilon} \frac{\partial^2}{\partial x \partial y} (H_x^{n+\frac{1}{2}} - H_x^n) \qquad \text{(A4-e)}$$

$$H_z^{n+1} = H_z^{n+\frac{1}{2}} + \frac{\Delta t}{2\mu} \frac{\partial E_x^{n+\frac{1}{2}}}{\partial y} - \frac{\Delta t}{2\mu} \frac{\partial E_y^{n+1}}{\partial x} - 4\frac{\Delta t^2}{8\mu\varepsilon} \frac{\partial^2}{\partial y \partial z} (H_y^{n+\frac{1}{2}} - H_y^n) \qquad \text{(A4-f)}$$

Similarly, equations for Method #2 can be obtained.

Appendix # B   Simplification of Dispersion Equation for 1-D DO-ADI-FDTD

In this appendix equation (6.16) is simplified to get equation (6.17)

$$\sin^2(\frac{k_x \Delta x}{2}) = \frac{\mu \varepsilon \Delta x^2}{B^2 \Delta t^2} \left(\frac{1}{\cos^2(\frac{\omega \Delta t}{2})} - 1 \right) \tag{B-1}$$

After simplification of above equation, obtained results are:

$$\sin^2(\frac{k_x \Delta x}{2}) = \frac{\mu \varepsilon \Delta x^2}{B^2 \Delta t^2} \left(\frac{1 - \cos^2(\frac{\omega \Delta t}{2})}{\cos^2(\frac{\omega \Delta t}{2})} \right)$$

$$\sin^2(\frac{k_x \Delta x}{2}) = \frac{\mu \varepsilon \Delta x^2}{B^2 \Delta t^2} \left(\frac{\sin^2(\frac{\omega \Delta t}{2})}{\cos^2(\frac{\omega \Delta t}{2})} \right)$$

$$\sin^2(\frac{k_x \Delta x}{2}) = \frac{\mu \varepsilon \Delta x^2}{B^2 \Delta t^2} \tan^2(\frac{\omega \Delta t}{2}) \tag{B-2}$$

In this equation, $k_x = \tilde{k} \cos\phi \sin\theta$ where $\tilde{k}$ is numerical wavenumber and for 1-D case in

x direction $\theta = 90°$ $\phi = 0°$ so $k_x = \tilde{k}$ and equation B-2 becomes

$$\sin^2(\frac{\tilde{k} \Delta x}{2}) = \frac{\mu \varepsilon \Delta x^2}{B^2 \Delta t^2} \tan^2(\frac{\omega \Delta t}{2}) \quad , \quad \tilde{k} = \frac{2}{\Delta x} \sin^{-1}\left(\sqrt{\frac{\mu \varepsilon \Delta x^2}{B^2 \Delta t^2} \tan^2(\frac{\omega \Delta t}{2})} \right)$$

Similarly equation B-1 can be written as:

$$\tilde{k} = \frac{2}{\Delta x} \sin^{-1}\left(\sqrt{\frac{\mu \varepsilon \Delta x^2}{B^2 \Delta t^2} \left(\frac{1}{\cos^2(\frac{\omega \Delta t}{2})} - 1 \right)} \right) \tag{B-3}$$

Appendix # C   Calculation of Optimization Parameter "*B*" for 1-D DO-ADI-FDTD

The value of B can be found by comparing the FDTD or analytical dispersion relation with that of the 1D ADI-FDTD dispersion equation.

The dispersion relation for optimized ADI-FDTD method is:

$$\sin^2(\frac{k_x \Delta x}{2}) = \frac{\mu \varepsilon \Delta x^2}{B^2 \Delta t^2} \left(\frac{1}{\cos^2(\frac{\omega \Delta t}{2})} - 1 \right)$$

(C-1)

and the dispersion of the FDTD method is:

$$\sin^2(\frac{\omega \Delta t}{2}) = \frac{c^2 \Delta t^2}{\Delta x^2} \sin^2(\frac{k_x \Delta x}{2})$$

It can be written as:

$$\sin^2(\frac{k_x \Delta x}{2}) = \frac{\Delta x^2}{c^2 \Delta t^2} \sin^2(\frac{\omega \Delta t}{2})$$

(C-2)

Comparing (C-1) and (C-2)

$$\frac{\Delta x^2}{c^2 \Delta t^2} \sin^2(\frac{\omega \Delta t}{2}) = \frac{\mu \varepsilon \Delta x^2}{B^2 \Delta t^2} \left(\frac{1}{\cos^2(\frac{\omega \Delta t}{2})} - 1 \right)$$

$$\frac{\Delta x^2}{c^2 \Delta t^2} \sin^2(\frac{\omega \Delta t}{2}) = \frac{\Delta x^2}{B^2 c^2 \Delta t^2} \left(\frac{1}{\cos^2(\frac{\omega \Delta t}{2})} - 1 \right)$$

$$B^2 \sin^2\left(\frac{\omega \Delta t}{2}\right) = \left(\frac{1 - \cos^2\left(\frac{\omega \Delta t}{2}\right)}{\cos^2\left(\frac{\omega \Delta t}{2}\right)}\right)$$

$$B^2 = \left(\frac{1}{\cos^2\left(\frac{\omega \Delta t}{2}\right)}\right) \qquad B = \left(\frac{1}{\cos\left(\frac{\omega_o \Delta x}{2c}\right)}\right) \qquad \text{(C-3)}$$

Another way to obtain value of B is by comparing with the dispersion relation of analytical results. The analytical dispersion relation for a plane wave in a continuous lossless medium for 1-D case is simply

$$\frac{\omega^2}{c^2} = k_x^2$$

Put value of k_x in (C-2)

$$\sin^2\left(\frac{\omega \Delta x}{2c}\right) = \frac{\mu \varepsilon \Delta x^2}{B^2 \Delta t^2}\left(\frac{1}{\cos^2\left(\frac{\omega \Delta t}{2}\right)} - 1\right)$$

after simplification

$$\sin^2\left(\frac{\omega \Delta x}{2c}\right) = \frac{\mu \varepsilon \Delta x^2}{B^2 \Delta t^2}\left(\frac{1}{\cos^2\left(\frac{\omega \Delta t}{2}\right)} - 1\right)$$

$$\sin^2\left(\frac{\omega \Delta x}{2c}\right) = \frac{\Delta x^2}{cB^2 \frac{\Delta x^2}{c}}\left(\frac{1 - \cos^2\left(\frac{\omega \Delta t}{2}\right)}{\cos^2\left(\frac{\omega \Delta t}{2}\right)}\right)$$

$$\sin^2(\frac{\omega \Delta x}{2c}) = \frac{1}{B^2} \left(\frac{\sin^2(\frac{\omega \Delta t}{2})}{\cos^2(\frac{\omega \Delta t}{2})} \right)$$

$$\sin^2(\frac{\omega \Delta x}{2c}) = \frac{1}{B^2} \left(\frac{\sin^2(\frac{\omega \Delta x}{2c})}{\cos^2(\frac{\omega \Delta x}{2c})} \right)$$

$$\sin^2(\frac{\omega \Delta x}{2c}) = \frac{1}{B^2} \left(\frac{\sin^2(\frac{\omega \Delta x}{2c})}{\cos^2(\frac{\omega \Delta x}{2c})} \right) \; , \; B^2 = \frac{1}{\cos^2(\frac{\omega_o \Delta x}{2c})} \; , \; B = \frac{1}{\cos(\frac{\omega_o \Delta x}{2c})} \qquad \text{(C-4)}$$

So equations (C-3) and (C-4) are the same with both FDTD and analytical dispersion results. Now this value of B will directly optimize the ADI-FDTD method depending on the spatial step. This variation of B with space step suggests the variation of dispersion of the ADI-FDTD method. It can be concluded that this is the difference between DO-ADI-FDTD and ADI-FDTD methods with different cell size.